NATIONAL TECHNICAL UNIVERSITY OF ATHENS

SCHOOL OF NAVAL ARCHITECTURE AND MARINE ENGINEERING
SHIPBUILDING TECHNOLOGY LABORATORY

DIPLOMA THESIS

"Application of non-destructive testing using ultrasound method for detection of defects in filament wound composite materials"

by

Konstantina Karteri

Supervisor:
Prof. N. Tsouvalis

Athens, November 2019

Contents

ACKNOWLEDGMENTS

This thesis was elaborated at the Shipbuilding Technology Laboratory of the School of Naval Architecture and Marine Engineering, National Technical University of Athens (NTUA), under the supervision of Professor N. Tsouvalis. With the end of my diplomatic work, I would like to thank the people who contributed to its completion.

First of all, I would like to thank Mr. Tsouvalis, Professor at NTUA, for the opportunity he gave me to deal with this subject, the trust he put in me throughout the diploma thesis and the permission to use the equipment that were located at the laboratory.

I would like to sincerely thank Ms. Sarafoglou, Dr. Mechanical Engineer at NTUA and member of the Special Laboratory Teaching Staff, for her guidance on the use of the ultrasonic equipment of the laboratory and her helpful comments on the procedure and the results. Her patience and willing to help made our cooperation pleasant and efficient.

Except for Mr. Tsouvalis and Ms. Sarafoglou, Assistant Professor K. Anifantis, Shipbuilding Technology Laboratory, NTUA, is also a member of my thesis committee and I genuinely thank him for his time and occupation.

I wish to acknowledge the help provided by Mr. A. Markoulis and Mr. Ch. Xanthis, Technical Staff of the Shipbuilding Technology Laboratory, NTUA, on technical and practical issues.

Finally, I would like to express my very great appreciation to my family and friends for their genuine concern and constant support.

ABSTRACT

The subject of this diploma thesis is the nondestructive inspection of a CFRP (Carbon Fiber Reinforced Polymer) wound tubular specimen through the ultrasonic technique, in order to detect teflon defects that simulate voids between laminates. Through A-Scan and C-Scan illustrations depth of the defects was specified.

More specifically, at the beginning it was necessary to get acquainted with the ultrasonic theory and equipment. After this preparation, an axial system was defined on the cylinder so that the theoretical position of the defects could be visually determined. The system contained the angle and the longitudinal position of the defects on the cylinder. This set the start of the experimental procedure, which continued with the approximation of the longitudinal sound velocity inside the specimen.

Then ultrasonic examination of the specimen began with the first method. Contact transducers were used to scan the areas of interest at the depth of each defect. According to the axes defined on the cylinder the area of the defect was detected. Then the signal from this area was compared with the signal of a neighboring “healthy” area. If any extra echo occurred at the depth of interest, the defect was considered to be detected. Several trials took place with various contact transducers, until the final ones were chosen. A-Scan illustration was used to present the results.

The second method used for the experimental procedure was the testing of the specimen with the use of an immersion tank. The specimen was sunk in the tank and an immersion transducer was scanning a rectangular area of the cylinder, according to the settings that the user applied. After several trials the final transducers were chosen. The recognition of the defects was allowed due to the 2D illustration that C-Scan provides.

Comparing the results of these two methods with each other and with the theoretical data, the reliability of each measurement was evaluated and conclusions were made.

1. COMPOSITE MATERIALS

Composite materials are defined as macroscopic combinations of two or more distinct materials having a discrete and recognizable interface separating them. Thus composites are heterogeneous materials, and many are naturally occurring; the most common is wood [1].

1.1 Structure and Manufacturing of Composites

The categorization of composite materials according to their structure is fibrous, particulate and laminated composites. For fibrous composites fibers have been introduced in the matrix. Fibers can be in different forms, e.g. fabrics, rovings etc. Particulate composites are consisted of tiny particles embedded inside the matrix and laminated composites are materials that are consisted of laminates of two or more different materials. Matrices can be organic, ceramic or metallic. This thesis deals with a specimen with organic matrix, which is resin. The resin can be epoxy, polyester, vinyl ester etc. Epoxy resins are very popular in marine, because of their low water absorption, better mechanical properties and their good behavior during automated methods. A negative aspect though is their high cost [2] [3].

There are numerous methods for fabricating composite components. Hand lay-up is the most basic, where layers (plies) of dry fabrics are being placed by hand onto a tool to form a laminate stack. Resin is applied to the dry plies after layup is complete. Other methods are open molding, resin infusion processes, high-volume molding methods etc [4].

The last category contains the method of this thesis' interest, which is called filament winding. This procedure is an efficient and low-cost method, which provides products with better mechanical properties through the use of continuous fibers. Continuous fibers, as tows or rovings, dry or preimpregnated with resin, are pulled from fiber packages in a creel, guided through a mixed-resin impregnating system (if fibers are dry), and then formed into a flat band. A filament winding machine has a fiber-band-dispensing carriage that traverses from one end of the form (mandrel, Figure 1.1) to the other (called a pass) and back again (completing a circuit). This motion alternately places a plus-angle fiber band in one direction and a minus-fiber band in the reverse direction as the form revolves. This sequence is repeated as required for either thickness or number of plies. Next, the form and winding are heated or otherwise treated to cure the resin. The tooling is removed from the winding, and finishing operations, if any, are performed [5].

Filament winding has plenty of advantages, as it is provides products with the cheapest and strongest form of fiber reinforcement. This method enables to orient the fibers to the direction of the stresses in the structure, leading to better behavior under mechanical stress. Furthermore, it is a high automated procedure with excellent control, meaning not only low production costs, as well as great productivity and low scrap rates. Products are always less in weight and can be less in cost than those of metal. The negative aspects of this method are also significant. There is a limitation at the shape of the products and often the outer surface is not smooth. It is also difficult or even impossible to remove the mandrel from a closed end winding [5][6].

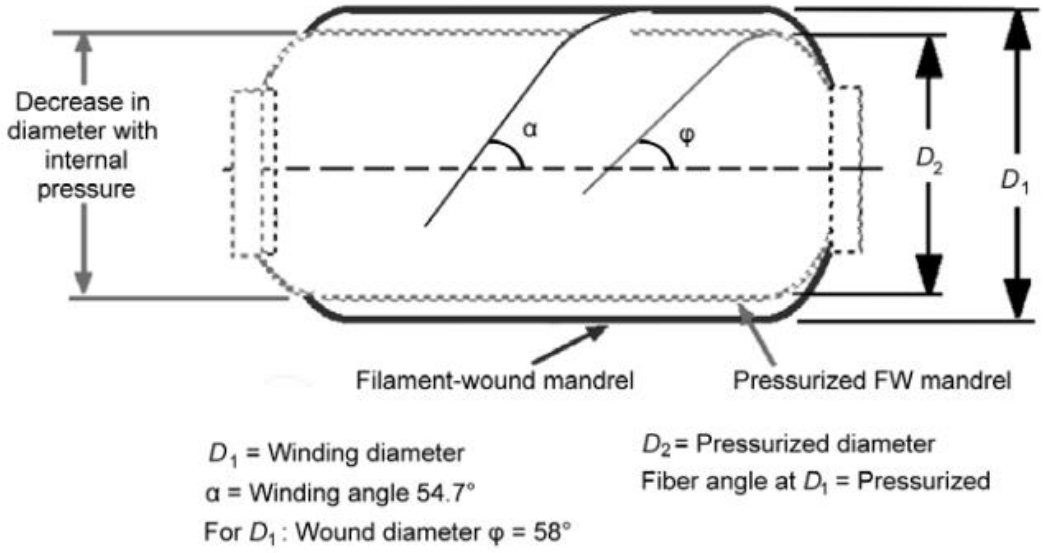

Figure 1.1 Filament-wound (FW) mandrel.

1.2 Advantages of Composite Materials

The first advantage is the light weight. Composites are light in weight, compared to most woods and metals. Their lightness is important in applications, where less weight means better fuel efficiency. Additionally, composites can be designed to be far stronger than aluminum or steel. Metals are equally strong in all directions, but composites can be engineered and designed to be strong in a specific direction. Strength Related to Weight ratio is a material's strength in relation to how much it weighs. Steel for example is very strong and heavy. Other materials can be strong and light. Such an example is composite materials that can be designed to be both strong and light. A composite can be made to resist bending in one direction, for example. In the case of a metal construction that greater strength is needed in one direction, the material usually must be made thicker. This adds weight to the construction. Composites can be strong without being heavy and have the highest strength-to-weight ratios in structures today. Corrosion resistance is also a very positive aspect of composites. They resist damage from the weather and from harsh chemicals that can eat away at other materials. Composites are good choices where chemicals are handled or stored. Outdoors, they stand up to severe weather and wide changes in temperature. Furthermore, composites can be made to absorb impacts (e.g. the blast from an explosion) efficiently. In many applications materials with high design flexibility are needed. Composites can be molded into complicated shapes more easily than most other materials. This gives designers the freedom to create almost any shape or form. Most recreational boats today, for example, are built from fiberglass composites because these materials can easily be molded into complex shapes, which improve boat design while lowering costs. The surface of composites can also be molded to mimic any surface finish or texture, from smooth to pebbly. Designers pay also great attention on part consolidation. A single piece made of composite materials can replace an entire assembly of metal parts. Reducing the number of parts in a machine or a structure saves time and cuts down on the maintenance needed over the life of the item. Dimensional stability is another advantage that composites have.

Composites retain their shape and size when they are hot or cool, wet or dry. They can be a better choice in situations demanding tight fits that do not vary. Composites are also nonconductive, meaning they do not conduct electricity. This property makes them suitable for such items as electrical utility poles and the circuit boards in electronics. Nonetheless if electrical conductivity is needed, it is possible to make some composites conductive. Composites contain no metals; therefore, they are not magnetic and can be used around sensitive electronic equipment. Radar signals pass right through composites, a property that makes composites ideal materials for use anywhere radar equipment is operating, whether on the ground or in the air. Furthermore, composites are good insulators, while having low thermal conductivity. Finally, structures made of composites have a long life and need little maintenance. It is not known how long composites last, because the end of the life of many original composites has not yet come. Many composites have been in service for half a century [4].

1.3 Applications of Filament Winding Composites in Marine

Composite materials are applied in marine the latest years in a greater extent than in the past. Filament wound composites though, because of the cylindrical shape of the produced pieces, apply to a narrower range of cases in marine. It is possible that other shapes are achieved as well, but the production method does not provide plenty of options. Filament wound products, though, find wide application in aerospace and automotive [7].

A very common application of filament winding method is pipelines. An example is the filament wound epoxy and vinylester resin based composite pipe system suitable for a wide range of applications as complete piping system alternative to traditional steel and metallic materials. It is estimated that this pipe systems is just a quarter the weight of comparable steel pipes and is easy to install without the need of heavy installation equipment, welding or protective coating. The installation cost of it is typically 80% of the cost of carbon steel. The smooth internal surface reduces the head loss resulting in lower pump energy consumption [8].

Offshore pressure vessels are also a significant application of filament wound composites. Not only are they corrosion resistant and lightweight, but also cost effective compared to metallic pressure vessels [9].

Filament wound storage tanks, such as containers, are also a very interesting development for the area of product transport. These tanks are applied for the storage of acids, alkalies, chlorinated brine, salts, oils and other corrosive products. Their prices in comparison with the galvanized steel tanks are lower, their weight is lighter, their corrosion resistance better and their maintenance cheaper [7].

Submarines have also turned their attention on composite wound materials. Example consist the launched missile’s capsules that are manufactured with a graphite, wet, filament-wound sandwich construction, metal honeycomb core and Kevlar reinforcements. Submarine technology focuses on research on possible future composite applications [10].

Other marine applications of composite filament wound products are masts, antenna tubes, vent cowlings, battery containers and car-top boats. All the above present similar advantages, as the above mentioned, e.g. lightweight, corrosion-resistant etc [7].

The possibilities for more marine applications are promising, as according to scientific research the production of filament wound hulls, decks, propulsion shafts and risers will be applicable in the future [10][11].

1.4 Defects

Some necessary definitions will be presented below. A defect is defined as a deviation from the ideal or specified geometric and/or physical built-up of a structure or component. A production defect is understood to be a defect that has arisen in the production process and includes material defects. An imperfection is related specifically to imperfections of shape and not generally to a defect. Like many other types of production defects, geometric imperfections can never be totally eliminated and it remains to set limits of acceptability for their size. Ideally a production control system that addresses quality assurance in a systematic way should include acceptance limits for all relevant types of production defects, including geometric imperfections. Damage is a deviation from the ideal or specified geometric structure or component that has arisen as a result of mechanical, thermal or other loading. Damage may occur during service or during production. Damage occurring during service may also be caused by the growth of a production defect.

Three categories of defects can be defined. These are structural defects, which affect the load carrying capability of a component, geometric defects, which include out-of-straightness or flatness, eccentricities and deviation from specified angles or thicknesses and, finally, cosmetic defects, which affect the appearance of the product but have little or no direct effect on the structural performance [12].

Most basic production defects that may occur in filament wound components are delaminations (Figure 1.2 [13]), dry zones, voids, poor curing, gel coat defects, regions of microbuckled fibers, thickness variations from non-uniform applied pressure, wrinkles in individual layers, and gaps or excessive overlapping of individual tows during winding [12][14].

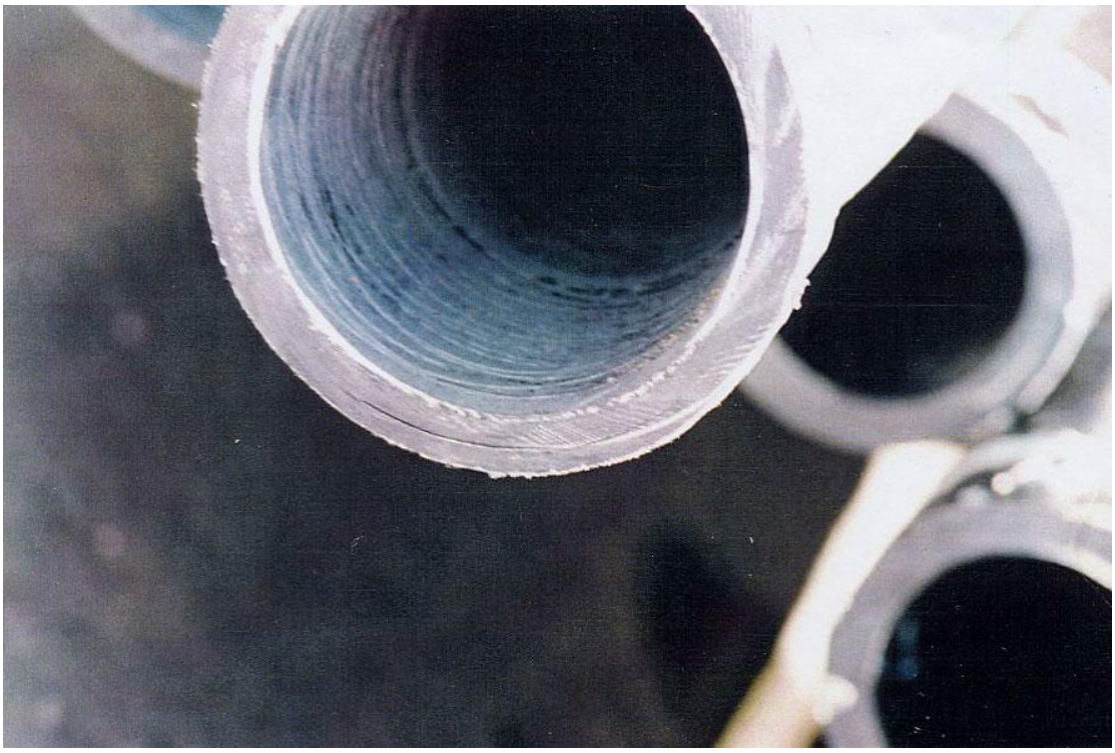

Figure 1.2 Internal delamination caused by improper curing (residual cure stresses resulting in cracking and delamination).

2. ULTRASONIC TESTING

Ultrasonic testing (UT) is a non-destructive inspection (NDI) method that uses the theoretical background of waves, and more specifically of ultrasonic waves, in order to examine an object or measure its thickness. NDI allows parts and material to be inspected and measured without damaging them. Therefore it provides an excellent balance between quality control and cost-effectiveness.

2.1. Waves in materials

Webster's dictionary [15] defines a wave as a disturbance or variation that transfers energy progressively from point to point in a medium and that may take the form of an elastic deformation or of a variation of pressure, electric or magnetic intensity, electric potential, or temperature. Russell [16] estimates that the most important thing about this definition is that a wave is “a disturbance or variation”, which travels through a medium. According to the ability of the waves to propagate in vacuum, they can be principally categorized in mechanical and electromagnetic waves. Ultrasonic waves are mechanical waves and that means that they, in conjunction with electromagnetic waves, cannot exist in vacuum. The particles of the medium do not travel with the mechanical wave, they just oscillate. Useful information is that a mechanical wave can propagate only in a medium that has the characteristics of inertia and elasticity.

The categorisation according to the frequency of the mechanical wave is infrasound (below 20 Hz), sound (20 Hz- 20000 Hz) and ultrasound (over 20000 Hz). The subject matter of this thesis is ultrasonic waves [22].

2.1.1. Mechanical Wave Types and Characteristics

The direction of the particles’ oscillation compared with the direction of the wave propagation leads to another wave categorization [17]. The first type is longitudinal waves, where the two directions are parallel, as seen in Figure 2.1 [16]. The wave causes compressions and rarefactions at the material’s particles. It can be propagated in all elastic materials.

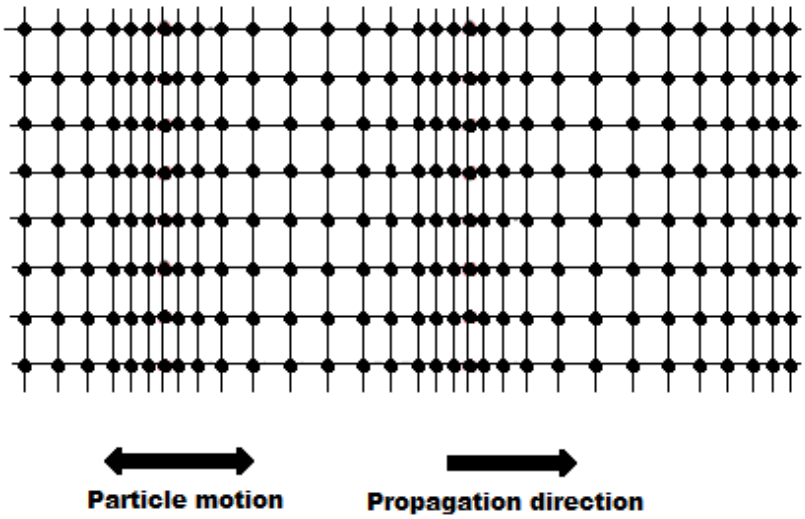

Figure 2.1 Longitudinal Wave.

Another type of wave is the transverse wave. In this case the two directions are perpendicular, while the particles oscillate vertically to the propagation's direction. As a result, crests and troughs appear (Figure 2.2). Transverse waves do not occur in liquids or gasses, but they occur in solid and specific viscously liquid mediums.

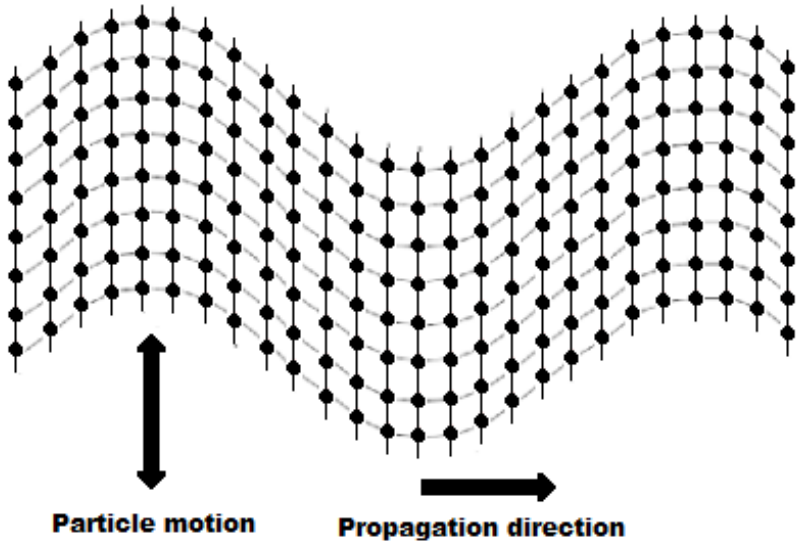

Figure 2.2 Transverse Wave.

Surface waves are more complicated and cause a combination of transverse and longitudinal wave, leading to an elliptical orbit of the molecules of a solid. As the depth into the solid increases the "width" of the elliptical path decreases (Figure 2.3) [16].

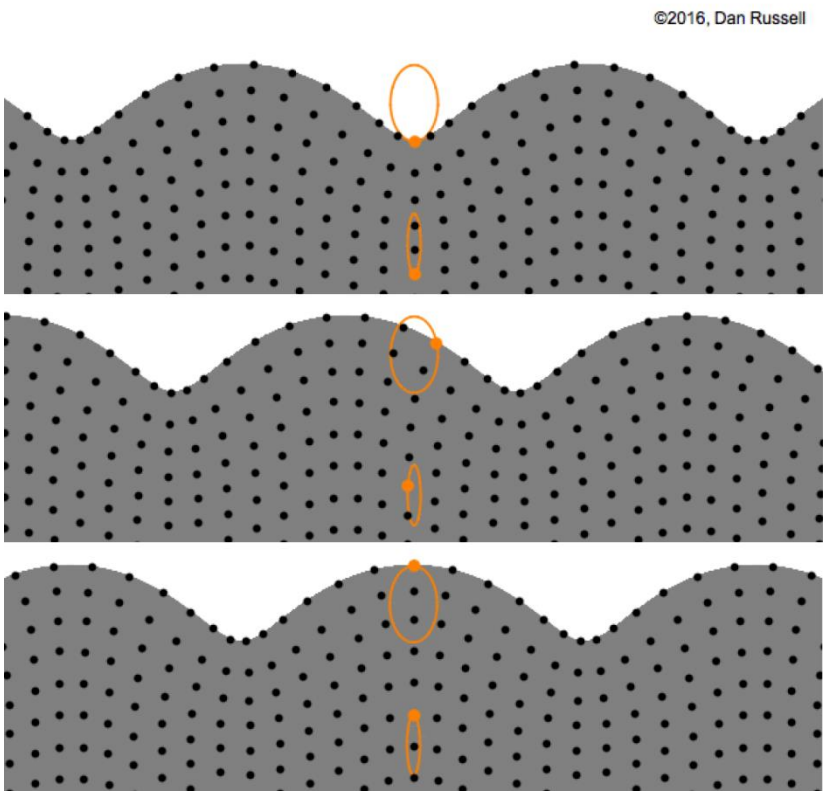

Figure 2.3 Rayleigh surface waves.

There are other types of waves as well, but making relative reference is beyond the scope of this thesis.

Among the properties of waves propagating in isotropic solid materials are wavelength, amplitude and frequency. All the properties mentioned have to do exclusively with the wave. Wavelength is the distance from one crest to another (for longitudinal waves: from one compression to another). Figure 2.4 [17] shows a comparison for both a longitudinal and a transverse wave between two different wavelengths. Wavelength is described by Eqn. 2.1 and is symbolized with λ.

$$\lambda = \frac{v}{f}$$

Eqn. 2.1

Explaining the symbols, v is the velocity and f is the frequency of the wave.

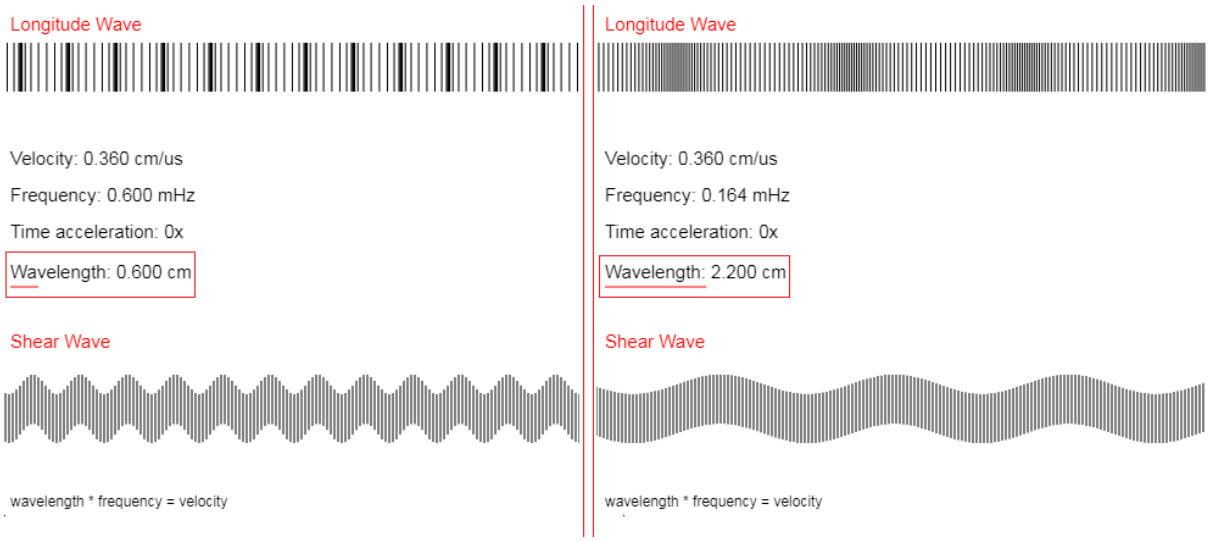

Figure 2.4 Different Wavelengths.

Amplitude is the maximum distance measured from the equilibrium position during the oscillation of the particles and is shown in Figure 2.5.

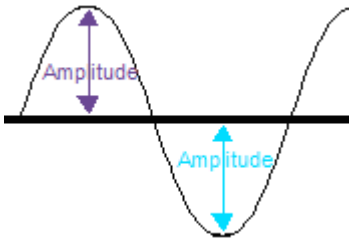

Figure 2.5 Amplitude of a Wave.

The frequency of the wave (Figure 2.6 [17]) describes how many waves (N) are passing a point per second and is explained through Eqn. 2.2.

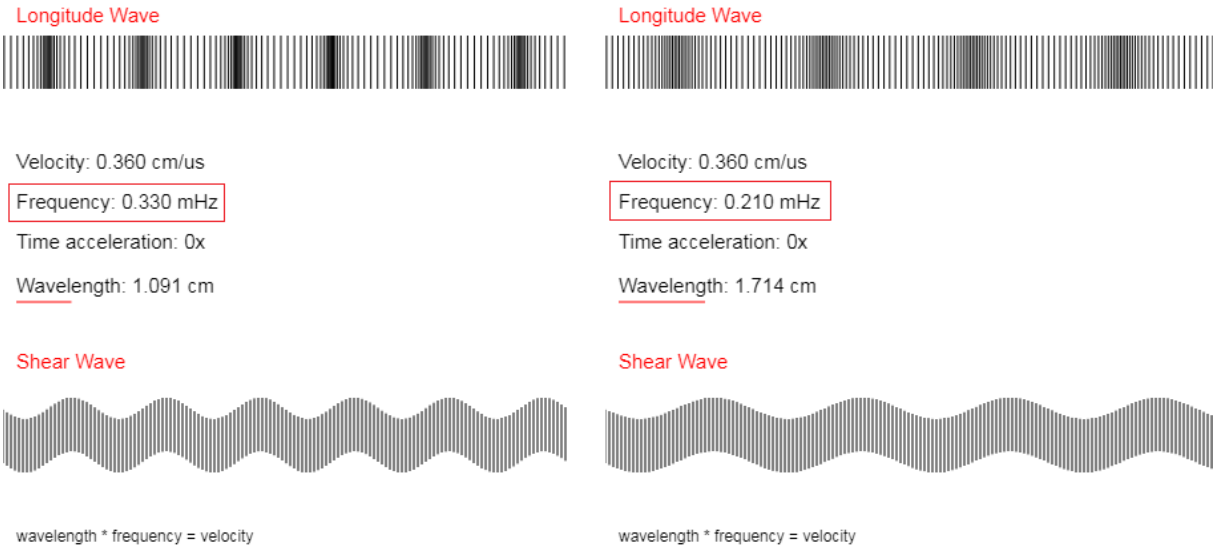

Figure 2.6 Frequency of a Wave.

$$f=\frac{N}{\Delta t}$$

Eqn. 2.2

2.1.2. Elastic materials

Elasticity is, as previously mentioned, an essential feature of the propagation medium. Material behaves elastically if the strains in a test specimen from a given load disappear when the load is removed. An ultrasonic wave may be visualized as an infinite number of oscillating particles connected by means of elastic springs. Each individual particle is influenced by the motion of its nearest neighbour and both inertial and elastic restoring forces act upon each particle [17][18].

The coefficient E of the material is the modulus of elasticity. It appears in Hook's Law equation (Eqn. 2.3 [18]) and associates directly proportional the plane stress applied (σ) with the resulting strain (ε).

$$\sigma=E\cdot\varepsilon$$

Eqn. 2.3

This equation is valid only until a specific stress limit, called yield strength (σ_Y).

When it comes to shear stress the coefficient that associates the stress (τ) with the shear strain (γ) differs and is symbolized with G (Eqn. 2.4 [18]).

$$\tau=G\cdot\gamma$$

Eqn. 2.4

Speed of sound is unique for every material and is independent of the characteristics of the wave propagated. The properties and the microstructure of the material influence the speed of sound through it.

$$v=\sqrt{\frac{C_{ij}}{\rho}}$$

Eqn. 2.5

Eqn. 2.5 provides the formula of velocity. C is the elastic constant. To be precise, C is G for the calculation of transverse velocity and E for the calculation of the longitudinal velocity. Letters i, j indicate the plane on which the stress is applied. The density of the material is ρ. Some materials are given as examples in Table 2.1 [17].

Table 2.1 Examples of Material Velocities.

Material	V longitudinal (cm/μs)	V shear (cm/μs)	Density (g/cm^3)
Aluminum	0.632	0.313	2.70
Steel, 1020	0.589	0.324	7.71
Teflon	0.135	N/A	2.2
Acrylic Resin	0.267	0.112	1.18

2.1.3. Attenuation of Waves and Acoustic Impedance of a Material

Sound has the characteristic that it is losing intensity during its propagation. Inside materials though, an extra weakening of sound is taking place. It is called attenuation of sound and is the combined effect of scattering and absorption of sound. Scattering is the reflection of sound into different undetectable directions. Absorption is the conversion of sound pressure, meaning the energy of the wave, to another form of energy. The formula that contains this term is Eqn. 2.6 and describes the loss of sound energy through a material.

$$A=A_o e^{-az}$$

Eqn. 2.6

Value A represents the final sound pressure after sound has travelled z length units, while A_O is the initial sound pressure. The attenuation coefficient is a. It is measured in Nepers /length and can be converted to Decibels/ length [17].

Microstructure of a material determines strongly the level of attenuation in it. The greater the grain size is, the stronger the attenuation. Other factors also define this level, such as temperature and frequency. Attenuation is usually increased with the temperature, especially in plastics and is also increased with high frequencies [19].

The result of attenuation is obvious in Figure 2.7[20].

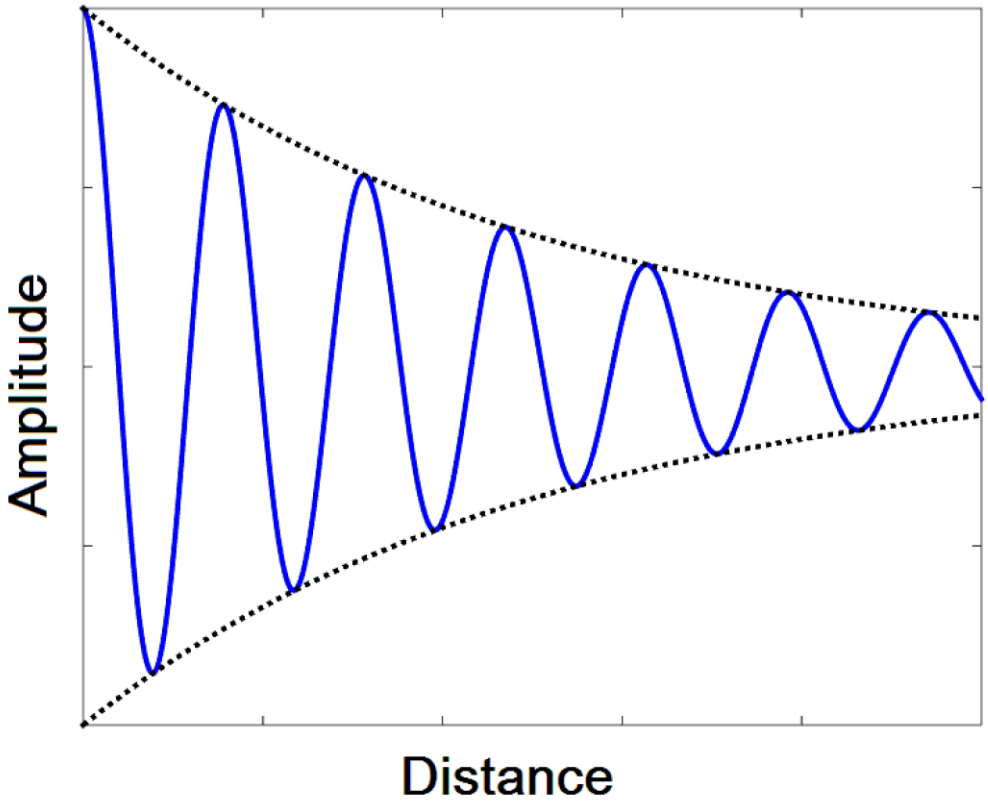

Figure 2.7 Attenuation of sound.

The acoustic impedance (Z) of a material is defined as the product of its density (ρ) and acoustic velocity (V), as seen in Eqn. 2.7 [17]. It is specific for each material.

$$Z=\rho V$$

Eqn. 2.7

Acoustic impedance expresses the opposition of a system to the acoustic flow. This value is important in the determination of acoustic transmission and reflection at the boundary of two materials that have different acoustic impedances, in the design of ultrasonic transducers, as well as in assessing the absorption of sound in a medium [21][22].

2.2. Incidence of a Wave on an Interface

During ultrasonic testing sound propagates to more than one materials. The interface in-between leads to several phenomena according to the angle of incidence of the wave. The following sections present the behavior of the wave based on this criterion.

2.2.1. Zero Angle of Incidence

A wave reaching an interface with zero angle of incidence can propagate and/ or reflect. Reflection is the change in the direction of the wave in a way, so that the wave or part of it returns back to the initial medium. In this case wave is being reflected with an angle of 180 degrees. The percentage of the sound pressure being reflected back to the initial medium

depends on the reflection coefficient (R) of the two materials. This coefficient is described in Eqn. 2.8, where Z_1 is the initial's medium acoustic impedance and Z_2 is the neighbouring's medium acoustic impedance. When these two impedances are equal, then reflection coefficient equals to zero. That means that the wave is not being reflected at all, but is entirely passing on to the next material. Likewise, transmission coefficient (T) is defined in Eqn. 2.9 and expresses the amount of the acoustic energy that is propagated to the next medium [21][22].

$$R=\frac{Z_2-Z_1}{Z_2+Z_1}$$

Eqn. 2.8

$$T=\frac{2Z_2}{Z_2+Z_1}$$

Eqn. 2.9

2.2.2. Oblique Angle of Incidence

A wave reaching an interface with an oblique angle can propagate, reflect, refract and/ or convert. The behaviour of the wave depends on the angle of incidence and will be explained below. We suppose that the initial wave is the red arrow seen in Figure 2.8.

Reflection is, as explained above, the change in the direction of the wave in a way, so that the wave or part of it returns back to the initial medium. The angle of incidence equals the angle of reflection (Snell's Law). Total internal reflection is occurred when the index of refraction of the first material (n_1) is greater than the one of the second material (n_2) [23].

Refraction is the propagation of the wave to the next material accompanied with change in the direction of the wave. The refraction angle can be found via the Snell's Law.

Conversion of wave type is common and depends on the angle of incidence, as it is explained below. The wave from longitudinal can be converted to shear or surface.

All the possible phenomena can be seen in Figure 2.8 below. Velocity is symbolized for longitudinal waves with V_L, for shear waves with V_T and for surface waves with V_S.

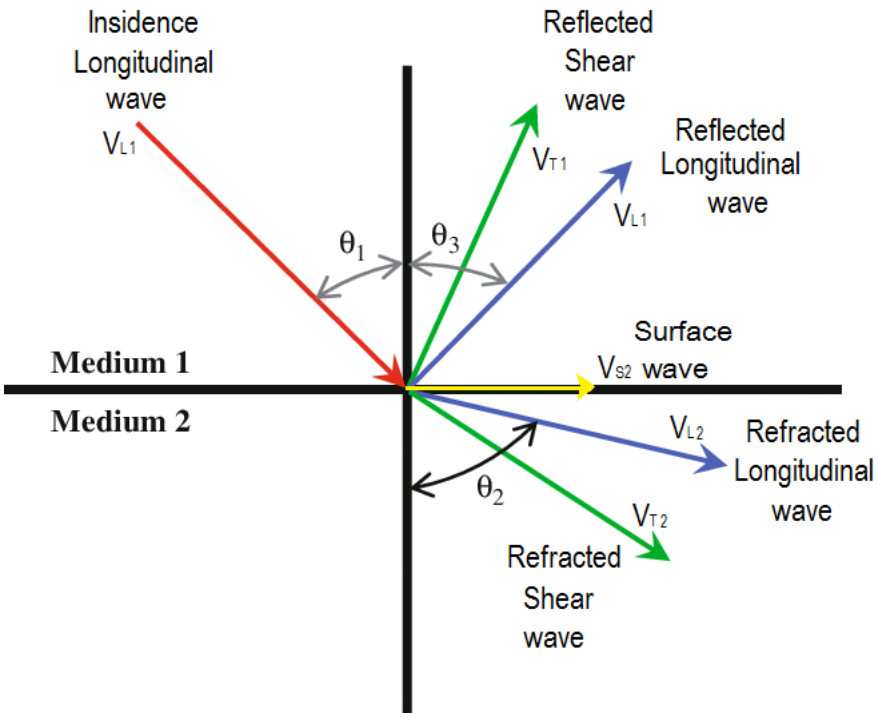

Figure 2.8 All phenomena at interface.

The behaviour of the wave when passing through an interface is determined by the material and the incidence angle (θ_1) and is described by Snell's law. To simplify the procedure, total internal reflection will not be a case for the rest of the section.

As regards the incidence angle (θ_1), there are three important values for every material, which determine the phenomena that will take place. The first value, which is common for almost all the materials, is 5°. The second and third values differ from case to case and are called respectively 2nd and 3rd critical angles. The accordance of these angles to the phenomena that will take place will be explained below.

All symbols used in the equations below are explained in the figures that follow them. When the angle of incidence is 0° (Figure 2.9), the wave can be both reflected to the 1st material and propagate to the 2nd material. The type of the wave is longitudinal and was described in a previous section (2.2.1.).

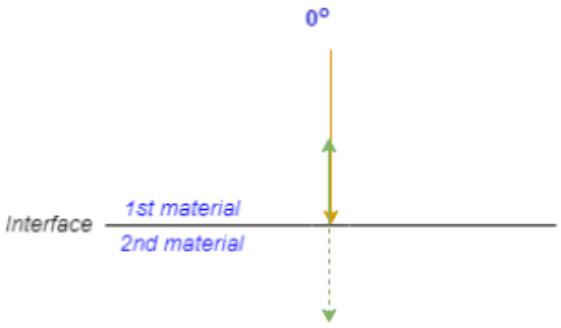

Figure 2.9 Zero incidence angle.

For angles between 0° and 5° the longitudinal wave is both reflected to the 1st material and refracted to the 2nd material. The wave is always longitudinal. Snell's law in this case is described by Eqn. 2.10, where α_1 is the angle of incidence and α_2 is the refraction angle.

$$\frac{\sin \alpha_1}{V_{L1}} = \frac{\sin \alpha_2}{V_{L2}}$$

Eqn. 2.10

Figure 2.10 below describes the parameters used in Eqn. 2.10.

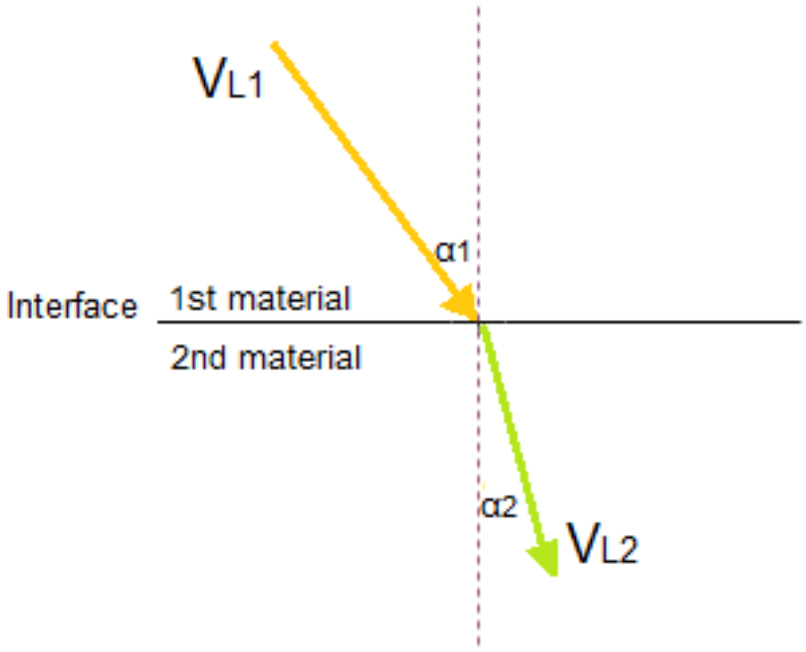

Figure 2.10 Zero to 5o incidence angle.

Between 5^O and the 1^{st} critical angle (Figure 2.11) the wave is reflected, refracted and partly converted to shear (V_{T2}, see Figure 2.11). Snell's law describes this behaviour:

$$\frac{\sin \alpha_1}{V_{L1}} = \frac{\sin \alpha_2}{V_{L2}} = \frac{\sin \beta_2}{V_{T2}}$$

Eqn. 2.11

When the incidence angle is equal to the 1^{st} critical angle, then the wave at the 2^{nd} material is fully converted to shear.

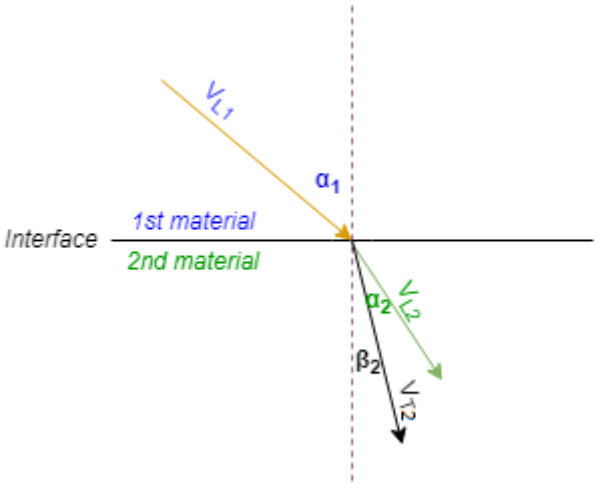

Figure 2.11 5º to 1st critical incidence angle.

Only shear refracted waves (V_{T2}) appear for angle values between the 1st and the 2nd critical incidence angle, as seen in Figure 2.12. Snell's law describes this behaviour through the Eqn. 2.12.

$$\frac{\sin \alpha_1}{V_{L1}} = \frac{\sin \beta_2}{V_{T2}}$$

Eqn. 2.12

When the incidence angle equals the 2nd critical angle, then at the second material only surface waves exist.

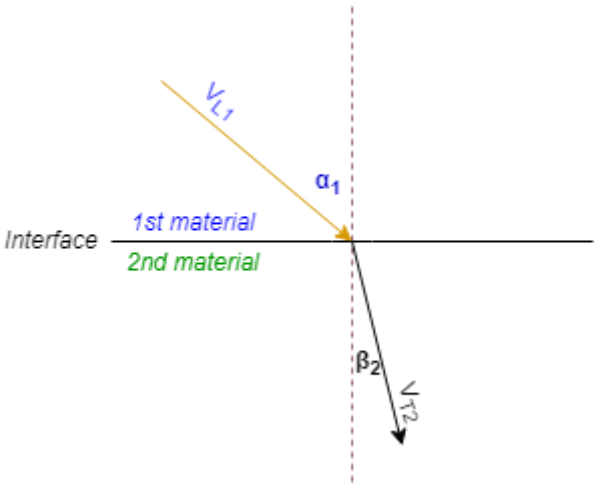

Figure 2.12 1st to 2nd critical incidence angle.

From the 2nd critical angle and over the waves of the second material are only surface waves. An overview of the above is given in Figure 2.13.

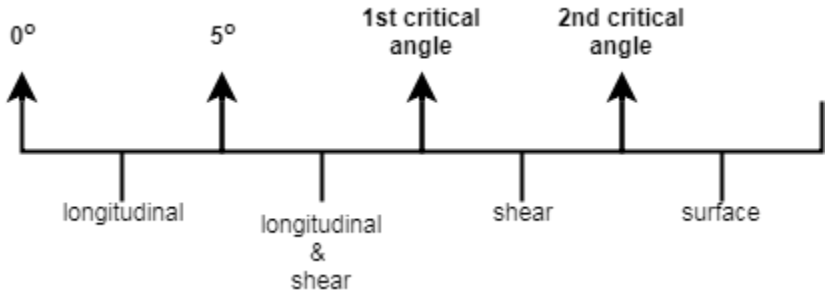

Figure 2.13 Wave type according to incidence angle.

2.3. Ultrasonic Transducers

Ultrasonic transducers produce ultrasonic waves. The generation of these waves is achieved by taking advantage of the piezoelectric effect, which will be explained below. The choice of the transducer is crucial for an ultrasonic examination, as the characteristics of the transducer and the transmitted beam define the success of the process. The choice of the transducer depends among others on the specimen's material and the examination method.

2.3.1. Piezoelectric Effect

Some materials (crystals, ceramics, etc.) can generate electricity or an electric polarization when subjected to mechanical stress. This phenomenon also occurs vice versa, namely the application of an electric field causes mechanical stress on these elements. That is called piezoelectric and reverse piezoelectric effect, respectively. Both effects are applied to the function of the piezoelectric ultrasonic transducers.

Reverse piezoelectric effect is useful for the generation of longitudinal waves. More specifically, during the reverse piezoelectric effect, compressive and tensile strain occurs (alternating according to the frequency of the applied A/C voltage) by applying electric potential at the two opposite sides of a piezoelectric element. The element is polarized, because of the applied electric potential, meaning that one side of every molecule becomes positively charged, while the other side becomes negatively charged. That causes the alignment of the element's molecules and therefore the element expands. The strain is proportional to the rate of the electric potential. The transducer though is formed in such a way, so that it constrains the deformation of the element in the directions of the compression and tensile strain, as seen in Figure 2.14. Consequently, the third dimension is deformed and it presses the neighbouring medium (water, air, metal, etc). This pressure is, as mentioned, synchronized with the frequency of the the A/C voltage, so it forces the molecules of the medium into oscillation. Thus, a longitudinal wave is created and transmitted through the medium (Figure 2.15). This is the procedure through which an ultrasonic piezoelectric transducer creates ultrasonic waves.

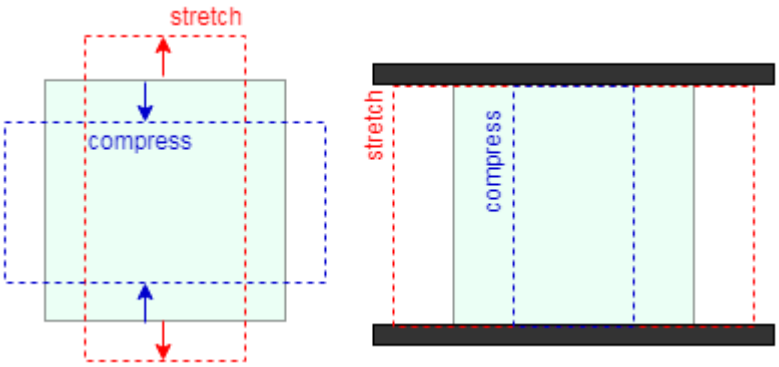

Figure 2.14 Free-to-move piezoelectric element vs. constrained piezoelectric element.

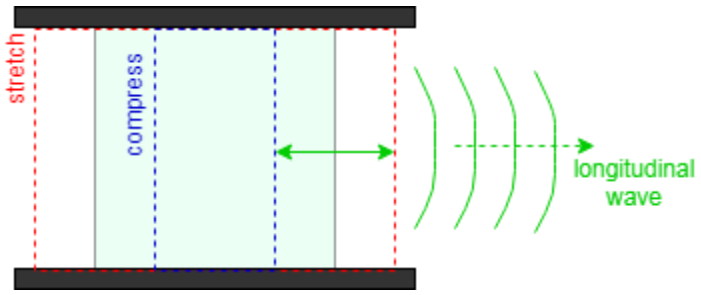

Figure 2.15 Reverse piezoelectric effect.

The simple piezoelectric effect is useful for the translation of the received waves from the transducer. The transducer receives longitudinal waves and transforms them through mechanical oscillation into electric potential. More specifically, the ultrasonic wave reaches the transducer and then the transducer is forced into alternating compression and tension. Because of the piezoelectric effect, two opposite sides of the piezoelectric element develop alternating electric potential. The frequency of the inversion of the polarity follows the frequency of the wave. In this way, the transducer can share the information it receives.

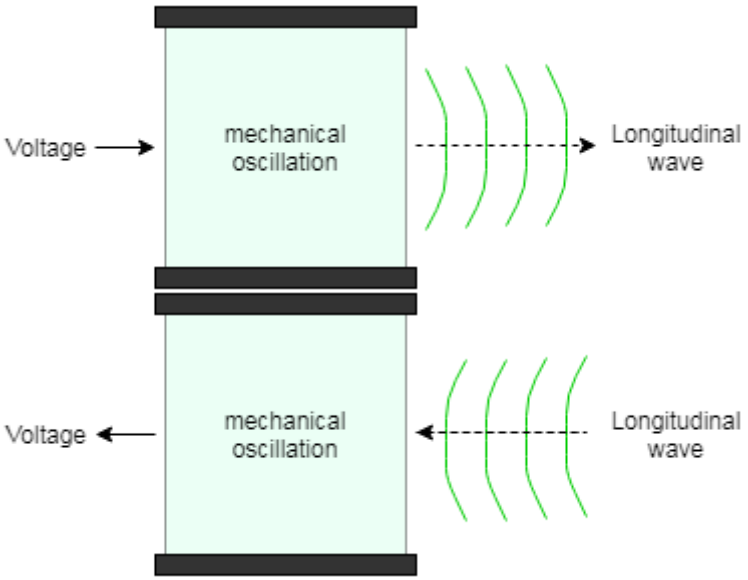

Figure 2.16 Generation and receipt of longitudinal waves.

To sum up, the heart of the transducer is the active element. It transforms electrical to acoustic energy and vice versa. As it is obvious in Figure 2.16, the transmission and the receipt of a longitudinal wave are both a consequence of the piezoelectric effect [24][25][26].

2.3.2. Parts and Materials of a Transducer

The parts of the transducer are also important to analyze. As seen in Figure 2.17 [24] a transducer consists of the piezoelectric element, which is constrained from the back with the backing material and is sandwiched between two electrodes. At the front of the piezoelectric element there are the matching element and the protective wear plate.

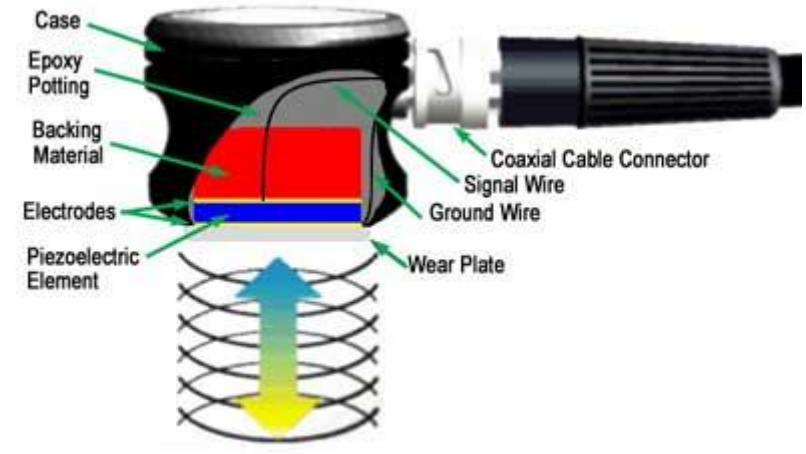

Figure 2.17 Inside of a transducer.

The desired frequency is ensured through the thickness of the active element. The thinner the element is, the higher the frequency. Contact transducers also incorporate a wear plate to protect the matching layer and the active element from scratching.

The materials used for the active element have changed throughout the years. Today piezoelectric ceramics are preferred (Figure 2.18 [24]), due to their easy manufacture in a variety of shapes and sizes and their good piezoelectric properties. These materials are also capable of working under desirable circumstances, such as low voltage and temperature up to 300 ^{o}C. Piezopolymers and composites are also used today as active elements in transducers, but to a lesser extent.

Figure 2.18 Piezoelectric ceramic element inside a cutten transducer.

The backing material influences the damping characteristics of a transducer. When the impedance of the backing material is similar to that of the active element, effective damping will be produced. Such a transducer will have a wider bandwidth and consequently a higher sensitivity. As the difference between the impedance of the active element and the backing material increases, a greater penetration but reduced sensitivity is achieved [24].

2.3.3. Transducer's Characteristics

In this section frequency and Signal-to-Noise Ratio will be examined, which are two very important characteristics of a transducer.

The noted frequency on a transducer is the central frequency and it depends among others on the backing material. The transducer though operates in a range of frequencies, the so called bandwidth. The highly damped transducers have to do with a wider range of frequencies and are accompanied by a high resolving power. The less damped transducers have a narrower field of frequencies and lead both to a lower resolving power and to a higher penetration capability. Low frequencies (0.5- 2.25 MHz) provide the examination with more energy and penetration, while high frequencies (15- 25 MHz) provide reduced penetration, but greater sensitivity to the detection of small discontinuities. In general transducer's frequency is considered proportional to the resolving power, the length of the near field (explained in 2.3.4 below), the attenuation and the noise. On the contrary, it is inversely proportional to the diameter of the beam and the penetration capability.

Another determinant factor for the characterisation of a transducer is the signal-to-noise ratio. The signal-to-noise ratio is a measure of how the signal from the defect compares to other background reflections, which are categorized as noise. The following formula relates some variables with this ratio:

$$\frac{S}{N} = \sqrt{\frac{16}{\rho \cdot v \cdot w_x \cdot w_y \cdot \Delta t}} \cdot \frac{A_{flaw}}{FOM}$$

Eqn. 2.13

ρ: density of material
v: sound speed in material
$w_{x,\,y}$: lateral beam width at flaw depth
Δt: pulse duration
A_{flaw}: flaw scattering amplitude at centre frequency
FOM: noise amplitude at centre frequency (FOM)

The minimum value of the ratio is 3. In general, it is proportional to the flaw size and the frequency and inversely relative to the beam width, the duration of the pulse, the density of the material and the velocity of the sound in the specific material. Signal-to-noise ratio is one of the main criteria, according to which not only the choice of a transducer, but also the evaluation of it is made [24][27][21].

2.3.4. Transmitted Beam

Since the inside of a transducer has been explained, now the beam that is generated will be examined. The generated beam is divided in the dead zone and two more fields, the near and the far field (Figure 2.19 [24]).

In dead zone it is not possible to detect defects. This is caused due to the lack of capability of the same probe to generate and at the same exact time receive signals. Therefore the initial pulse's width is considered to be the width of the dead zone. This problem can be overcome by using twin crystals, one transmitting and one receiving or by using a delay line, which means shifting the dead zone in an extra wedge on the transducer. Furthermore, high frequency transducers lead to shorter dead zone [19].

The near field is characterised by remarkable amplitude fluctuations, which are caused by the wave interference near the transducer. That leads to difficult evaluation of the flaws that are included in the near field. Near field's length is described through Eqn. 2.14.

$$N = \frac{a^2 \cdot f}{4 \cdot v}$$

Eqn. 2.14

α: radius of transducer
f: frequency of transducer
v: velocity in the material

After N length, which is presented in Figure 2.19 [24], far field exists. The amplitude is there more uniform, as it smoothly declines. The area right after the end of the near field is appropriate for optimal detection, because the amplitude is uniform and the strength maximum.

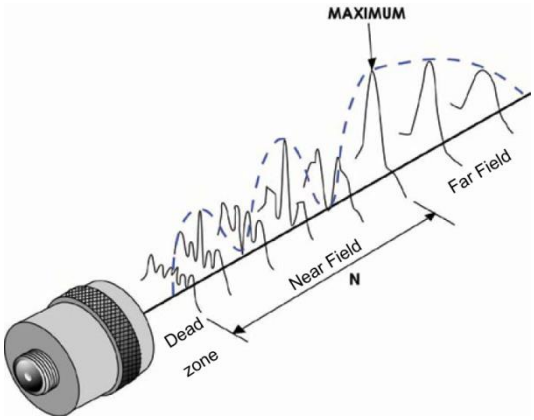

Figure 2.19 Near and far field amplitude formation.

Firstly the geometrical beam characteristics will be presented. The diameter, the length and the spread of the beam determine the geometry of it. The beam's shape is not a cylinder, it is a cone. The generation of a wave means energy transmission. The mechanical energy though is not always transmitted from molecule to molecule in alignment with the direction of the wave propagation. This variation in the direction of the energy transmission leads to the non-cylindrical shape of a cone. Beam spread is the angle that is formatted and is twice the beam divergence, as seen in Figure 2.20 [24] below.

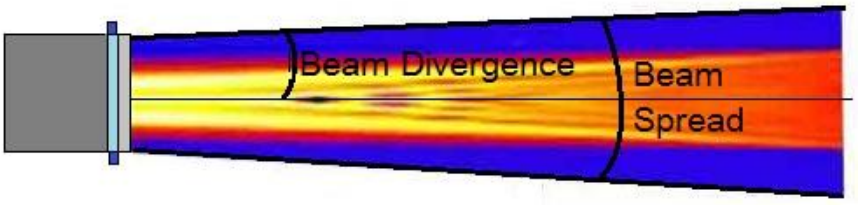

Figure 2.20 Beam spread.

Beam spread is low, when frequency and diameter are high. Big beam spread affects negatively the amplitude of the reflections received and consequently it complicates the signal interpretation. Beam divergence is expressed through this formula:

$$\sin\left(\frac{\theta}{2}\right)=\frac{0.514\cdot v}{2\cdot a\cdot f}$$

Eqn. 2.15

α: radius of transducer
f: frequency of transducer
v: velocity in the material

Secondly, three qualities of the beam will be discussed. These are resolution, sensitivity and attenuation. Resolution is the ability to separate two really close defects. Sensitivity is the ability to detect very small defects. Both are positively affected from high frequencies. Attenuation is caused because of the scattering and the absorption of the beam. When the beam is transmitted through an oblique angle, then at the interface it is reflected, refracted and converted into other wave types (e.g. shear). That is scattering. Absorption is the direct conversion of the mechanical energy into heat. High frequency leads to higher absorption.

Acoustic pressure's decrease, because of the attenuation, is described through Eqn. 2.16 [24][27][21].

$$P=P_{o} \cdot e^{-ad}$$

Eqn. 2.16

α: attenuation coefficient [dB/mm]
d: depth [mm]
P_o: initial acoustic pressure

2.3.5. Types of Transducers and Examination Methods

Two basic categories of ultrasonic transducers are contact and immersion. Contact transducers contain many subcategories, such as single element or duel element transducers, delay line transducers, angle beam transducers, normal incidence shear wave transducers etc. For the specific thesis single element contact transducers were used, as well as immersion transducers. Therefore, no further reference will be made for the rest types of transducers. Contact transducers are used for direct contact inspections, and are generally hand manipulated. Immersion transducers do not contact the component. These transducers are designed to operate in a liquid environment and all connections are watertight. Single element transducers, as seen in Figure 2.21 [28], contain one element both for transmitting and receiving the signal, while duel element transducers use one element for the transmission and another for the reception of the signal [24][28].

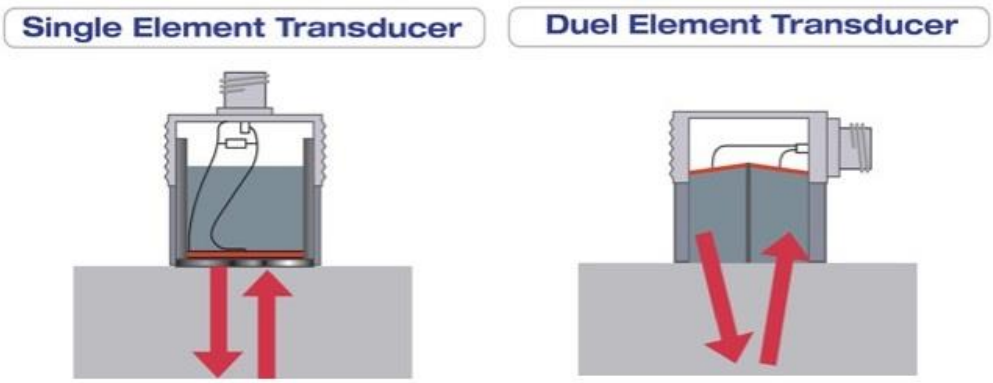

Figure 2.21 Single vs. duel element transducer.

There are various examination techniques, but in this case only pulse echo method was used. Pulse-echo ultrasonic measurements can determine the location of a discontinuity in a part or structure by accurately measuring the time required for a short ultrasonic pulse generated by a transducer to travel through a thickness of material, reflect from the back or the surface of a discontinuity, and be returned to the transducer. The two-way transit time measured is divided by two to account for the down-and-back travel path and multiplied by the velocity of sound in the test material. The result is expressed in the well-known relationship:

$$d = \frac{vt}{2} \text{ or } v = \frac{2d}{t}$$

Eqn. 2.17

, where d is the distance from the surface to the discontinuity in the test piece, v is the velocity of sound waves in the material, and t is the measured round-trip transit time. This method requires access only from one surface of the tested material. In Figure 2.22 an example of pulse echo method is presented on a calibration block, accompanied by the A-Scan illustration. A-Scan illustration is a method of presenting the information drawn from scanning and will be explained below.

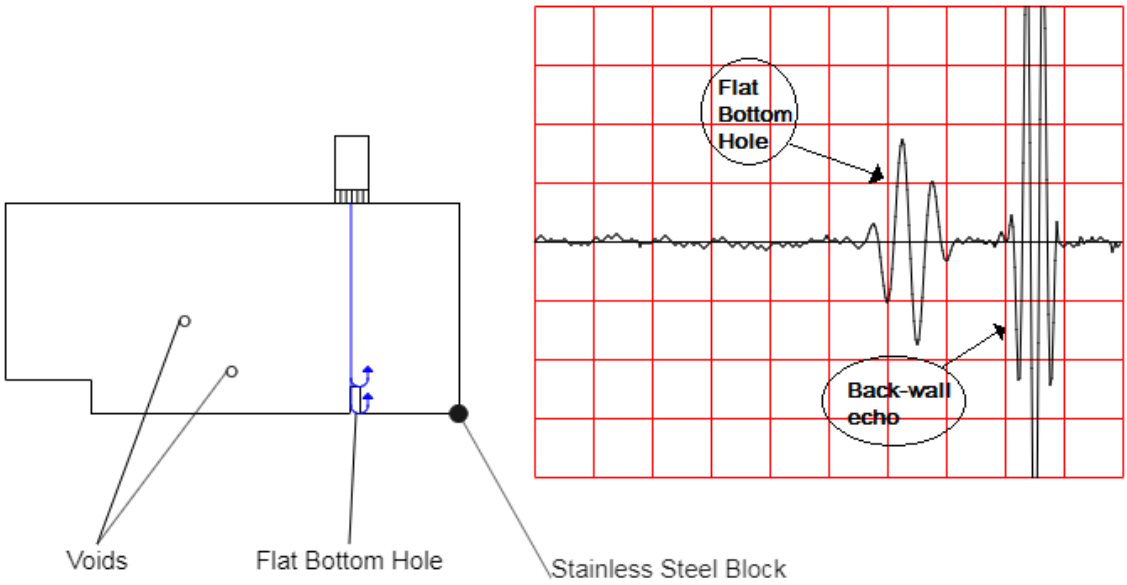

Figure 2.22 A-Scan illustration of an artificial defect on a stainless steel calibration block.

It is known that low frequencies serve high penetrability, while high frequencies provide better resolution. Therefore, thick materials with high acoustic attenuation and scattering should be examined with lower frequency probes. Thin, non-attenuating and non-scattering materials are advised to be examined with higher frequency transducers, in order to achieve better resolution. Composite materials belong to the first group of materials, where high penetrability is needed [24].

2.4. Inspection of a Specimen using Ultrasound

2.4.1. Testing Methods

Two basic testing methods will be mentioned. The first is pulse-echo technique, which is actually used in this thesis, and the second is through transmission technique.

Pulse-echo is a widely used non-destructive testing technique. A pulse of ultrasonic energy is transmitted into the specimen in a direction normal to the surface. The pulse is reflected from any interface of two materials back to the transducer. Figure 2.23 (a) [29]

shows a typical pulse-echo set-up. The signals which travel back towards the probe are detected and the position and size of a flaw is determined.

This method can be applied for the detection of a delamination, smaller flaws such as voids and foreign inclusions.

The pulse-echo technique advantages are that size and location (in the direction of the ultrasonic beam) of the defect can be defined. It can be used in cases, where access only from one side is possible. This is a particularly useful advantage as such testing situations often occur in practice.

This technique has also some disadvantages. There is a time period approximately equal to the pulse length, during which the probe cannot detect signals, because it is either emitting a pulse or reverberating. This is the dead zone. This problem can be limited by using a shorter pulse, immersion testing, a standoff probe, or employing a duel element probe. A similar problem occurs with defects very near to the front surface of the component. The solution here may be to increase the frequency and thereby shorten the pulse length, or scan from the opposite side of the specimen.

Through-transmission technique uses two transducers, one transmitting and one receiving. These two transducers have to be positioned opposite each other, having the component in between. It measures total attenuation within the material caused by features that attenuate the beam. Comparisons can be made of the attenuation between different specimens and between different regions of the same specimen.

Through-transmission testing (Figure 2.23 (b)) is used to detect delamination, porosity, some inclusions, fiber volume fraction changes and displaced fibers. Cracks can also be detected but, as with pulse-echo, their alignment should not be parallel with the beam direction.

Compared with pulse echo there is no 'dead zone' which means that flaws can be detected at all depths throughout the thickness of the specimen at the measurement location.

One disadvantage of through-transmission is that it does not provide any information about flaw depth. Furthermore, the transmitter and detector must be kept well aligned making the inspection of contoured surfaces very difficult. Also, it requires access from both sides and this may not be possible [29].

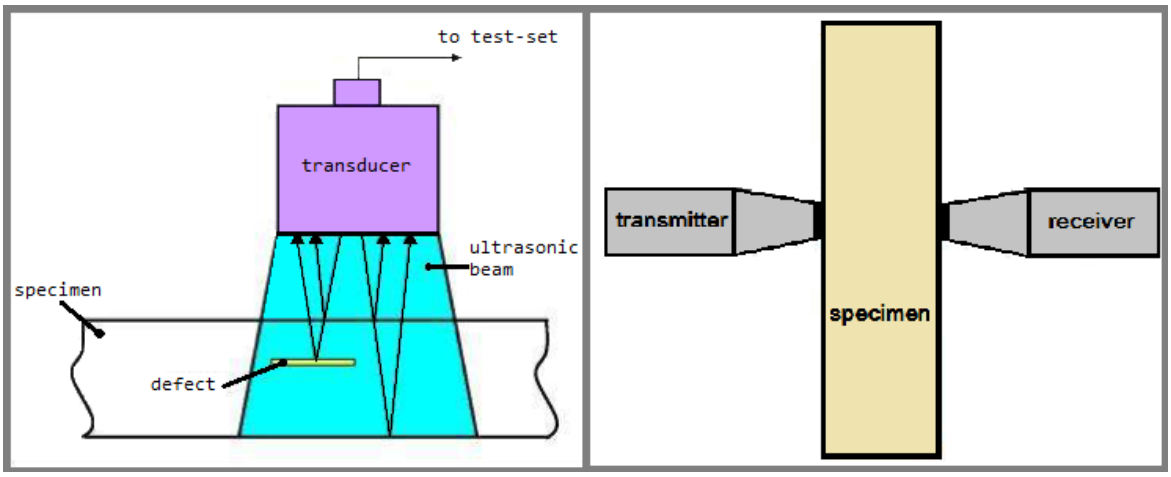

Figure 2.23 (a)Pulse-echo technique (b) Through Transmission technique.

2.4.2. Data Presentation Methods

For ultrasonic inspection there are three data presentation methods. These are amplitude scan (A-Scan), brightness scan (B-Scan) and contrast scan (C-Scan). This thesis dealt only with A-Scan and C-Scan.

The A-scan method is the most widely used and appears on portable control set ups. Automated dipping controls enable the user to use all three imaging modes depending on the desired information.

More specifically, A-Scan describes the information through two axes. One axis (X-axis) is time, where zero is the moment that the initial pulse was transmitted, but it can be set wherever the user decides, e.g. at the front surface of the component. This axis shows the period of time that the pulse needed to return to the transducer, because of an interface, a defect, a back-wall echo etc. The second axis (Y-axis) shows the relative amount of energy received, meaning the amplitude of the pulse. In the A-scan presentation, relative discontinuity size can be estimated by comparing the signal amplitude obtained from an unknown reflector to that from a known reflector. Reflector depth can be determined by the position of the signal on the horizontal axis. Other techniques of sizing also exist, but are not in the field of interests of this thesis. Figure 2.24 [30] relates a real component that has a reflector with its A-Scan illustration. Gate is the blue line in Figure 2.25 [31] and is also useful for B and C-Scan. As seen in Figure 2.25 a gate can be adjusted at the amplitude height and moment that information has to be extracted.

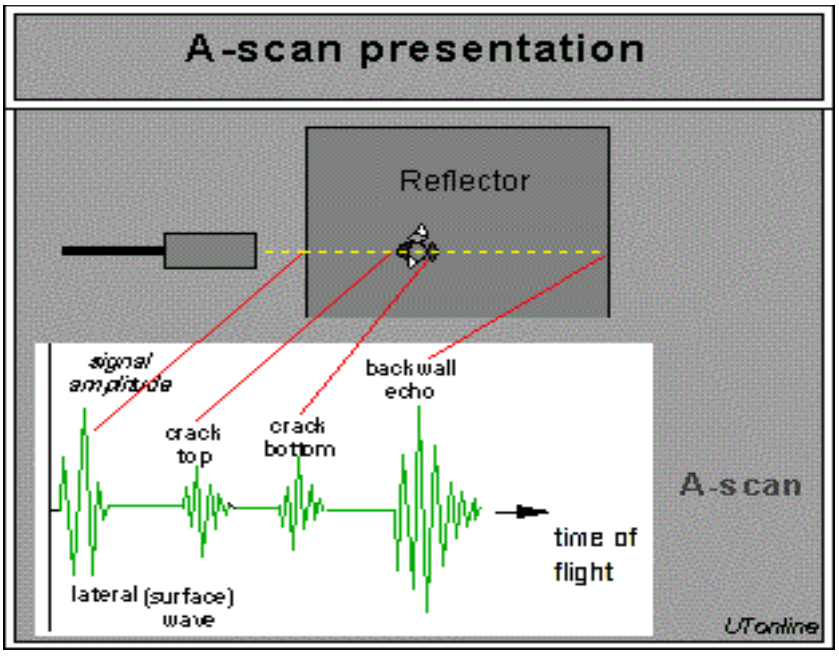

Figure 2.24 A-Scan explanation of signals.

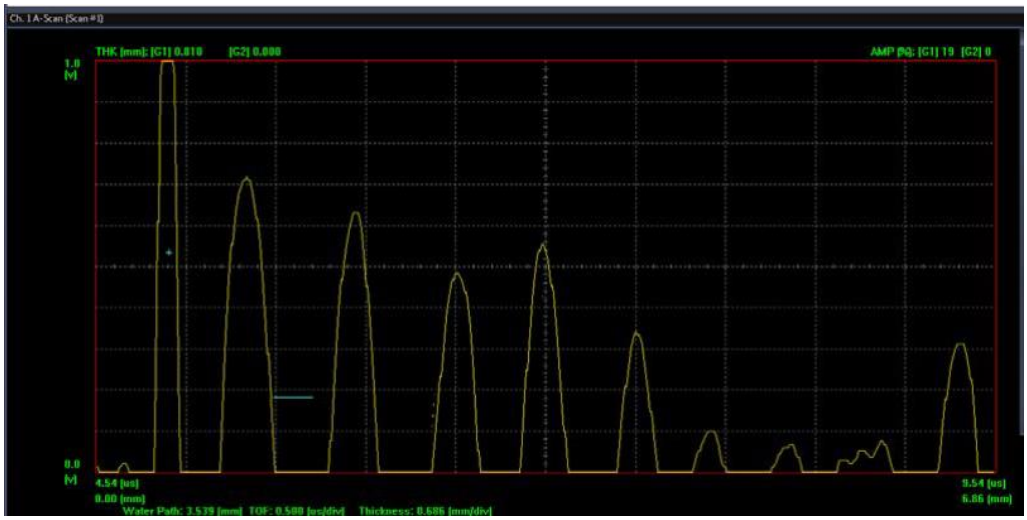

Figure 2.25 A-Scan presentation example.

In case of an echo of a reflector, the position of which is already known, it is possible to determine the velocity of the material. In setups that contain other presentation methods as well, the A-scan is the basis for adjusting the various parameters to extract the B-scan and C-scan images [24].

Brightness scan (B-Scan) illustrates a horizontal section of the specimen and the position of the defect on the scan direction and on the direction of the depth. Figure 2.26 [31] illustrates a real component that has A, B and C reflectors and the corresponding B-Scan presentation. Gates, which are set at the A-Scan setup at a specific “height” (amplitude), determine the lower limit of the signals’ amplitude that can be illustrated. Any echo with lower amplitude is not illustrated, while every echo with higher amplitude is creating a new point on the illustration [31].

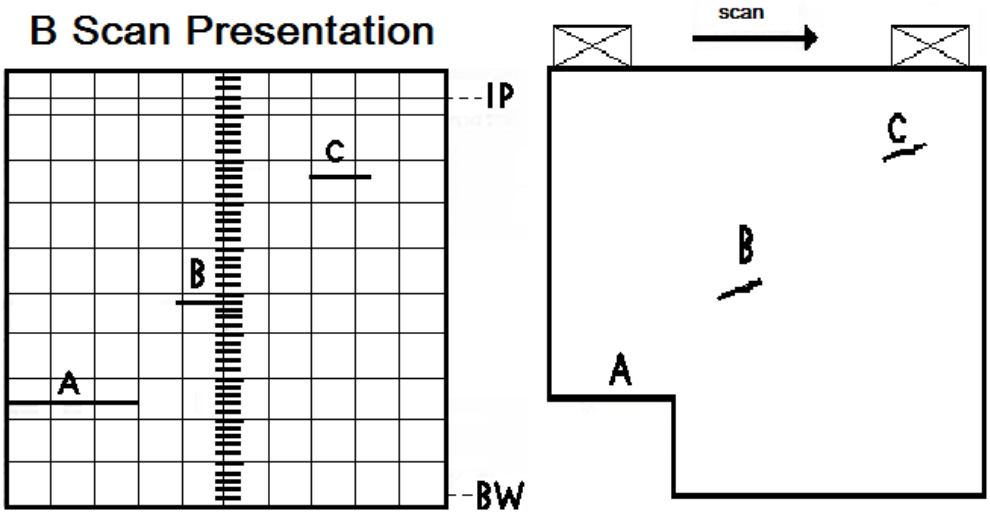

Figure 2.26 B-Scan presentation example.

During C-Scan the transducer scans the surface of the component and illustrates for each position the higher amplitude received and the depth that corresponds to that amplitude. In this case as well, gates determine the lower limit of the signal’s amplitude that is taken under

consideration from the setup. The route of the transducer is the one seen in Figure 2.27 and is defined from the user in more detail.

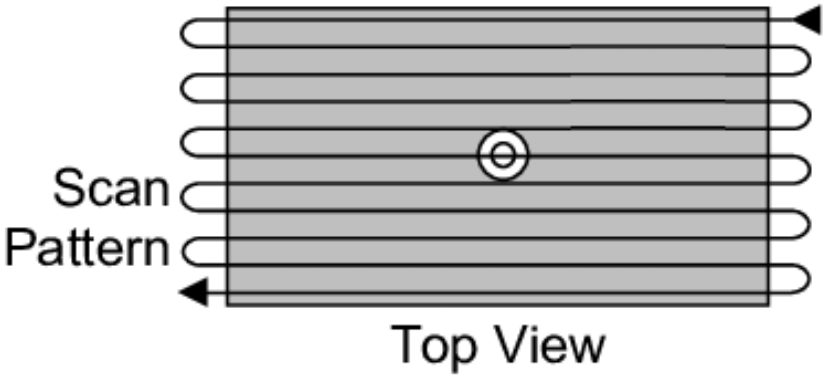

Figure 2.27 Transducer's route during C-Scan.

The produced C-Scan illustration conveys the above mentioned information with color scaling, as seen in Figure 2.28 [31].

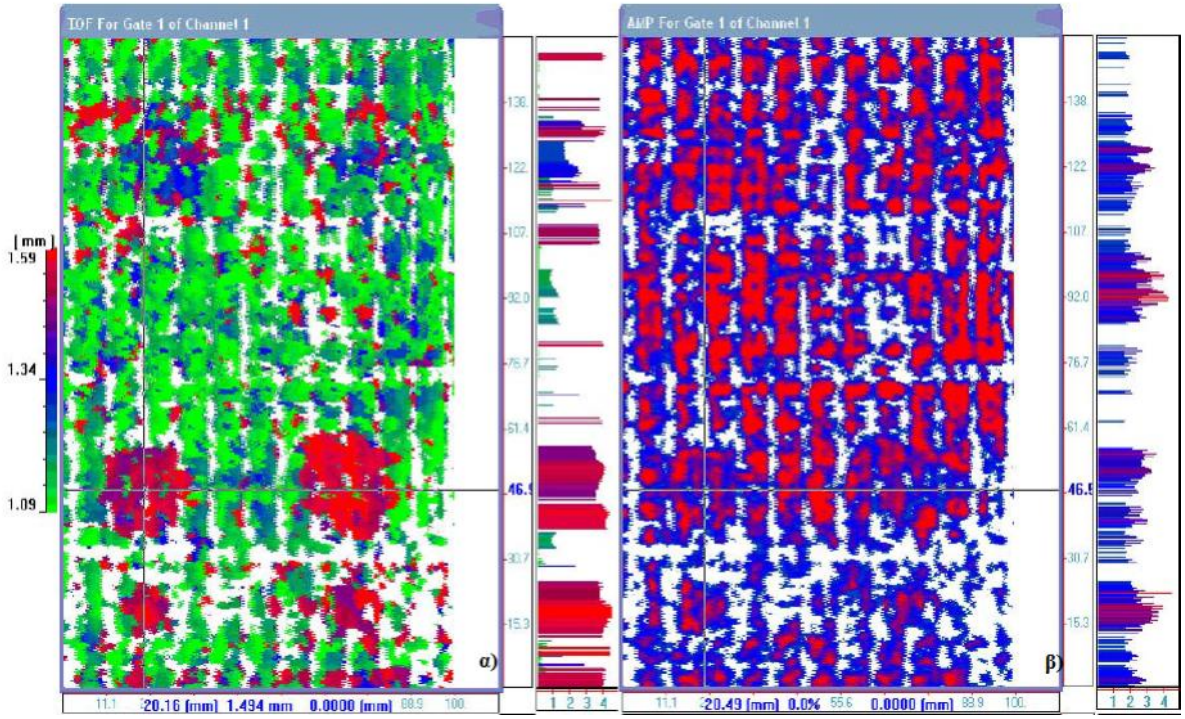

Figure 2.28 C-Scan presentation example.

At this point it is useful to mention DAC method. It was used during the experimental procedure of this thesis and is a method of compensating for the fact that the pulse-echo response of a reflector will decrease as the distance of the reflector from the ultrasonic probe increases. This occurs because of the attenuation of the transmitted energy as it travels from the probe to the reflector and so the further the reflector is from the probe, the lower the energy of the sound that actually hits the reflector is. Similarly, the further the reflected pulse has to travel, the lower is the energy that is received back at the probe.

The DAC is generated by plotting the amplitude of a known calibration reflector at different distances from the probe. The DAC is generated by plotting a curve through these amplitudes. As seen in Figure 2.29 [32], by plotting the amplitudes received from the reflector D for positions A, B and C of the transducer, DAC is produced. Using this curve, gain is corrected according to the time [32].

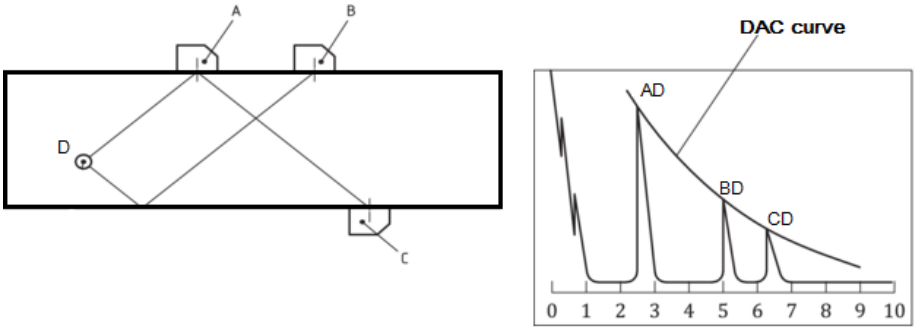

Figure 2.29 DAC explanation.

2.4.3. Parameters' meaning

During ultrasonic testing specific parameters should be defined. An example of a software's required parameters is shown in Figure 2.30.

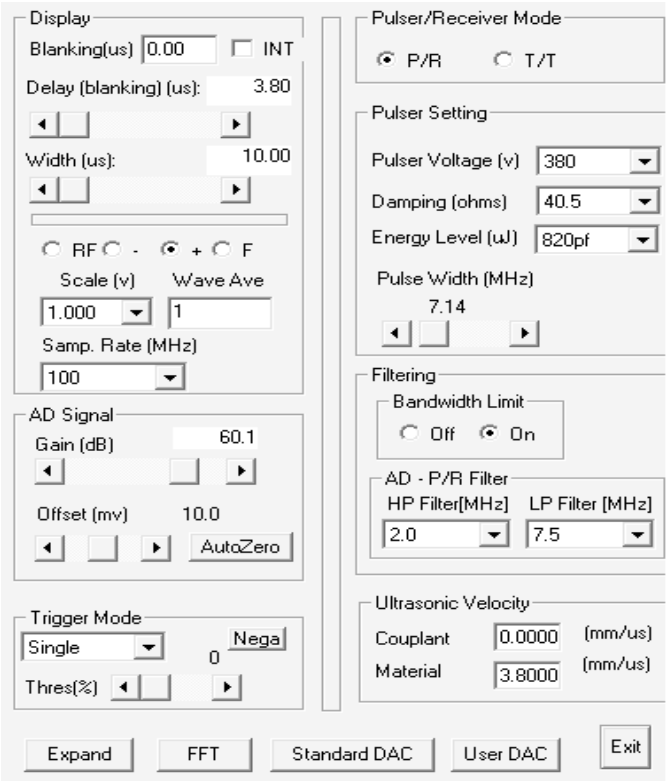

Figure 2.30 Window with parameters.

In this section the meaning of most of them will be analyzed. To start with, at the 'Display' section Delay and Width had to be defined. Delay expresses the time that is chosen as the start of the screen. All the information before are being hidden from the user. Width

expresses the length of the screen, meaning the duration of the time period being examined. Both of them are measured in μs. At the 'AD Signal' section two crucial parameters should be defined. Gain allows the amplification of the signal. The equation that relates Gain (dB) with signal height is Eqn. 2.18 [33]. Ratio H_1 to H_2 expresses the ratio of the new height of the signal after amplification to the old one.

$$dB=20*\log_{10}\frac{H_1}{H_2}$$

Eqn. 2.18

Offset is measured in mV and defines the lower limit of Voltage for the signals that are illustrated. Signals of lower Voltage are being ignored and that leads to absence of "noise" [31]. Gain and Offset are useful for the easy and efficient understanding of the screen's information from the operator. Trigger mode should also be defined. The options are threshold, external, single, auto and positional. Throughout this Thesis Pulser/ Receiver (P/R) Mode was used. 'Pulser Settings' are of great importance. Increase in Pulser Voltage leads to maximization of the penetration ability of the ultrasonic wave and decrease leads to better near surface resolution. Damping setting is obviously a resistance, as it is measured in Ohms. The damping control selects a resistor that modifies the shape of the outgoing waveform. Lower damping resistance increases pulse damping and improves near surface resolution, while higher damping resistance reduces damping and improves penetration. Frequency Filters, named HP/ LP Filter, can often improve signal-to-noise ratio or near surface resolution by filtering out unwanted high or low frequency components of the signal. It is obvious that in 'Ultrasonic Velocity' Settings the sound velocity in the material should be inserted. If the period of time that sound travels through the couplant is ignored through the Delay parameter, then couplant velocity does not need to be inserted [34].

3. LITERATURE REVIEW

3.1. Comparison of Ultrasonic Testing between Metals and Composites

Many differences occur during an ultrasonic examination of a metal and a composite specimen. Firstly, the acoustic impedance of these materials is different. As seen in Table 3.1 [35][36], where some materials' impedances are shown, metals present greater value in contrast to carbon or glass. Resin's acoustic impedance could be estimated from 2.77 to 3.6 $\frac{10^5*gr}{cm^2s}$ [22]. Therefore, the total acoustic impedance of a glass or carbon composite material would be lower than the acoustic impedance of a metal.

Table 3.1 Acoustic impedance of various materials.

Material	Acoustic Impedance ($\frac{10^5*gr}{cm^2s}$)
Aluminum	17.10
Stainless Steel	44.8
Steel	46.5
Carbon	13.33
Glass	14.5
Teflon	2.97
Resin	3.2

Another characteristic of materials is attenuation. Composite materials absorb ultrasound quicker than metals, something that means greater attenuation of the wave [37]. When it comes to composites, hand-layup method gives even more attenuating products than fabrication method. Fabrication methods result in low porosity in the product, while hand-layup method ends to enwrap air between the layers. That makes them more attenuating [38].

The greater attenuation of sound in composite materials requires special high penetration pulser/ receivers and lower frequencies in comparison to metals. For the examination of steel components transducers of frequency between 1 MHz and 5 MHz are preferred. Suited frequencies for composite material examination are considered to be between 0.25 MHz and 2.25 MHz. However, the use of low frequency transducers decreases resolution [37][38].

Composites generally allow poorer flaw resolution than microscopically homogenous materials because of the greater contribution of noise from fibers' or particles' boundaries (although large-grained metals present a similar problem) [39]. According to Bergant these high noise levels of course limit the detection accuracy. Reflected pulses in composites have more complex waveforms and less time separation between the reflected pulses than in the case for steel. Therefore multiple echoes cannot reliably be used in signal interpretation [38].

As mentioned before, each material is accompanied by a specific speed of sound. Sound typically travels faster in metals that in composite materials. More particularly, speed of sound in GRP varies from 2 to 4 mm/μs, carbon fiber reinforced plastic varies from 3 to 4 mm/μs and differ from that of steel, which is around 6mm/μs [38][41]. Time-of-flight is the time that sound propagates inside a material and is useful for the calculation of the depth of

the scatterer responsible for any echo. Time-of-flight measurements are of less interest for composites than for metals since it is usually sufficient to merely identify the presence of a defect. However, if this method is used to estimate how deep a particular defect is, the user should be aware that the sound velocity may vary locally within the laminate based on fiber content and orientation [38]. The longitudinal wave velocity increases almost linearly with an increase of the fiber content, as seen in Figure 3.1, where a specimen consisted of glass woven fabrics is examined [42]. These are important to remember when calibrating equipment or when comparing ultrasonically and physically measured thicknesses.

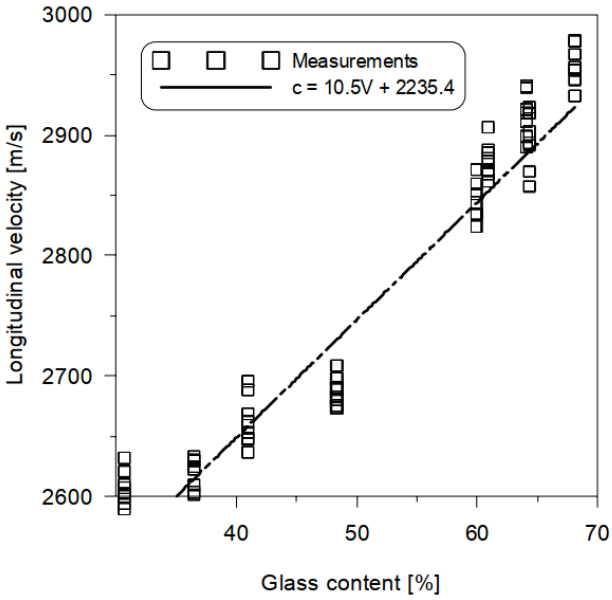

Figure 3.1 Relationship between the ultrasonic wave velocity and the glass content.

Calibration blocks are typically required before the examination of any specimen. These blocks should be manufactured with the exact method and the materials used for the specimen. For metals ready to use calibration blocks can be bought, but for composite materials each specimen requires a unique calibration block to be manufactured [38]. Inspection procedure differs between metals and composites in other areas as well. Through Transmission (T/T) inspection method is preferred for composites, while Pulse Echo (P/E) method is preferred for metals. For high-attenuating materials, such as composites, T/T method allows to save some wave energy by avoiding the extra attenuation caused of the travelling time from the defect back to the receiver [43]. Some composite materials also absorb moisture and therefore any technique that involves substantial wetting of the surface should be avoided where possible. This is a risk that examination of metals does not entail [39].

A fact of interest is that, while very detailed specifications regarding the case of ultrasonic inspection of metals exist, no official specifications for inspection requirements for composites are published. This makes clear the multiparametric and volatile circumstances under which ultrasonic inspection in composites is being performed.

3.2. Comparison of Ultrasonic Testing between Cylindrical and Flat Surfaces

Curved surfaces are more complex to inspect with the ultrasonic technique. Firstly, the size of the transducer should be reduced, in order to achieve as much contact with the surface as possible. In order for better contact to be achieved special transducers exist as well, such as the ones with the spring loaded swivelling head. As seen in Figure 3.2, the transducer follows with good precision the path of the specimen's surface. A system with an immersion transducer would definitely provide good results as well. In this case, the orientation of the transducer must be controlled with a high degree of precision in order to adequately follow the part contour and maintain probe orientation, as seen in Figure 3.3 [44]. It is also logical that coupling efficiency is reduced, as the coupling medium may not totally connect the transducer with the specimen's surface. Therefore, immersion systems are ideal in order to achieve good coupling [37].

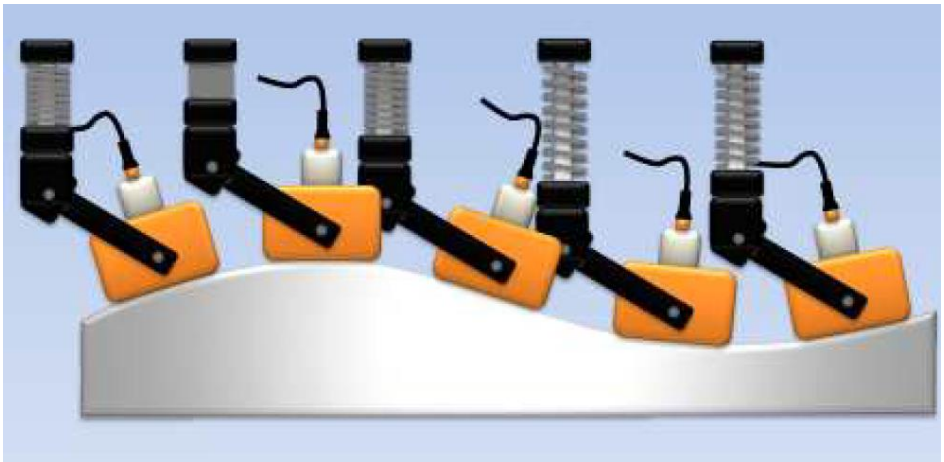

Figure 3.2 Spring loaded swivelling head.

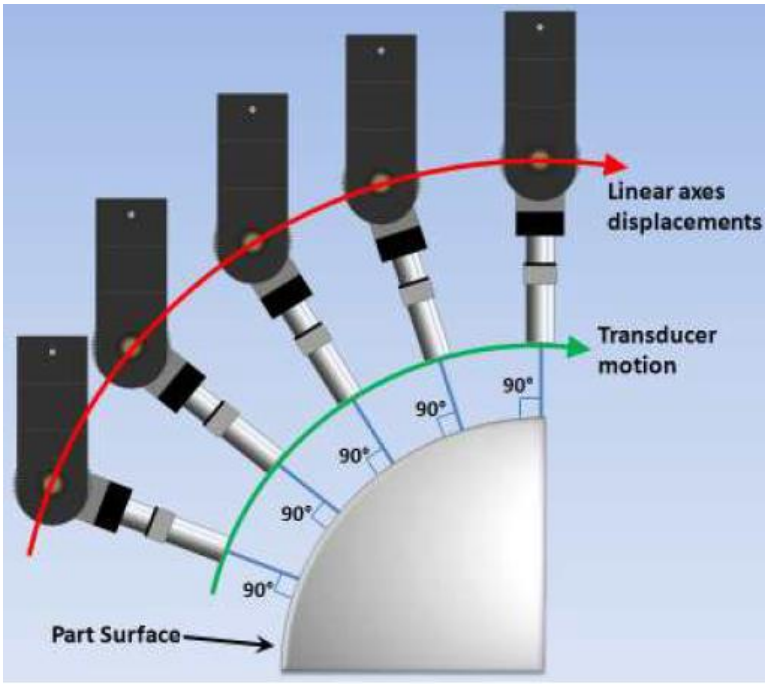

Figure 3.3 Immersion system with constant water path and beam entry angle.

It is possible to inspect a specimen by scanning it with the use of a turntable or by scanning a rectangular area. Cylindrical specimens can be examined with both techniques, while flat ones only with the second one [44]. An advanced immersion system for ultrasonic inspection, which contains a turntable, is shown in Figure 3.4 [45].

Figure 3.4 Immersion tank with a turntable.

According to ASTM, Pulse Echo Twin-Probe Method provides better results for specimens with curved surfaces, as the first back-wall echo is more representative of depth or time than a later back echo [43].

During ultrasonic inspection, specimen curvature has a significant effect on both the ultrasonic response and the scanning resolution requirements. When an ultrasonic beam is entering the specimen sound velocity changes. Waves are being refracted and the ultrasonic beam directivity and amplitude pattern can be affected in different ways. Concave surface tends to focus the ultrasonic beam as it enters the material surface, while convex has the opposite effect. In Figure 3.5 all the possible cases are illustrated. A concave surface is

practically the inner surface of the cylinder, while convex is the outer surface of the cylinder. In general, it is preferred for the inspection to get a focused beam rather than a spread one. Therefore, examination of a cylinder from the inside would be ideal, but geometrical limitations and difficulties could occur [44].

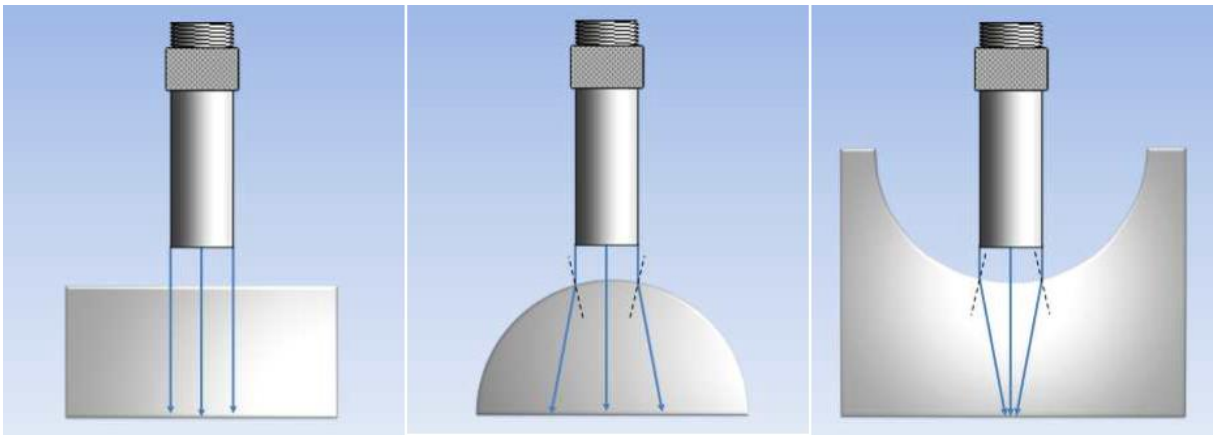

Figure 3.5 Illustration of the beam pattern modifications caused by wave refraction for a flat, convex and concave surface.

Using a calibration block (Figure 3.6) to test the detection abilities of a transducer according to the surface curvature, specific conclusions are reached. The dotted lines of the figure indicate transitions between different curvatures. The rectangles on top represent the unwrapped surfaces. Individual groups of five identical side-drilled holes (SDH) were machined at the same depths below each surface type. In Figure 3.7 peaks identified in red represent the SDH that is closest to the surface. Peaks identified in blue represent the second shallowest set of SDH. Red and blue dotted lines represent the expected echo amplitude of these SDH referred to the areas 1 and 2 (both flat). Peaks identified by a circle correspond to SDH in flat areas, while square are for convex and concave areas. As seen in the figure, concave surfaces lead to better resolution for deeper defects, while convex surfaces do not allow the detection of them [44].

It is common that flat composite specimens are layered, while cylindrical are filament wound. Ultrasonic inspection of these two cases has differences. The distance of each layer from the external surface for a flat specimen is specific and has less margin of error than a wound one. In a filament wound specimen a specific layer is not at the same distance from the external surface for every point of the surface, due to the construction method. A specific and stable definition of the depth of the intermediate layers is very useful for the detection of defects in a composite material.

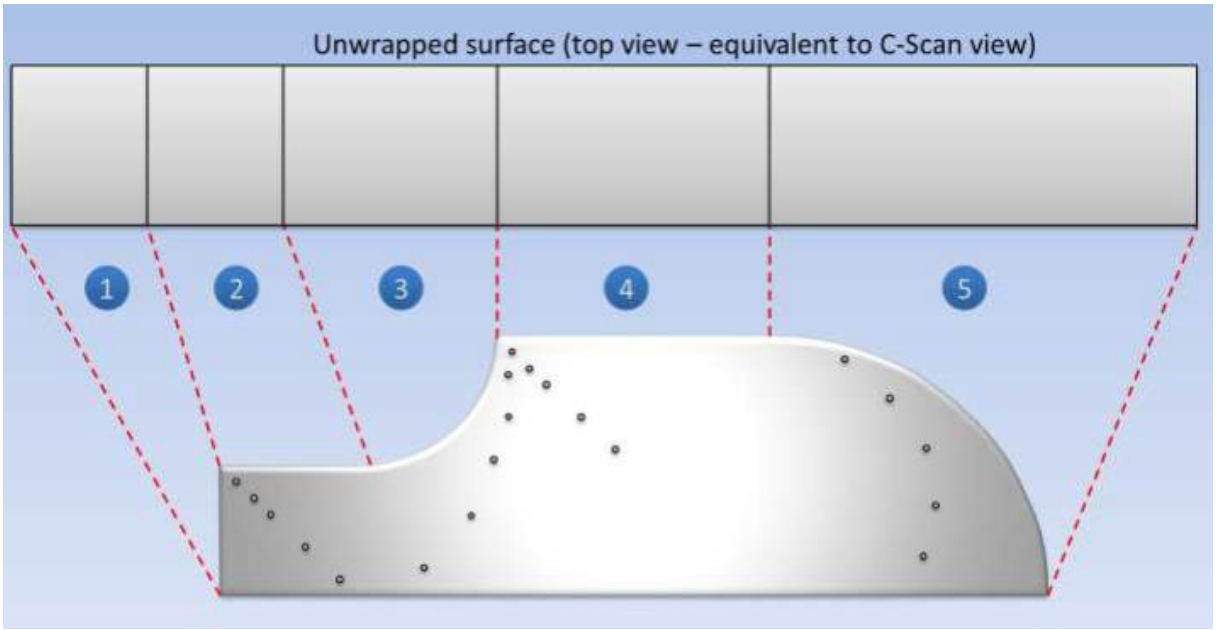

Figure 3.6 Calibration curvature block.

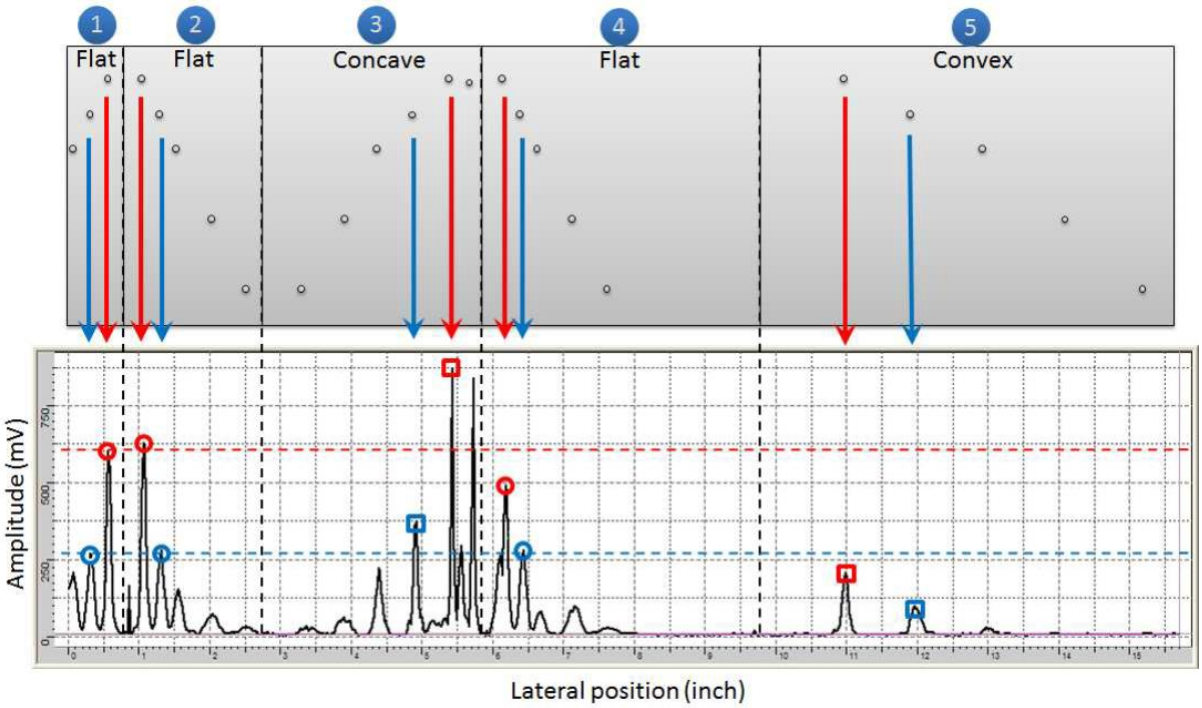

Figure 3.7 Lateral plot of the amplitude of the C-Scan across the surface of the block (bottom) compared to the position of the SDH and the different curvatures (top).

4. EXPERIMENTAL PROCEDURE

Before the examination of the cylinder, it was important to get to know the equipment and practice ultrasonic testing. A weld and three composite specimens from the diploma thesis of Mr. Themelakis were examined with A-Scan for this cause. The procedure is not directly related to this thesis and therefore will be presented in Appendix A.

In order to proceed to scanning the specimen of this thesis interest, it was necessary that the specimen was properly prepared. After the preparation of the specimen, the choice of the appropriate ultrasonic transducers was made. Namely, for A-Scan the probes of 2.25 MHz and 5 MHz and for C-Scan the probes of 2.25 MHz and 3.5 MHz were chosen. Then the parameters were adjusted and A-Scan took place. This step led to results, but not for all the defects. Afterwards, the procedure continued with C-Scan, which led to confirmation of the A-Scan results and to results for the defects that were not originally detected with A-scan.

4.1. Specimen's Description

The specimen studied in this thesis is a cylinder from carbon fibers wound at +/-55^{o} and epoxy resin. The manufacturing method of the cylinder is filament winding.

For the experimental procedure to begin, it was necessary to create a visual system on the CFRP cylinder, which would allow the specification of the defects' theoretical positions. Therefore, all the angles that represented defects, as well as the longitudinal positions of the defects were illustrated on the cylinder. The result is obvious in Figure 4.1. Therefore, each defect has its own coordinates, according to the angular position (φ), the longitudinal position (L) and the depth (d). These coordinates will be presented throughout the text with the following order No (φ, L, d), for example defect's No.2 coordinates are 2(200, 50mm, 14.5mm), see Table 4.1.

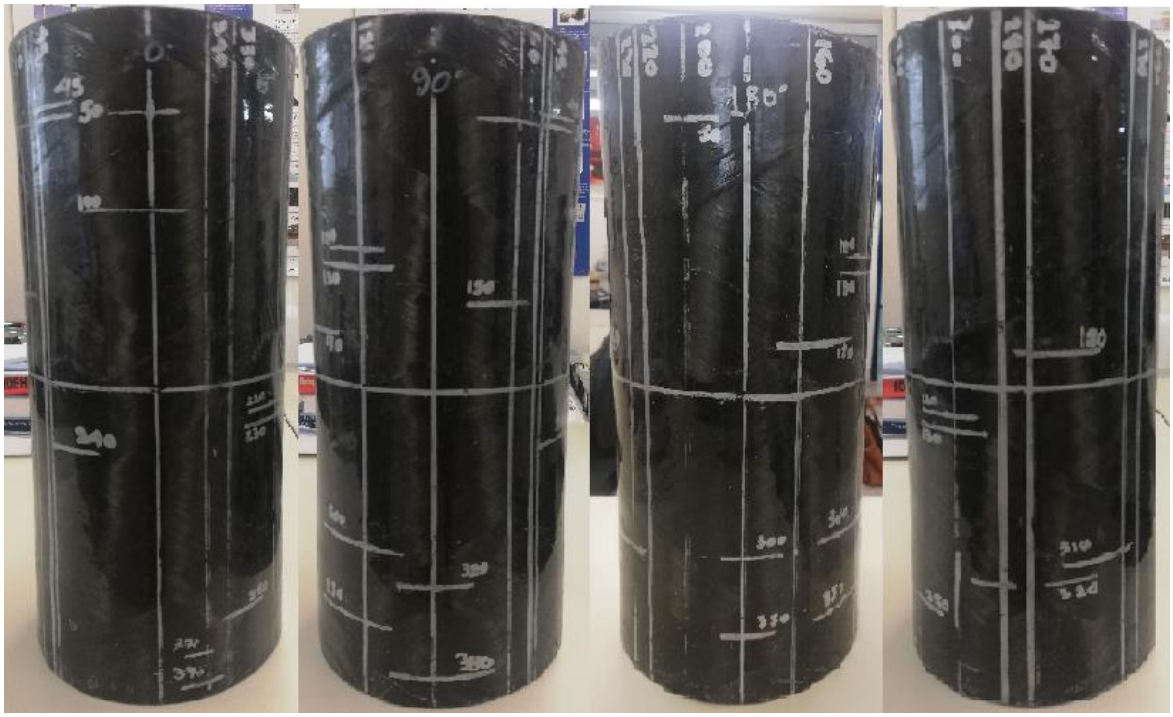

Figure 4.1 Cylinder's angles.

The geometrical characteristics of the cylinder are illustrated in Figure 4.2. Namely, the length is 400 mm, the external diameter is 182 mm and the internal one is 149.5 mm, which equals to nominal thickness of 16.25mm [46].

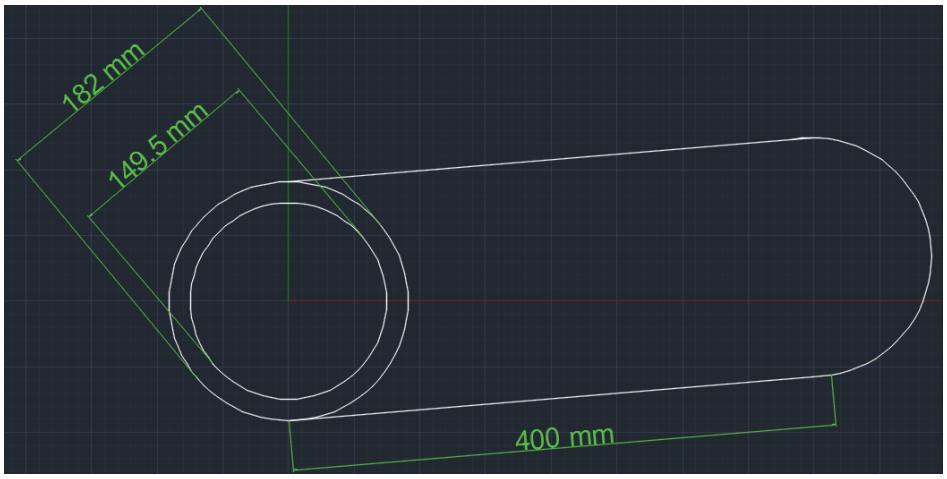

Figure 4.2 Cylinder's geometry.

The final positions of the defects are stated from the B&T Composites Company and are very close to the positions ordered from the laboratory [47]. In total there are 30 defects throughout the cylinder. Six of them were not taken under consideration, as their diameter was very small and equal to 0.2 mm. These defects are highlighted with yellow color in Table 4.1 and, from this point on, they will be considered as non-existed. There are three layers of defects, which correspond to three different depths, 14.2 mm, 9.25 mm and 4 mm, respectively, measured from the external surface. Each layer contains eight defects, approximately 0.1 mm thick, from Teflon. Some of them are thicker, namely 2mm thick, as seen in Table 4.1. The position of each defect is determined from a layer, a longitudinal position and an angle. The radiuses of the Teflon defects vary among 10 mm, 20 mm, 30 mm and 40 mm. In more detail, this information is contained in Table 4.1. An exploded view of each layer is also illustrated in Figure 4.3 for better understanding.

Table 4.1 Defects' position with new numbering
[code= Layer(1,2,3),Color(Green, Cyan, Magenda, Pink), Number(01-24)].

No	Lx (mm)	φ (°)	color	defect code	defect diameter
1	50	50	green	1G01	1cm
2	50	200	magenda	1M02	2cm
3	170	160	pink	1P03	4cmx 2 thickness
4	180	270	cyan	1C04	3cm
5	240	45	magenda	1M05	2cm
6	320	280	pink	1P06	4cm
7	320	90	cyan	1C07	3cmx 2 thickness
8	390	340	green	1G08	1cm
-	50	0	yelow	1Y09	0.2mm
-	350	180	yelow	1Y10	0.2mm
9	45	50	pink	2P11	4cm
10	180	270	green	2G12	1cmx2 thickness
11	50	60	cyan	2C13	3cm
12	220	300	magenda	2M14	2cmx 2 thickness
13	120	120	green	2G15	1cm
14	310	230	cyan	2C16	3cm
15	130	120	magenda	2M17	2cm
16	350	330	pink	2P18	4cm
-	200	0	yelow	2Y19	0.2mm
-	350	120	yelow	2Y20	0.2mm
17	40	85	green	3G21	1cmx 2 thickness
18	50	200	pink	3P22	4cmx 2 thickness
19	150	60	magenda	3M23	2cm
20	200	220	green	3G24	1cmx 2 thickness
21	300	120	cyan	3C25	3cmx 2 thickness
22	230	300	cyan	3C26	3cm
23	380	90	pink	3P27	4cm
24	370	340	magenda	3M28	2cmx 2 thickness
-	100	0	yelow	3Y29	0.2mm
-	300	180	yelow	3Y30	0.2mm
	variation + - 2%				

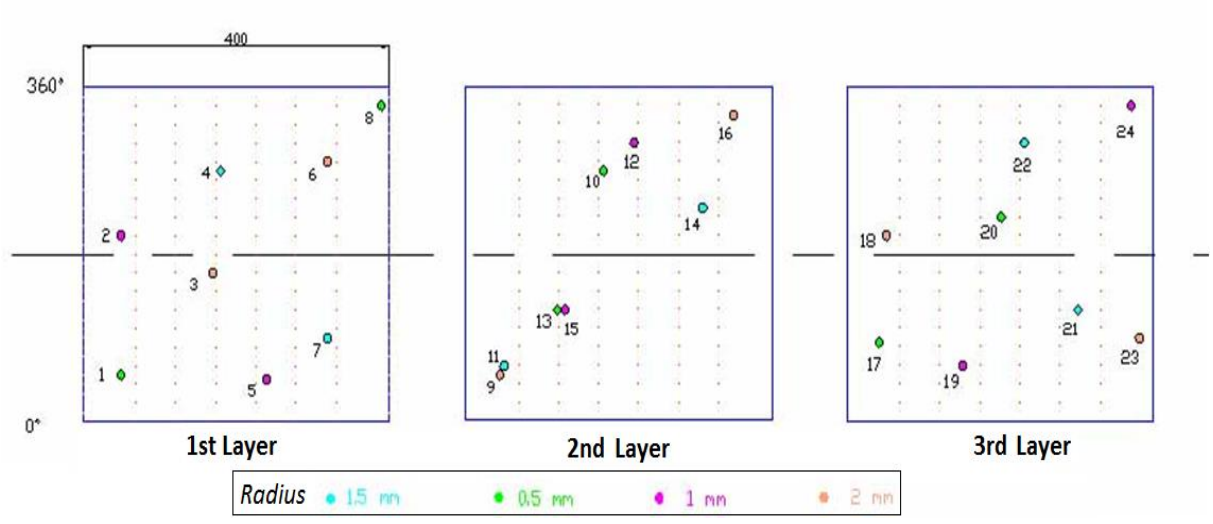

Figure 4.3 Cylinder's defects extended view.

It is important to be mentioned, that this information comes from the manufacturing company and has not been amended on quality control. Therefore, it is possible that this description of the cylinder does not accurately reflect the reality.

4.2. Choice of Ultrasonic Transducers and Velocity Approximation

For the choice of the transducer's frequency some parameters had to be taken under consideration. First, the choice was made according to the availability of the laboratory's transducers. Secondly, ASTM Standards were taken under consideration. According to them, for many fiber- reinforced composites, probe pairs with center frequencies ranging from 0.5 to 5 MHz prove useful, as for example pairs of 2.25 MHz damped probes [48]. Low frequencies serve good penetration, which is necessary for composite materials. In addition to the above, several trials took place in the laboratory in order to decide which probes will be used. Taking all the above under consideration Olympus microscan transducers of 2.25 MHz (Nominal Element size: 0.5 in., Part No: M1036) and 5 MHz (Nominal Element size: 0.5 in., Part No: M109-SM) were chosen for the A-Scan and immersion transducers of 2.25 MHz (Nominal Element size: 0.5 in., Part No: V306-SU) and 3.5 MHz (Nominal Element size: 0.5 in., Part No: V382-SU) were chosen for the C- Scan process. In Table 4.2 the transducers used are cumulatively shown. From Figure 4.4 to Figure 4.7 below the used transducers according to the above mentioned order are shown. Near field does interfere with the echoes of the inside of the material, but it was not possible to get a smaller value, as the available transducers had neither a smaller diameter nor a lower frequency.

Table 4.2 Transducers used.

		A-Scan		C-Scan	
	Olympus	M1036	M109-SM	V306-SU	V382-SU
Frequency	f (MHz)	2.25	5	2.25	3.5
Nominal Diameter	d (in)	0.5	0.5	0.5	0.5
Near Field Length	N (mm)	23.9	53.1	60.6	94.3

Figure 4.4 Microscan transducer M1036, 2.25 MHz.

Figure 4.5 Microscan transducer M109-SM, 5 MHz.

Figure 4.6 Immersion transducer V306-SU, 2.25 MHz.

Figure 4.7 Immersion transducer V382-SU, 3.5 MHz.

Due to lack of a calibration block, velocity approximation had to be done on the specimen itself. Using the thickness of the specimen was considered a less reliable option than using the position of the defects for the calculation of the velocity. Defects find place in various depths. That leads to increased reliability of the final velocity approach. Furthermore, at this initial stage of the process, it was far from easy to distinguish the back – wall echo with certainty. Using the trial and error method, velocity was estimated to be 3.8 mm/μs. The attempts were considered to be successful, when specific defects could be detected at their theoretical position. An initial approach was 3.45 mm/μs according to literature [49]. Defects No.1(50, 50, **14.2**), 16(330, 350, **9.25**), 21(120, 300, **4**) and 23(90, 380, **4**) were used as scatterers. The depth calculated using velocity equal to 3.45 mm/μs was not close to the nominal depth. After each measurement the velocity that would give the correct depth was estimated and was used for the next measurement. The process ended, because the velocity approach of 3.8 mm/μs gave satisfying results for all the defects.

4.3. Experimental Setup and Parameters

The ULTRAPAC II device is installed at the Laboratory of Marine Engineering. It is an automated, high-resolution ultrasound system that enables the materials to be examined, both by contact and by immersion, using one of the two basic test methods, either pulse echo or through transmission. The results are presented in real time by a personal computer with the A-scan, B-scan and C-scan illustrations. The ULTRAPAC II device consists of the following parts:

Immersion tank made of Plexiglas accompanied by an adapted carriage for moving the piezoelectric transducer as shown in Figure 4.8 [50]. The carriage consists of two horizontal arms that allow the transducer to move in two directions. On this system, a perpendicular to the other two arm is also attached, at the end of which the transducer is placed. This way the vertical movement of the probe is achieved. The arm is driven by electric motors, but there is also the possibility of manual movement.

The computer includes the AD-IPR-1210 excitation and analog-to-digital signal conversion card and the PAC-SMC4 transducer-drive servo control unit. The AD-IPR-1210 card is a 12 bit analog to digital signal conversion device with a pulser-receiver card integrated. The AD-IPR-1210 card is adjusted to the PC motherboard on a PCI port. It provides the ability to transmit pulses of 300-400 Volts with duration of less than 10 nsec, which adjusts their pulse repetition rate, energy and other characteristics. The signal reception section provides various settings, such as the frequency range of the received signals, between 0.5-30 MHz, amplification from -20 to 80 dB and the use of high pass-low pass filters. The PAC-SMC4 card controls the movement of the arms, which can move at a speed that can reach 20 in/sec (500 mm/sec) with a step of 0.00275 in (0.07 mm). Of course, these speeds are determined by the desired resolution, the probe used, and other factors as well.

ULTRAWIN is a control, recording and illustrating software. It allows real-time collection, storage and graphic illustration of the data. It runs in Windows XP and allows the control and configuration of the AD-IPR-1210 and PAC-SMC4 cards.

Figure 4.8 ULTRAPAC II immersion tank.

During the testing process, some parameters of the device that apply, both in touch and immersion, must be properly adjusted in order to obtain the most reliable results possible.

In the AD-IPR Setup tab of Figure 4.9 [50], it is possible to specify the parameters of both the pulser-receiver (P/R Mode) and the analog-to-digital signal (A/D Signal) conversion card. The parameters will be presented, not in the order shown in Figure 4.9 [50], but in the order that they are adjusted when examining the specimen. At the same time, the A-scan display of the specimen is also open on the computer screen, allowing the user to monitor the changes made to the received signals. The first thing to determine is the test method. The software provides us with two options, the P/R (Pulser/ Receiver) method and the T/T (Through transmission) method. For the purposes of the present work, the examination will be performed by the P/R method.

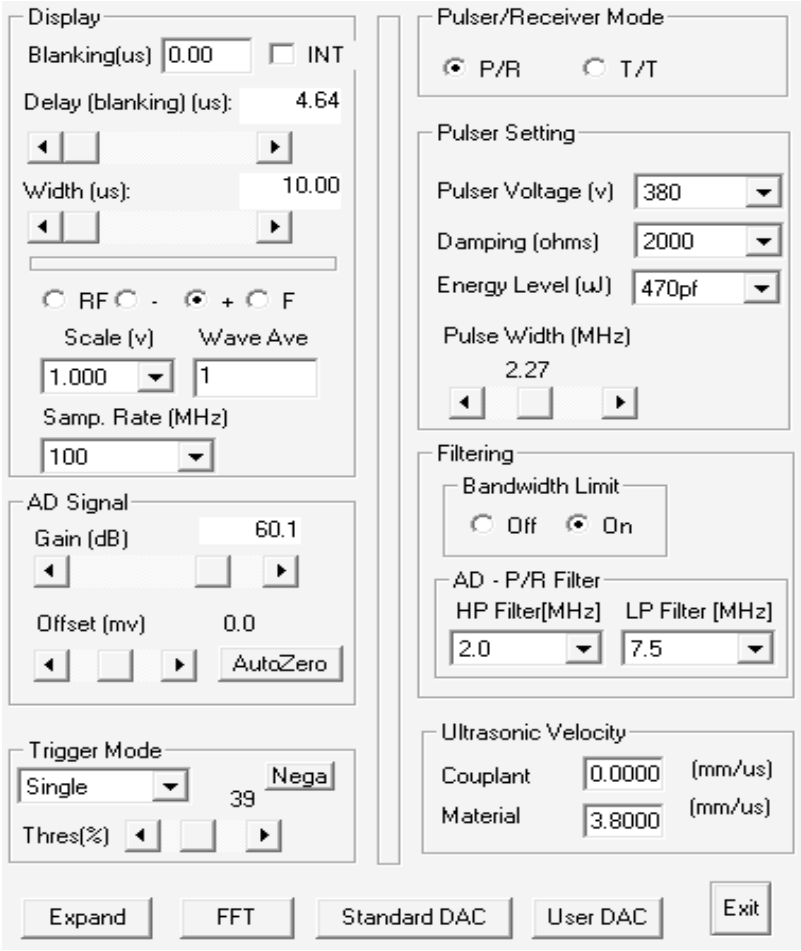

Figure 4.9 A/D and P/R setup.

Next, the A-scan illustration from the Display tab is chosen. With the Delay and Width options the user determines the time period to observe. In more detail, with the Delay command the start of the A-scan illustration is moved, in order to observe a specific time period of the ultrasound waves. In case of composite materials it is advisable to observe the first set of reflections after the initial pulse, because, due to their high attenuation, they usually have a very weak second set, making it difficult and sometimes impossible to utilize. The Width option determines the length of the time period, meaning the thickness of the specimen for display. This option is adjusted so that all useful reflections are visible.

The user can then choose how the echoes can be displayed through the options (RF), (-), (+), (F). The user can monitor the full waveform (RF), only the positive rectified waveform (+), only the negative one (-), or finally the fully rectified waveform (F). The various illustrations are shown in Figure 4.10 [50].

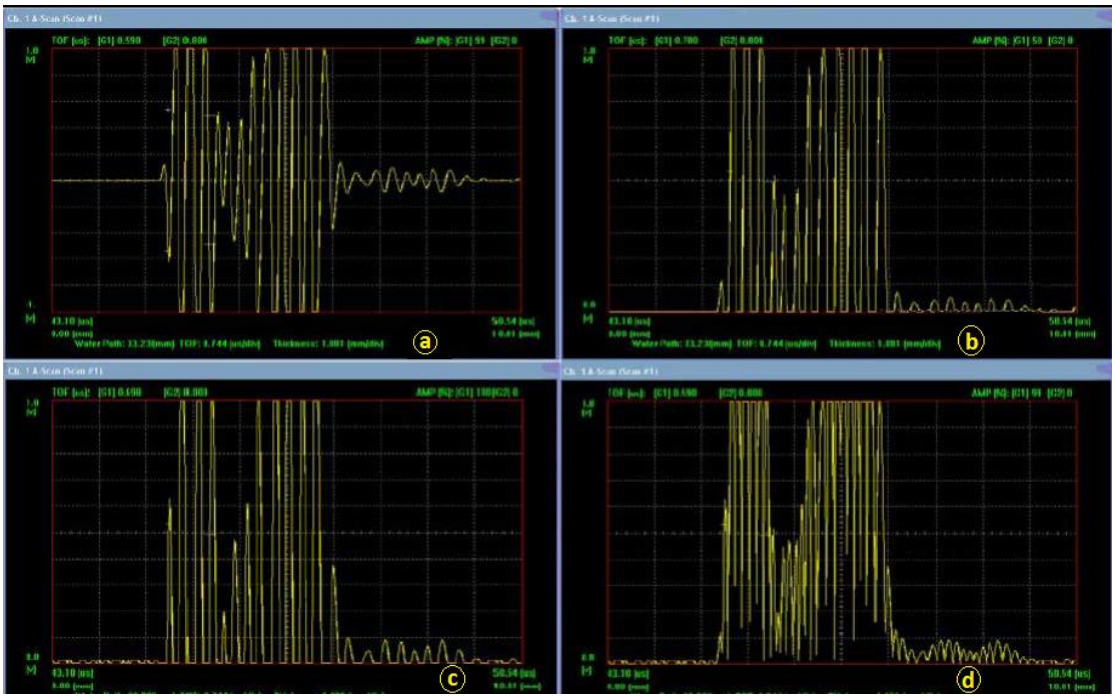

Figure 4.10 Possible waveforms a)Full waveform b)Positive rectified waveform c) Negative rectified waveform d)Fully rectified waveform.

The Display option also determines the Scale of the vertical axis in the A-scan window, the Wave average, and the Sample Rate (MHz). In order to have a complete and accurate A-scan illustration, in the Ultrasonic Velocity section the coupling media and test material velocities are entered.

Having adjusted the A-scan window to test the composite material, it is observed that the attenuation is very large, to the point where the reflection of the back surface of the material does not occur. To the AD signal section, Gain is increased and so the entire waveform is amplified by a specified number of dB. The amplification should be such that the pulses of the first reflections are slightly below 100% FSH. At the same point in the dialog box stands the Offset (mV) option. This option determines the lowest limit of the mV, on which the amplifier will apply the Gain. This choice is particularly important, as noise and useless reflections with less intensity (mV) can be excluded from amplification and thus not be confused with reflections from layers or imperfections.

Gates allow the observation of specific reflections, meaning specific thickness of the material. The gate is a time window, defined by the user of the Ultrapac device, that monitors a specific time period and that records any pulses that may occur during that time. The determination of the gates' height and width is particularly important in order to get the right results. ULTRAPAC II enables the user to fix two gates, gate 1 and gate 2. In the gates dialog box, shown in Figure 4.11 [50], there is the option to activate one gate or both gates at the same time marking On. In the Gates tab, the Sync option allows the user to synchronize the gates either with the Initial Pulse or the First echo. The first echo is considered the first signal viewed on the screen and is the echo of the front surface of each specimen under examination. This option is very important if the test surface is not perpendicular to the ultrasound beam in the test piece. The gates will also move relative to the first echo and will constantly monitor the given area of material, which is not the case if the gates are synchronized with the Initial Pulse. In this case, the gates are immovable and follow a

specific area on the axis of time, which, however, may not correspond to the volume of material that we have decided to examine. Since we have selected gates to synchronize with the first echo for the purpose of this examination, the Sync Thres setting is important. This parameter determines the lower percentage of the peak that is considered reliable to receive as the first echo and therefore reliable to synchronize the activated gate with. Then, in the gates dialog box, you will find the Detection Thread option. This option determines exactly the height of the gate. Next, the gate is positioned on the time axis, with the Start option specifying the distance or time from the initial pulse. Width sets the width of the gate and indirectly defines the end of the gate. After determining the position and width of the gate, the way in which the gate will record the echoes that intersect must be determined. ULTRAWIN software offers four options, or detection strategies. As shown in Figure 4.11 [50] there are two groups. The first group includes the First and Max options and the second the Thres and Peak options. These options must always be a combination of one from the first group and one from the second. That leads to four signal capture strategies, which are presented in Figure 4.12 and are discussed below.

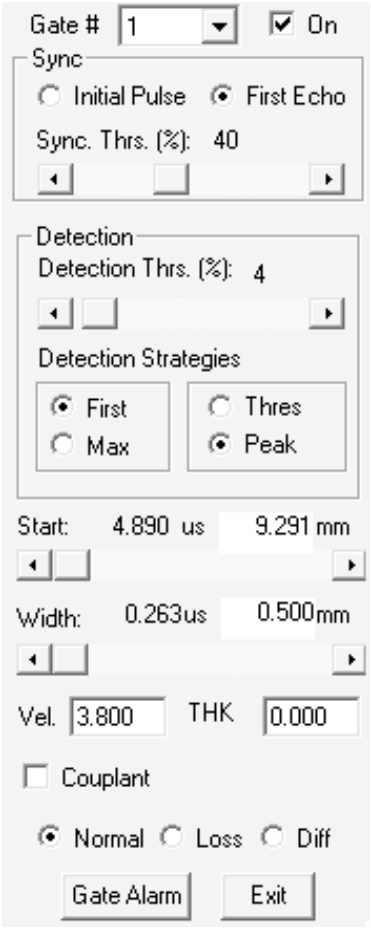

Figure 4.11 Gate setup.

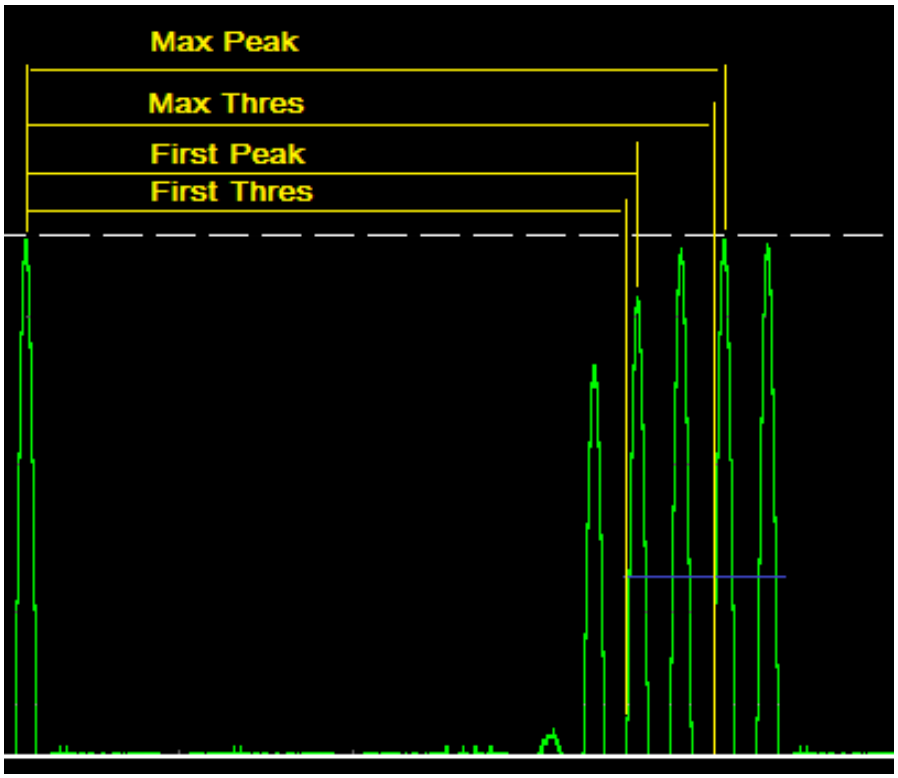

Figure 4.12 Detection strategies.

The strategies mentioned above are:

• First Peak: The gate records the first peak that intersects and the TOF (TIME of flight) is calculated according to the point of the peak.

• Max Peak: The gate records the peak with the maximum amplitude from those that intersect and the TOF is calculated according to the point of the peak.

• First Thres: The gate records the first peak that intersects and the TOF is calculated according to the point where the left side of the peak intersects the Gate.

• Max Thres: The gate records the maximum peak of those who cut it and the TOF is calculated as in the First Thres strategy.

Finally, the Gates dialog box defines the velocity of longitudinal waves inside the test material (Vel.) and the thickness of the material measured by mechanical means.

There is also one more important setting available; the usage of DAC (Distance Amplitude Correction) Curves in order to balance the strong attenuation of the wave far from the external surface of the specimen. That means that amplification is applied on the received signal. The starting moment has to be defined as well as the ending moment. Additionally, the starting and ending gain have to be determined. According to these settings amplification is applied on the signal, but not linear. DAC Curves determine the growth rate of the gain. In Figure 4.13 some typical DAC settings are presented.

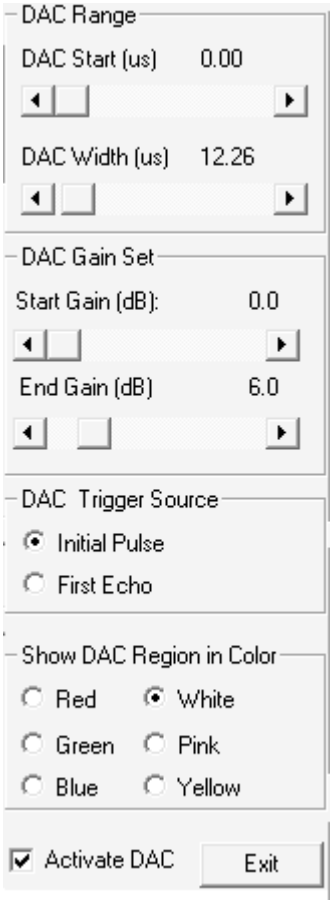

Figure 4.13 Typical DAC settings

At this point, it should be noted that all of these parameters have to do with A-scan examination. However, during the experimental process, the specimen was tested also by immersion, something that required some additional parameters to be adjusted. First, the scanning area must be defined. By saying scanning area, the area over which the piezoelectric head scans is mentioned.

The setting starts from the Scanner set up dialog box, shown in Figure 4.14 . Initially, the Scan Axis is selected, which may be any of the X or Y axes. The X-Y axes are at a plane parallel to the bottom of the tank, where the specimen lays. On the Z axis the head is located and is perpendicular to the X-Y plane. For the selected Scan Axis, the Length, the Speed at which the head will move and the Resolution are determined. The Index Axis is also defined, which cannot be the same as the Scan Axis. In the Length setting the dimensions of the specimen are entered. Resolution is defined as the distance between two consecutive points from which data are recorded, both in the Scan Axis and in the Index Axis. The resolution can reach 0.07 mm (0.00275 in). The speed of the two axes can be as high as 500 mm/sec.

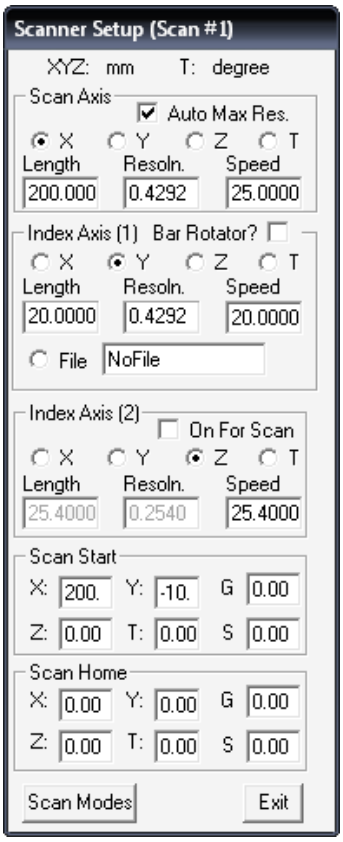

Figure 4.14 Scanner setup.

The last parameter to be set for the scan to start correctly is the reference point. The Scanner Jog dialog box (Figure 4.15 [50]) specifies the scan reference point. The reference point is the beginning of the x-y-z axis system and is located on the piezoelectric element of the head. Based on this point, the device records the distances, both at the X-Y plane and on the Z axis. The beginning of the axle system defines the point of the tank according to which, after the end of the scan at the plane X-Y, the dimensions of the specimen and the thickness of the material will be recorded along the Z axis.

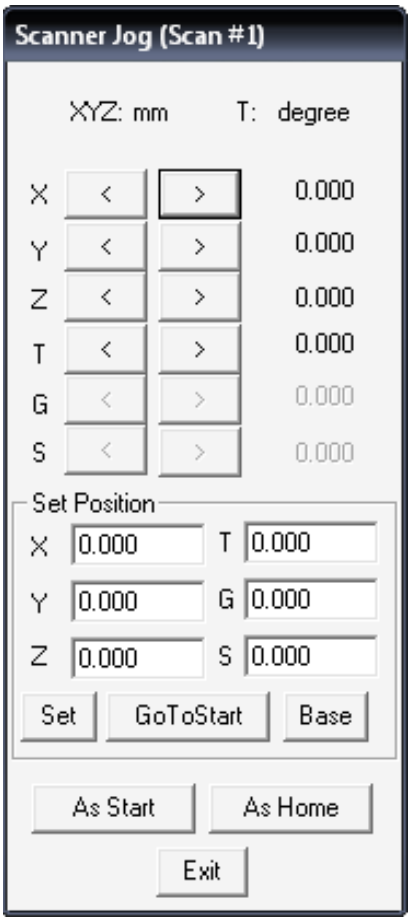

Figure 4.15 Scanner jog setup.

4.4. A-Scan Procedure and Difficulties

The rationale behind the detection of the defects during A-Scan was to make a comparison between the signal received from a theoretically "healthy" area (with no defects) near the defect and the signal received from the defect's position. If an extra echo was noticed at the under examination depth, then it was considered to be the defect. The range of the depth that was chosen varied according to the defect. For each defect several tries were made in order to end up to the depth range that provided clear image of the defect. The ideal situation is to examine a depth range that covers the area between two layers, where the defect is.

For the A-Scan to start, all the parameters had to be defined. It was necessary to decide for each defect separately which settings were ideal. The general rule is that for the deeper defects higher voltage and damping was chosen, while for the closer defects lower voltage and damping was chosen. The gain was maintained at the same level for all the depths. The settings used for each defect are presented below at Table 4.3. Glycerin was used in order to achieve contact between the probe and the surface.

It is underlined that near field interferes with the entire thickness of the specimen. No second set of echoes was available, due to the strong attenuation of the beam. Therefore detection of defects had to be done inside the near field, something that led to a high level of difficulty. More particularly, near field's length was 23.9 mm for 2.25 MHz transducer and 53

mm for 5 MHz transducer, while the thickness of the specimen was calculated around 17.7 mm, as seen later in section 4.5.

More specifically, with the 2.25 MHz frequency transducer more defects were detected than with the 5 MHz frequency transducer. The reason is that lower frequency provides higher penetration, which is necessary during the ultrasonic testing of composite materials. Table lines signed with "-" are the defects that could not be detected with the A-Scan method. The reason could be the cylindrical shape of the specimen, which allowed no full and stable contact of the probe with the surface. Furthermore, the transducer during A-Scan is controlled manually. That always entails the risk of human error. It is also very important to note, that the internal structure of the specimen is complex and can lead to signals that do not represent the real situation inside the cylinder. The user should also be aware that the sound velocity may vary locally within the specimen based on carbon content and fiber orientation and therefore lead to variations in results [51]. The fact that near field interferes with the observed echoes could also lead to lack or wrong estimation of the depth of a defect. All the above associated with the lack of confirmation of the constructive data from a competent laboratory could be reasons that lead to inadequate results.

Table 4.3 A-Scan settings.

			2.25 MHz			5 MHz		
	No	Depth (mm)	Voltage (V)	Damping (Ohms)	Gain (dB)	Voltage (V)	Damping (Ohms)	Gain (dB)
Group 1	1	14.2	380	2000	60.1	-	-	-
	2	14.2	-	-	-	-	-	-
	3	14.2	380	2000	60.1	-	-	-
	4	14.2	380	2000	60.1	380	2000	60.1
	5	14.2	380	2000	60.1	-	-	-
	6	14.2	-	-	-	-	-	-
	7	14.2	380	2000	60.1	-	-	-
	8	14.2	380	2000	60.1	380	2000	60.1
Group 2	9	9.25	360	2000	60.1	360	2000	60.1
	10	9.25	360	2000	60.1	-	-	-
	11	9.25	-	-	-	360	2000	60.1
	12	9.25	360	2000	60.1	-	-	-
	13	9.25	360	2000	60.1	-	-	-
	14	9.25	360	2000	60.1	-	-	-
	15	9.25	360	2000	60.1	-	-	-
	16	9.25	380	2000	60.1	-	-	-
Group 3	17	4	380	40.5	60.1	360	43.8	60.1
	18	4	380	40.5	60.1	-	-	-
	19	4	-	-	-	360	43.8	60.1
	20	4	380	40.5	60.1	-	-	-
	21	4	360	43.8	60.1	380	43.8	60.1
	22	4	380	40.5	60.1	-	-	-
	23	4	360	43.8	60.1	-	-	-
	24	4	-	-	-	360	43.8	60.1

Special reference is required for defects No. 13 and No. 15, which are consecutive inside the cylinder and constitute two tangent circles. Therefore they were dealt as one big defect. Additionally, the surface that the probe had to scan for the detection of defects No.2 (200, 50, 20) was very uneven, as seen in Figure 4.16, something that led to lack of results.

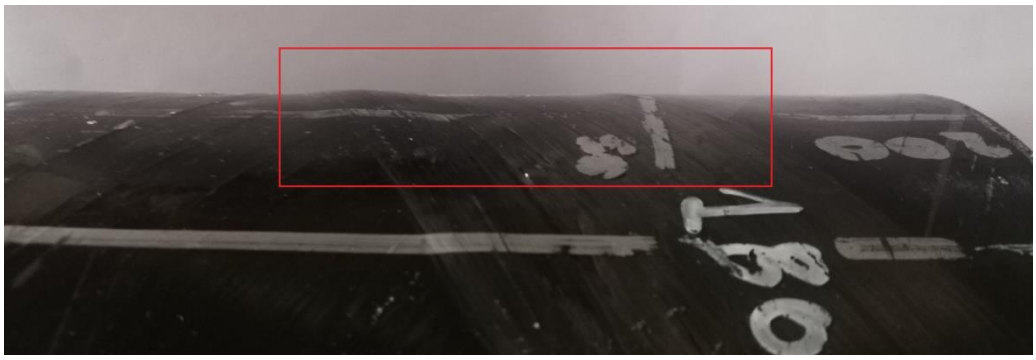

Figure 4.16 Uneven surface at 200 degrees, 50mm.

4.5. C-Scan Procedure and Difficulties

The rationale behind C-Scan examination was to scan a specific area of a specific length and width for a predefined depth range. The result was to receive an image that would illustrate the maximum amplitude's depth for each position of the probe. The echo with the maximum amplitude is supposed to be the echo of the defect.

The specimen had to be sunk inside a tank filled with deionized water (Figure 4.17), which was the coupling liquid for this procedure. The velocity of the water was measured 1.497 mm/ μs. It is underlined that near field does not interfere in this case with the thickness of the specimen. More particularly, near field's length was 60.6 mm for 2.25 MHz transducer and 94.3 mm for 3.5 MHz transducer, while the distance from the transducer to the external surface of the specimen was 100 mm, which was the water path. That led to a more reliable examination of the received echoes.

Before the beginning of the detection procedure, a thickness measurement took place. Due to manual rotation of the cylinder, thickness measurement has been done only for the four basic angles, namely 0 deg, 90 deg, 180 deg, 360 deg, and not for the whole cylinder. The scanned width was 10 mm and the scanned length was 400 mm, meaning the entire length of the cylinder. In Figure 4.18 to Figure 4.21 are shown the results of the measurements. In this case the echo with the maximum amplitude stands for the back- wall echo.

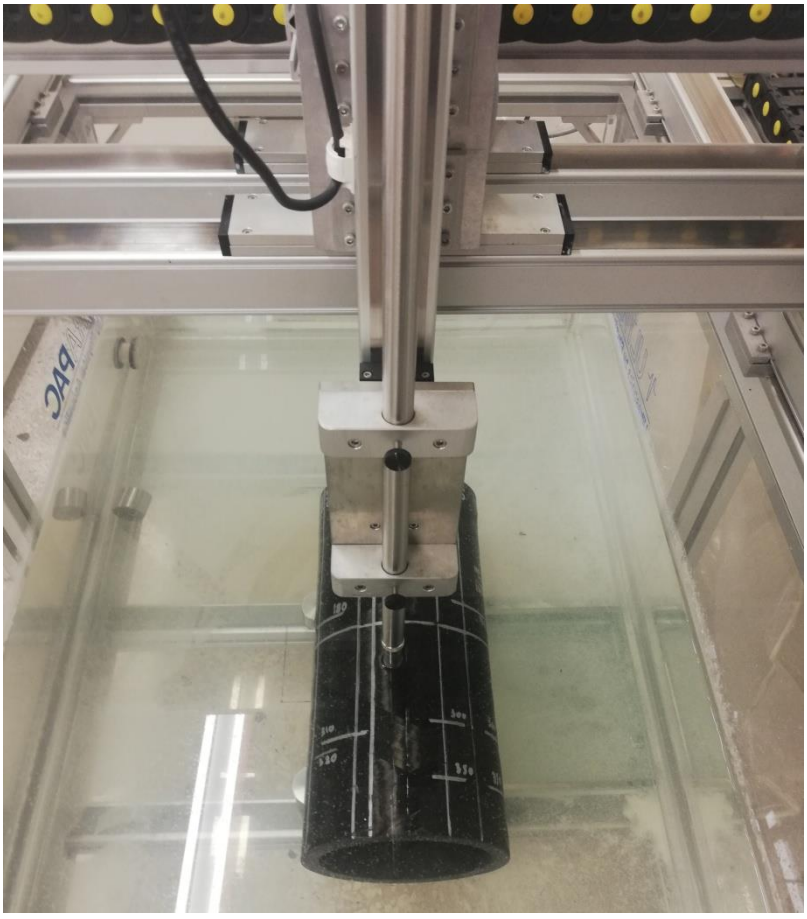

Figure 4.17 CFRP cylinder in examination tank.

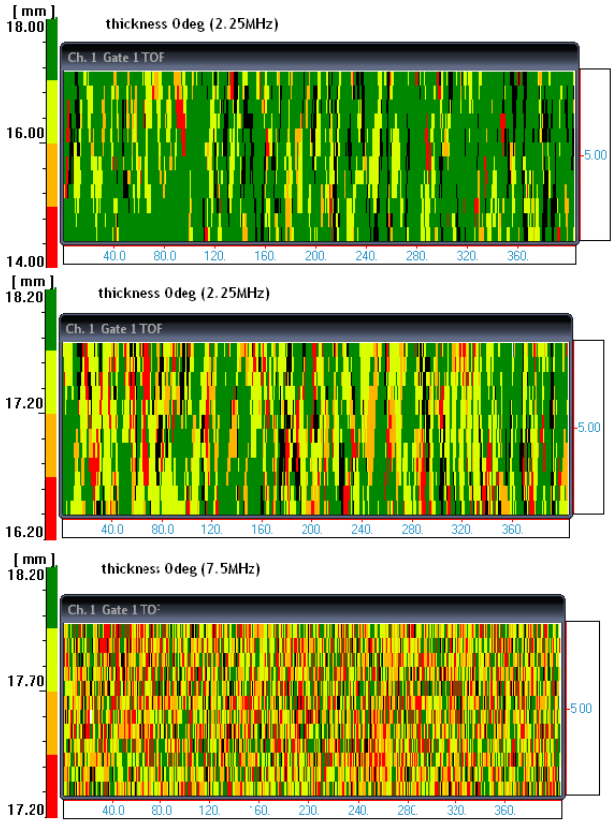

Figure 4.18 C-Scan thickness measurement at 0 degrees.

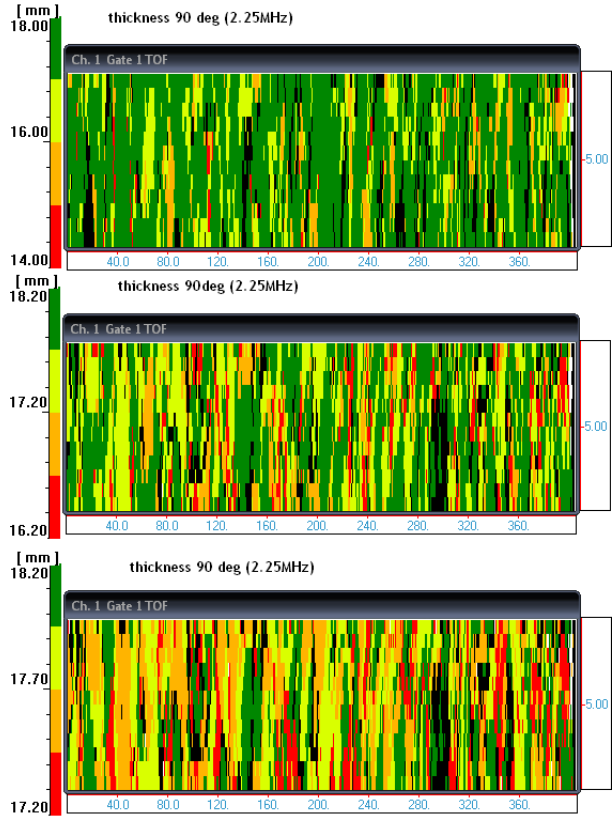

Figure 4.19 C-Scan thickness measurement at 90 degrees.

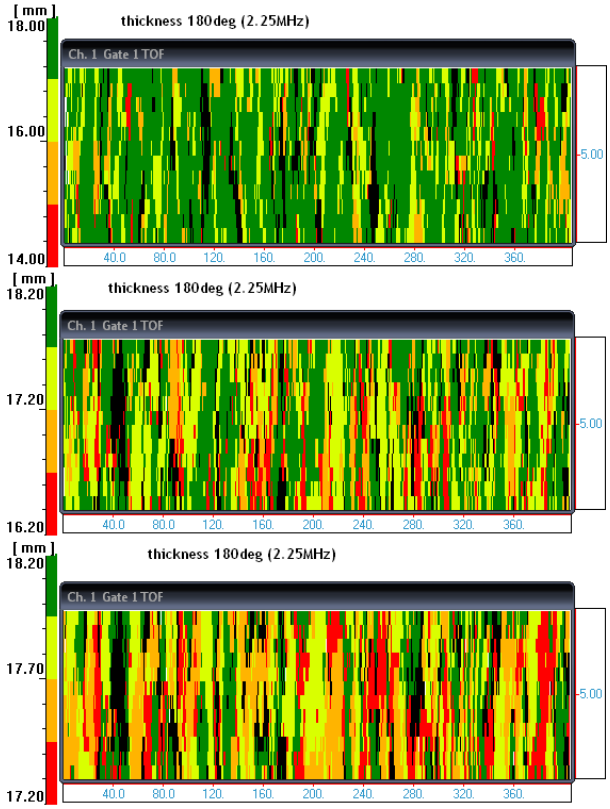

Figure 4.20 C-Scan thickness measurement at 180 degrees.

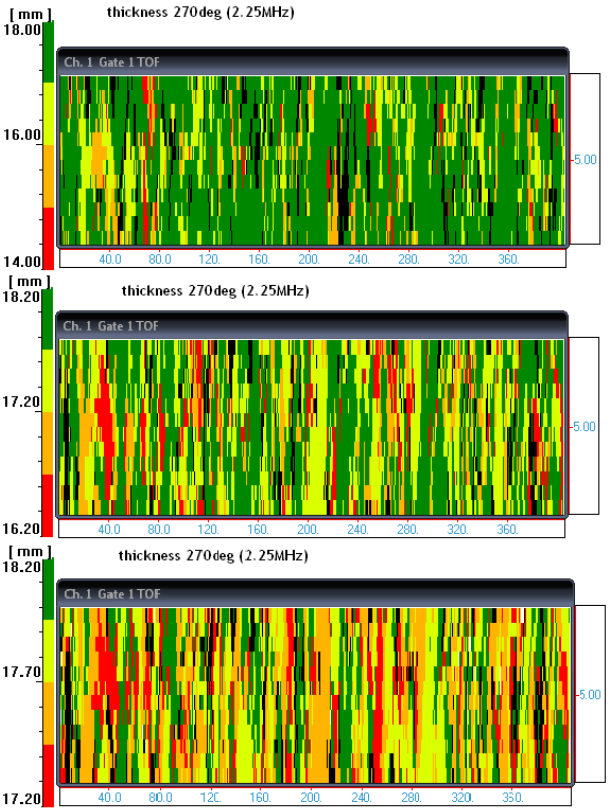

Figure 4.21 C-Scan thickness measurement at 270 degrees.

In order to prevent repetition, only the angle of zero degrees will be discussed. All other four angles follow the same pattern. At the beginning a wide range of depth was chosen, namely from 14 mm to 18 mm depth. As seen in the figure above most of the produced image is green, which means, according to the scale on the left, that thickness is basically between 17 mm and 18 mm. The depth range got limited between these two values, as it is obvious in the third line. The most of the produced image is yellow and orange, which means that thickness varies between 7.45 mm and 17.95 mm. In Table 4.4 the approximation of thickness for all four angles is illustrated according to this method.

Table 4.4 C- Scan thickness measurements.

Angle	Thickness		
	Lower limit	Upper limit	Average
(deg)	(mm)	(mm)	(mm)
0	17.45	17.95	17.7
90	17.45	17.95	17.7
180	17.45	17.95	17.7
270	17.45	17.95	17.7

The settings used for these measurements are presented in Table 4.5.

Table 4.5 Settings for THK measurement with 2.25 MHz probe.

Transducers Frequency (MHz)					2.25	
Gain	Offset	Pulser Voltage	Damping	Energy Level	HP Filter	LP Filter
dB	mV	V	Ohms	μJ	MHz	MHz
15.5	8	380	2000	820 pf	2	7.5

At this point, it could be considered useful to change the nominal depths accordingly with the thickness deviation. This step was not made, firstly because the increase in thickness did not necessarily affect all the layers, e.g. the deepest layer, which was first manufactured, could be on the nominal diameter and the deviation from the nominal data could start from the second layer on. Secondly, such a change would increase the nominal depths up to 1.2 mm, something that leads to deviations between the nominal and the calculated results up to 2mm. Therefore new A-Scan measurements would have to be taken, something that did not prove for the most part necessary after seeing the C-Scan results, which confirmed the already A-Scan measured depths of the defects.

Afterwards, the process of defects' detection began. After rotating the cylinder to the appropriate angle, the scanning length was chosen and was always 200 mm. If the defect belonged to the first half of the cylinder, then the scan start was chosen at L= 0 mm, if it belonged to the second half, then the scan start was chosen at L= 200 mm. If the defect was at L= 200 mm, then the scan start was set at L=100 mm. Another parameter was the scanning width, which was always 20 mm. This width allowed good quality at the produced image without large blank spaces. Due to the cylindrical geometry of the specimen, no signal could be received far from the center line. Figure 4.22 shows a typical set up of the scanner. Then the appropriate depth range had to be chosen. This parameter is very important and was always defined after various trials, up until the produced image actually depicted the under examination defect. The colors of the scale were chosen for each defect according to the opinion of the operator, in order to make defects as obvious as possible. In Table 4.6 the basic settings of the setup can be seen, for each defect.

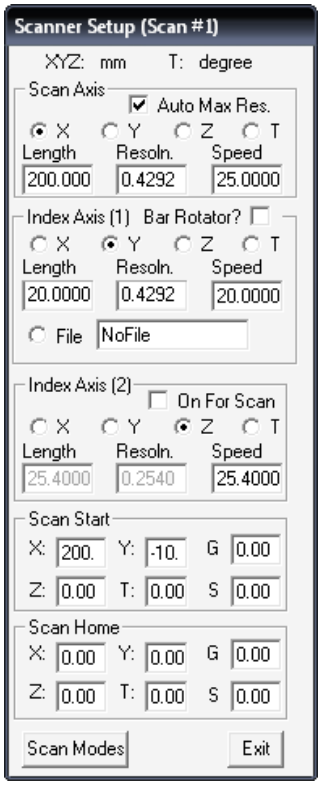

Figure 4.22 Scanner setup.

Table 4.6 C-Scan settings.

			2.25 MHz			3.5 MHz		
	No	Depth (mm)	Voltage (V)	Damping (Ohms)	Gain (dB)	Voltage (V)	Damping (Ohms)	Gain (dB)
Group 1	1	14.2	380	2000	45	-	-	-
	2	14.2	380	2000	45	-	-	-
	3	14.2	380	2000	45	-	-	-
	4	14.2	380	2000	45	-	-	-
	5	14.2	380	2000	45	-	-	-
	6	14.2	-	-	-	-	-	-
	7	14.2	-	-	-	-	-	-
	8	14.2	380	2000	45	-	-	-
Group 2	9	9.25	380	2000	45	-	-	-
	10	9.25	380	2000	45	-	-	-
	11	9.25	380	2000	45	-	-	-
	12	9.25	-	-	-	-	-	-
	13	9.25	380	2000	45	-	-	-
	14	9.25	-	-	-	-	-	-
	15	9.25	380	2000	45	-	-	-
	16	9.25	380	2000	45	-	-	-
Group 3	17	4	380	2000	45	-	-	-
	18	4	380	2000	45	-	-	-
	19	4	380	2000	45	-	-	-
	20	4	380	2000	45	360	2000	45
	21	4	380	2000	45	-	-	-
	22	4	380	2000	45	360	2000	45
	23	4	380	2000	45	-	-	-
	24	4	380	2000	45	-	-	-

The transducer during C-Scan is controlled automatically, something that eliminates the risk of human error. It is also very important to note, that the internal structure of the specimen is complex and can lead to signals that do not represent the real situation inside the cylinder. The lack of confirmation of the constructive data from a competent laboratory is something that should be reminded and taken under consideration.

5. EXPERIMENTAL RESULTS

5.1. A-Scan Results

5.1.1. Detailed Presentation of the A-Scan Results

The previously described procedure led to the results shown in the following figures (Figure 5.1 to Figure 5.27). In the figures below the waveform of each measurement is illustrated. The first snapshot corresponds to a healthy area, while the second one shows the defect's area signal. The echo that is considered to represent the defect is in a red box. The measurement received from the Gate is enlarged in the figure in order to be readable. Furthermore, a table with the basic settings of the equipment is available for each defect. For some defects DAC setting was used. All the measurements with the 5 MHz probe for Group 1 and 2 needed this setting, due to the combination of the lower penetrability of the probe and the longer distance of the defects. DAC setting is obvious, as in this case the echoes are colored white.

Starting with Group 1 (d=14.25mm), the results for each defect will be presented. No.1 and No.3 defects were detected only with the 2.25 MHz probe, while No. 2 defect was not detectable at this point of the experimental procedure.

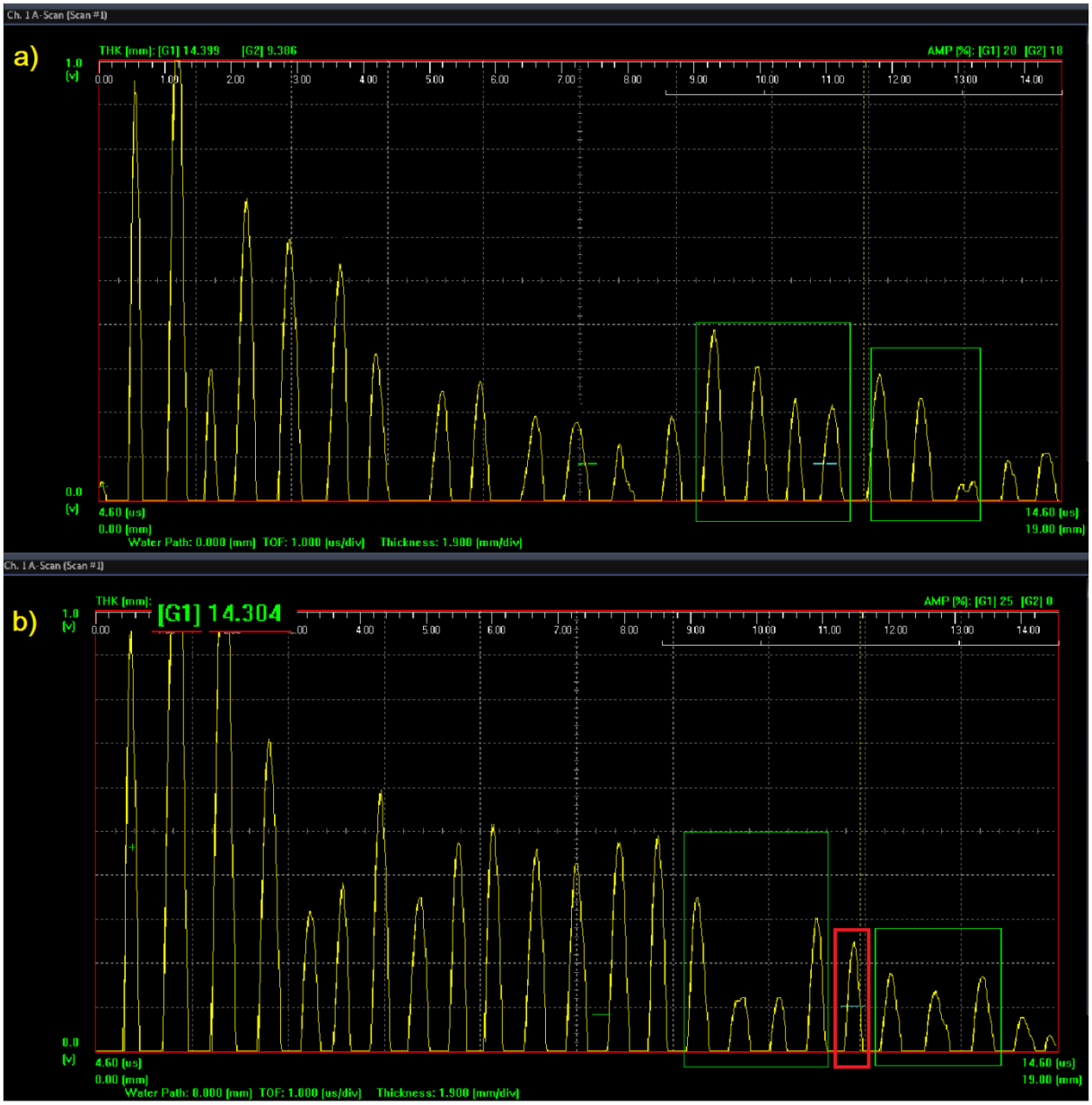

Figure 5.1 a) A-Scan on healthy area around defect No.1 b) A-Scan on defect No.1 (2.25 MHz).

Table 5.1 A-Scan settings for defect No.1 (2.25 MHz).

Transducers Frequency (MHz)					2.25		
No	Gain	Offset	Pulser Voltage	Damping	Energy Level	HP Filter	LP Filter
	dB	mV	V	Ohms	μJ	MHz	MHz
1	60.1	0	380	2000	470 pf	2	7.5

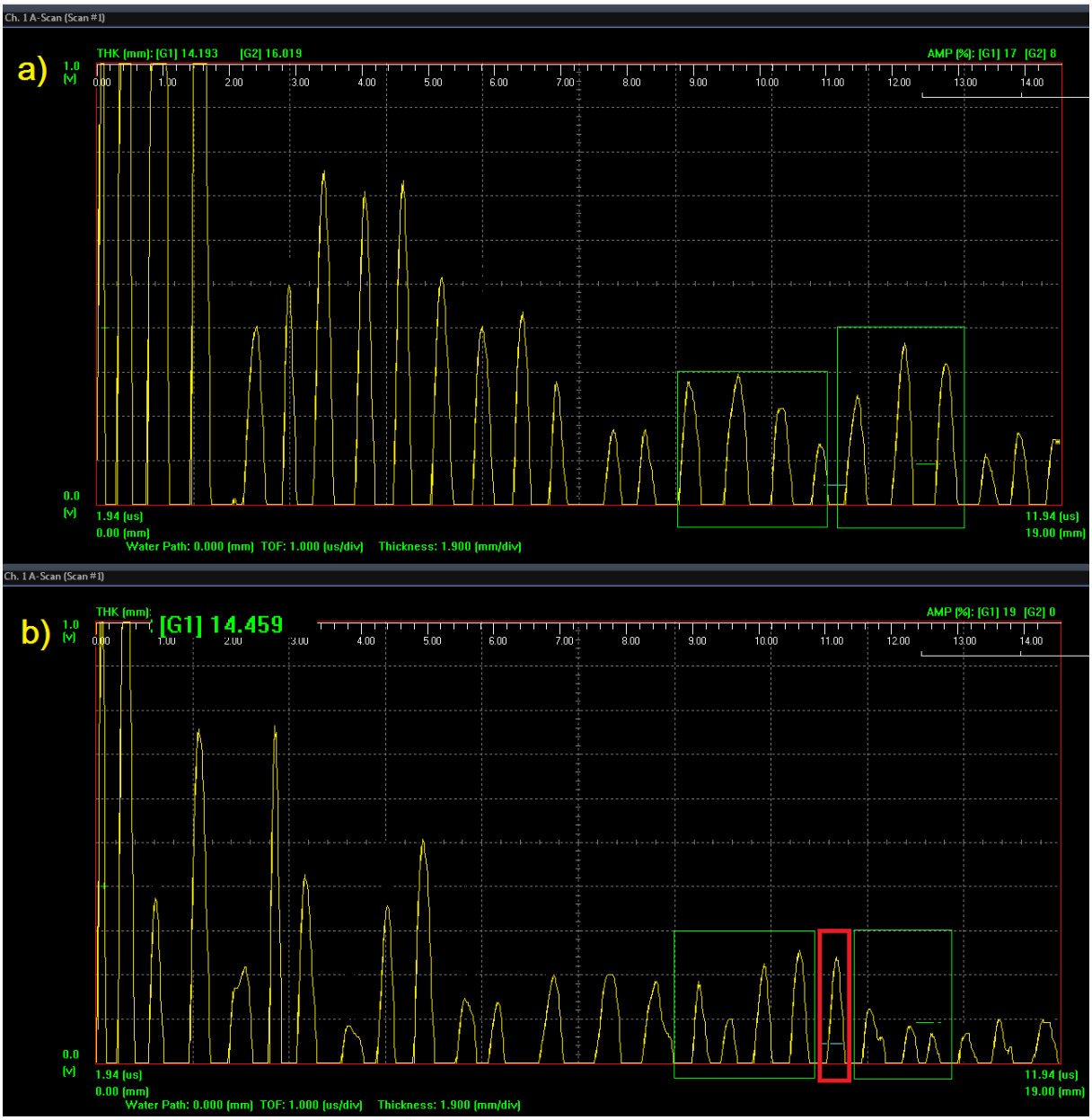

Figure 5.2 a) A-Scan on healthy area around defect No.3 b) A-Scan on defect No.3 (2.25 MHz).

Table 5.2 A-Scan settings for defect No.3 (2.25 MHz).

Transducers Frequency (MHz)					2.25		
No	Gain	Offset	Pulser Voltage	Damping	Energy Level	HP Filter	LP Filter
	dB	mV	V	Ohms	µJ	MHz	MHz
3	60.1	0	380	2000	470 pf	2	7.5

For No.4 defect results were found with both the transducers of 2.25 MHz and 5 MHz.

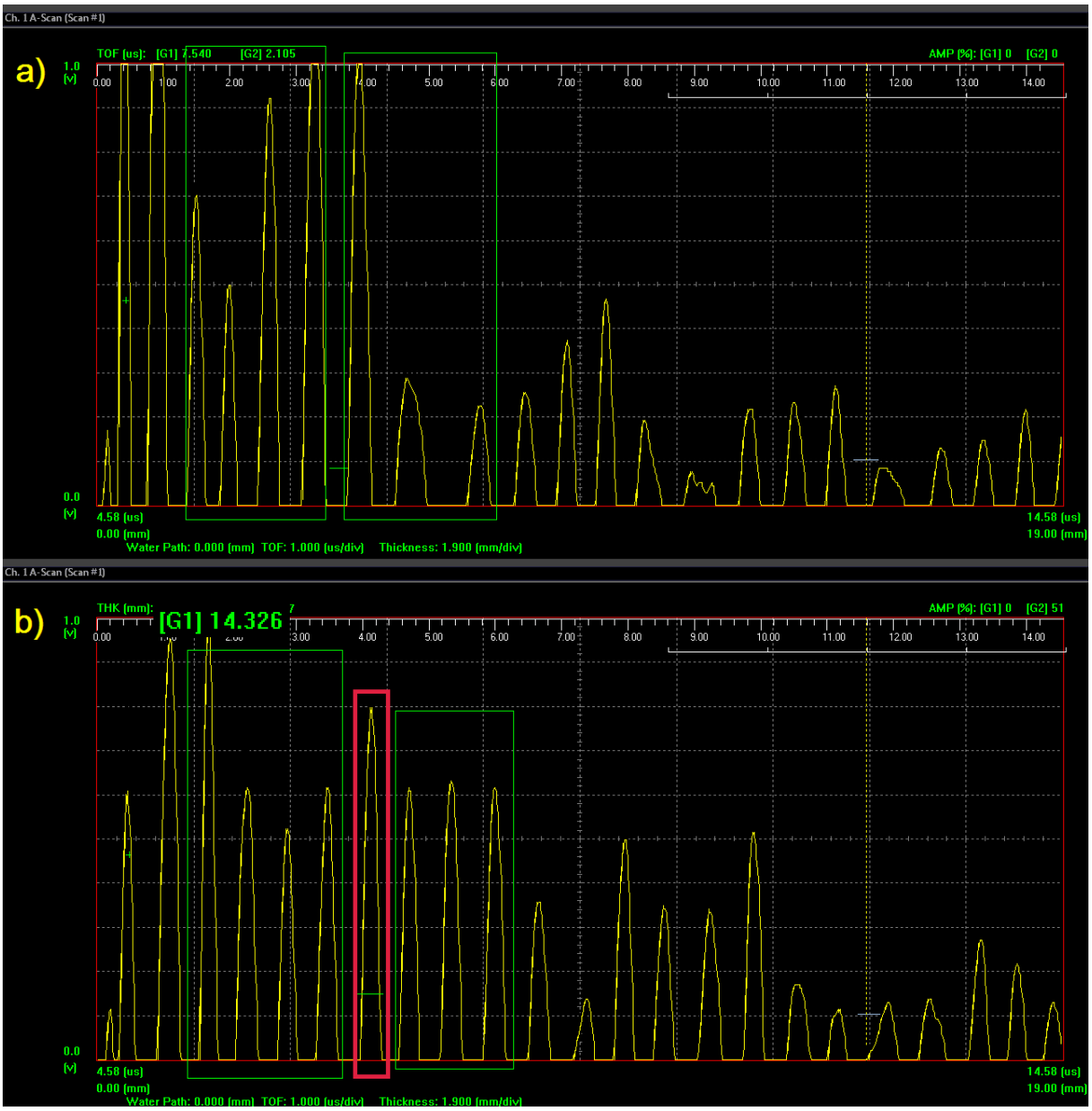

Figure 5.3 a) A-Scan on healthy area around defect No.4 b) A-Scan on defect No.4 (2.25 MHz).

Table 5.3 A-Scan settings for defect No.4 (2.25 MHz).

Transducers Frequency (MHz)					2.25		
No	Gain	Offset	Pulser Voltage	Damping	Energy Level	HP Filter	LP Filter
	dB	mV	V	Ohms	µJ	MHz	MHz
4	60.1	0	380	2000	470 pf	2	7.5

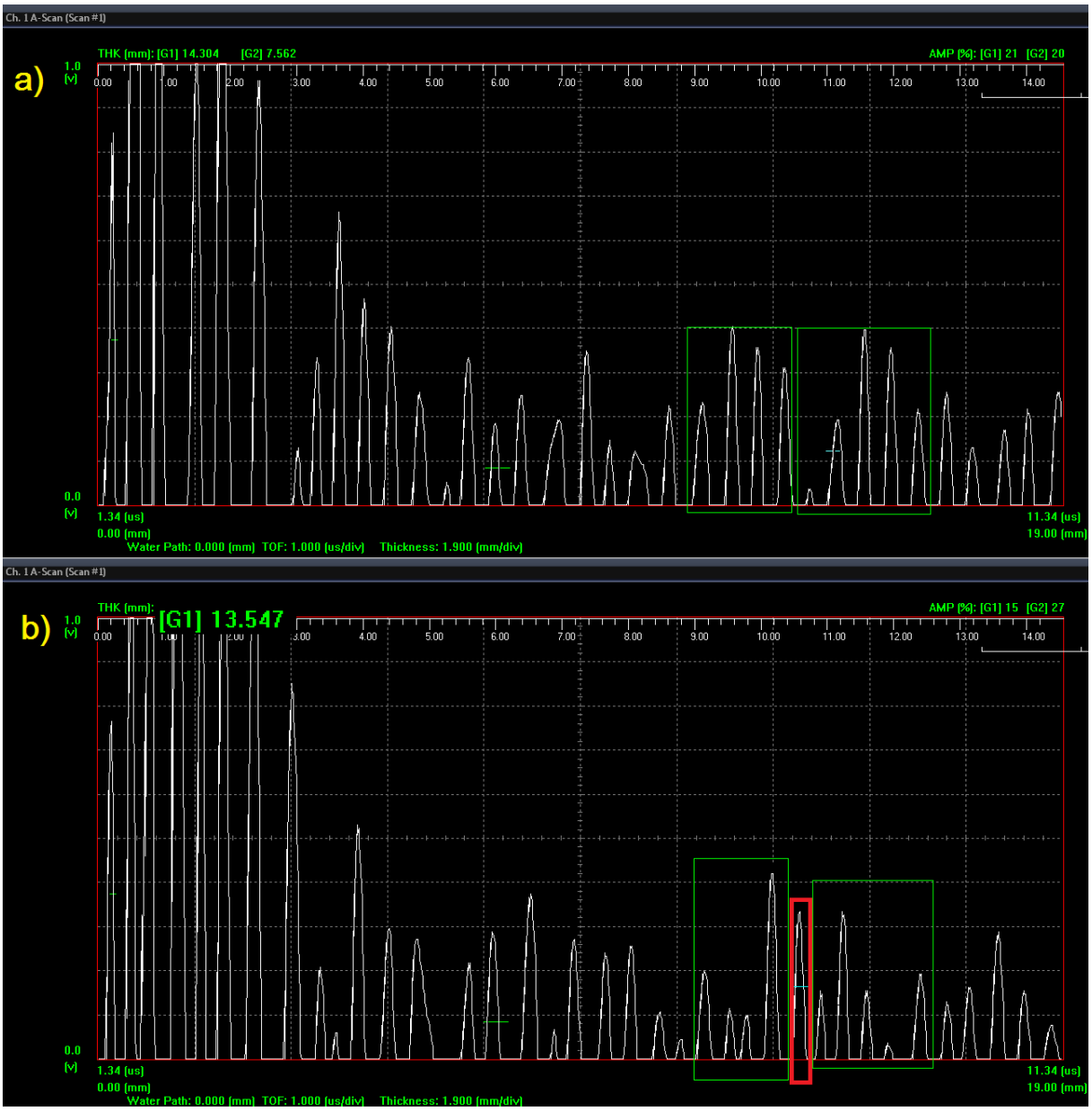

Figure 5.4 a) A-Scan on healthy area around defect No.4 b) A-Scan on defect No.4 (5 MHz).

Table 5.4 A-Scan settings for defect No.4 (5 MHz).

Transducers Frequency (MHz)					5		
No	Gain	Offset	Pulser Voltage	Damping	Energy Level	HP Filter	LP Filter
	dB	mV	V	Ohms	µJ	MHz	MHz
4	60.1	0	380	2000	470 pf	2	7.5
DAC SETTINGS							
Start Gain		End Gain		DAC Start		DAC End	
dB		dB		µs		µs	
0		7.5		0		12	

No. 5 and No.7 defects were detected only with 2.25 MHz transducer, while No.6 defect was not detected at this phase of the experimental procedure.

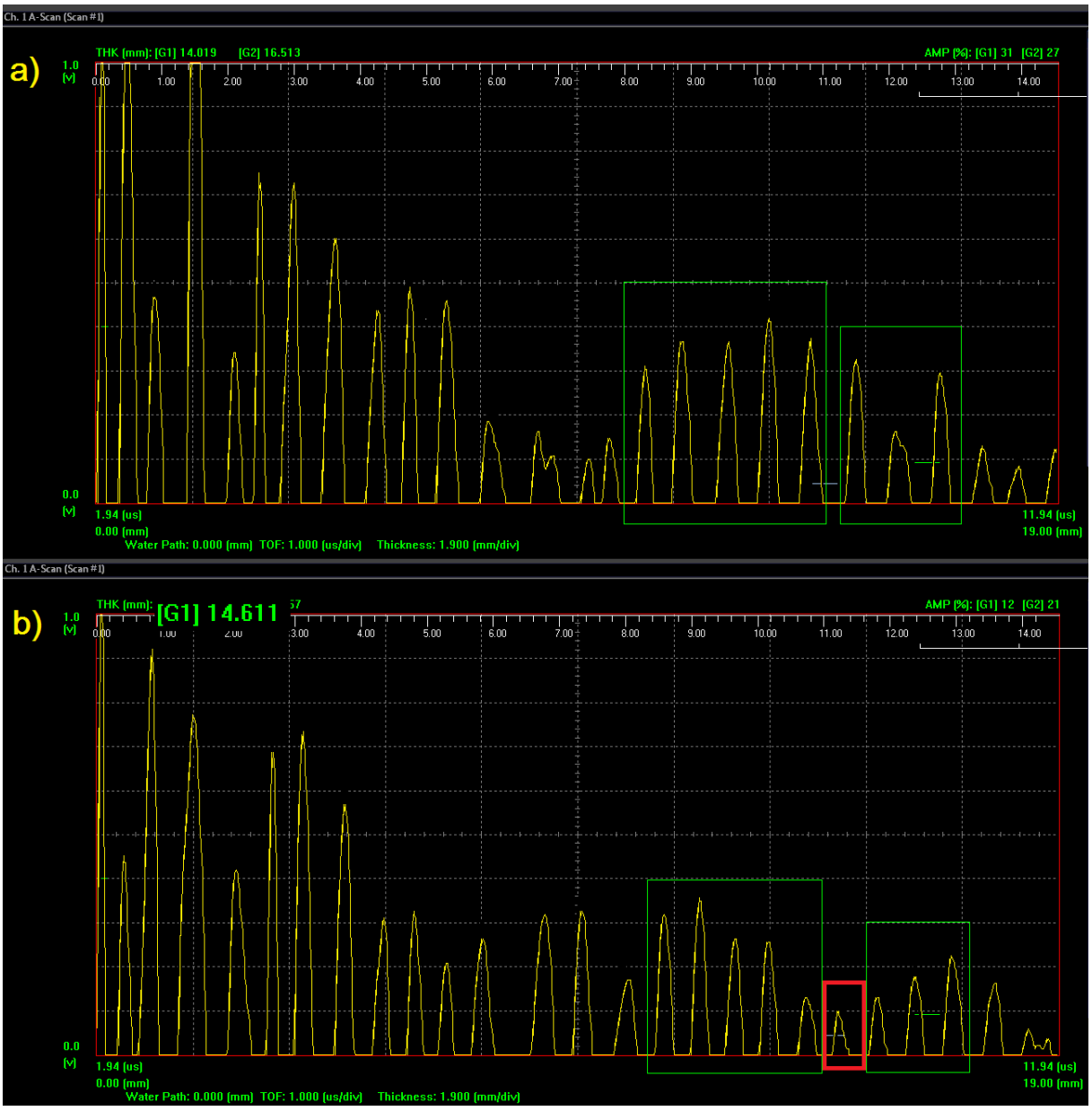

Figure 5.5 a) A-Scan on healthy area around defect No.5 b) A-Scan on defect No.5 (2.25 MHz).

Table 5.5 A-Scan settings for defect No.5 (2.25 MHz).

Transducers Frequency (MHz)					2.25		
No	Gain	Offset	Pulser Voltage	Damping	Energy Level	HP Filter	LP Filter
	dB	mV	V	Ohms	µJ	MHz	MHz
5	60.1	0	380	2000	470 pf	2	7.5

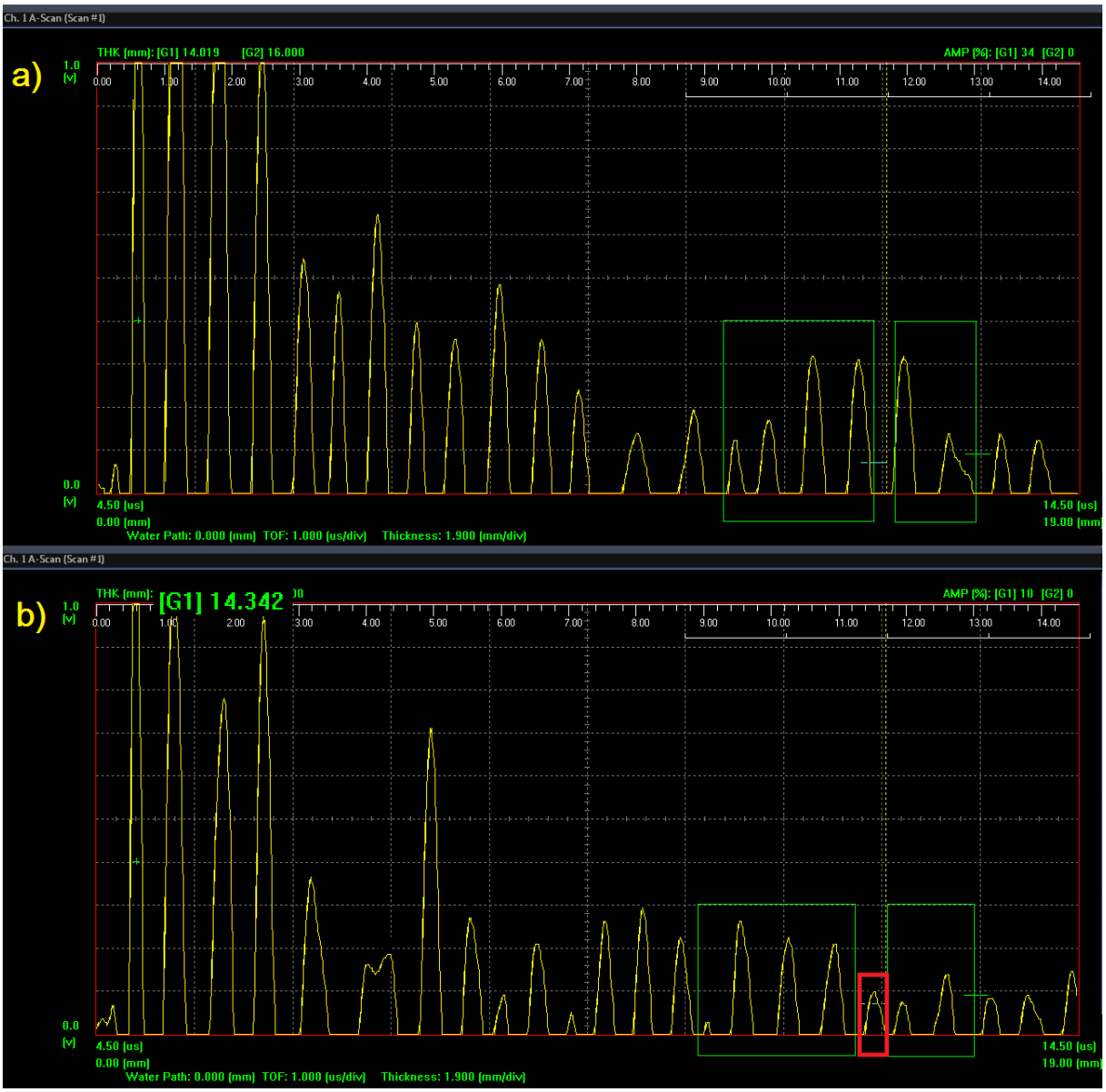

Figure 5.6 a) A-Scan on healthy area around defect No.7 b) A-Scan on defect No.7 (2.25 MHz).

Table 5.6 A-Scan settings for defect No.7 (2.25 MHz).

Transducers Frequency (MHz)					2.25		
No	Gain	Offset	Pulser Voltage	Damping	Energy Level	HP Filter	LP Filter
	dB	mV	V	Ohms	µJ	MHz	MHz
7	60.1	0	380	2000	470 pf	2	7.5

The last defect of the 1st Group, No.8, was detected with both the probes.

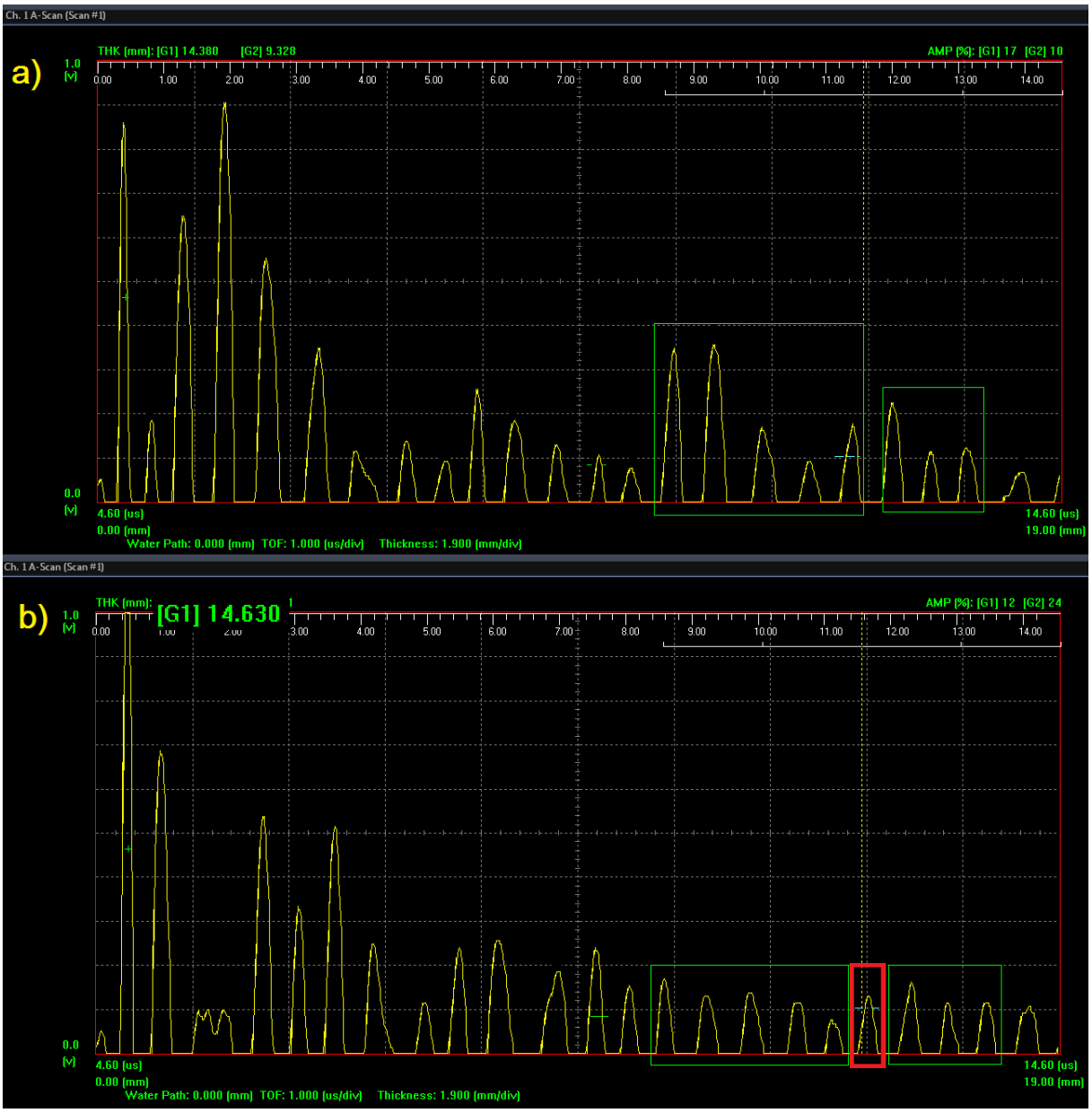

Figure 5.7 a) A-Scan on healthy area around defect No.8 b) A-Scan on defect No.8 (2.25 MHz).

Table 5.7 A-Scan settings for defect No.8 (2.25 MHz).

Transducers Frequency (MHz)					2.25		
No	Gain	Offset	Pulser Voltage	Damping	Energy Level	HP Filter	LP Filter
	dB	mV	V	Ohms	µJ	MHz	MHz
8	60.1	0	380	2000	470 pf	2	7.5

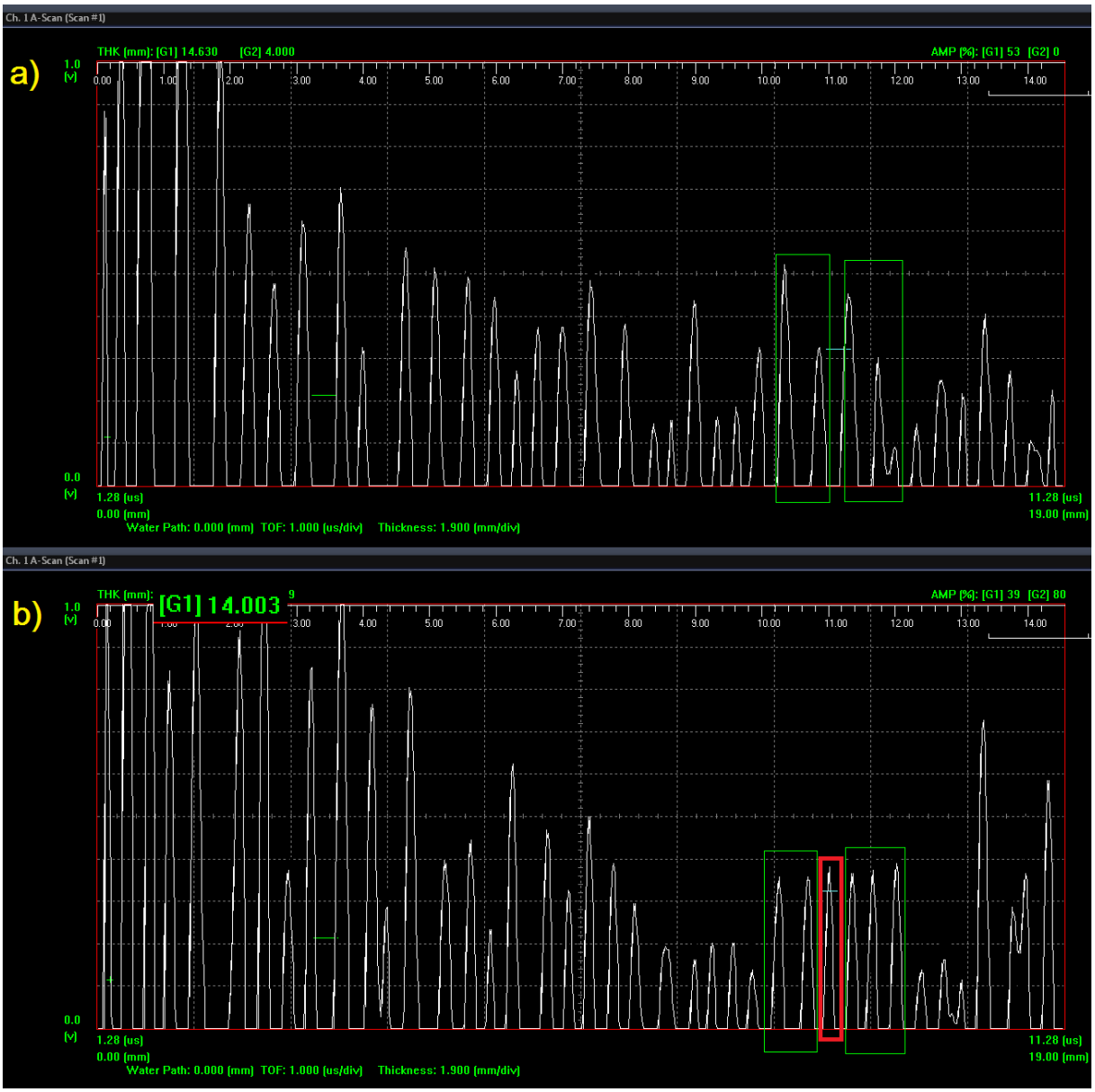

Figure 5.8 a) A-Scan on healthy area around defect No.8 b) A-Scan on defect No.8 (5 MHz).

Table 5.8 A-Scan settings for defect No.8 (5 MHz).

Transducers Frequency (MHz)					5		
No	Gain	Offset	Pulser Voltage	Damping	Energy Level	HP Filter	LP Filter
	dB	mV	V	Ohms	µJ	MHz	MHz
8	60.1	0	380	2000	470 pf	2	7.5
DAC SETTINGS							
Start Gain		End Gain		DAC Start		DAC End	
dB		dB		µs		µs	
0		7.5		0		12	

Moving on to the 2nd Group of defects (d=9.25 mm), No.9 was detected with both transducers.

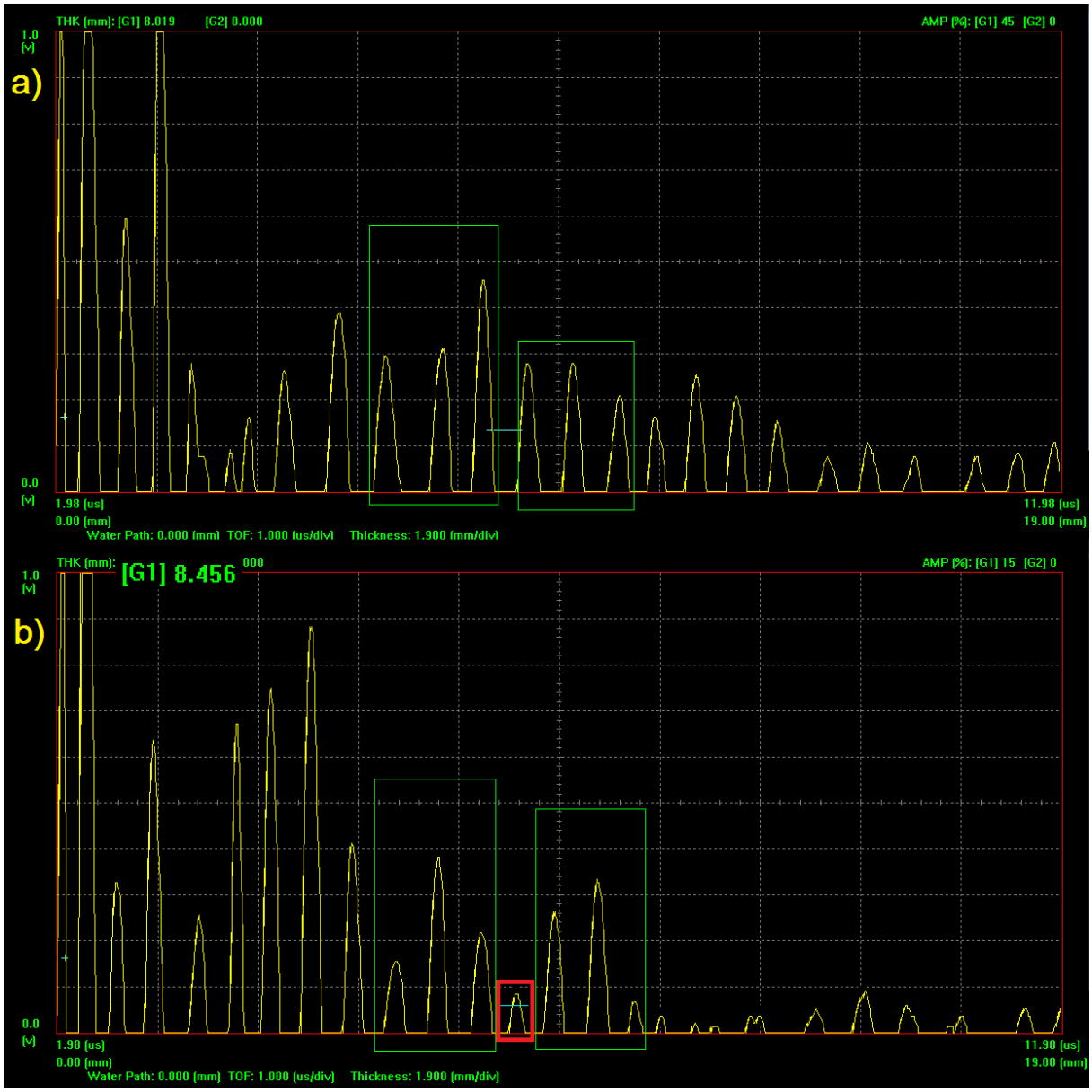

Figure 5.9 a) A-Scan on healthy area around defect No.9 b) A-Scan on defect No.9 (2.25 MHz).

Table 5.9 A-Scan settings for defect No.9 (2.25 MHz).

Transducers Frequency (MHz)					2.25		
No	Gain	Offset	Pulser Voltage	Damping	Energy Level	HP Filter	LP Filter
	dB	mV	V	Ohms	µJ	MHz	MHz
9	60.1	6	360	2000	820 pf	2	5

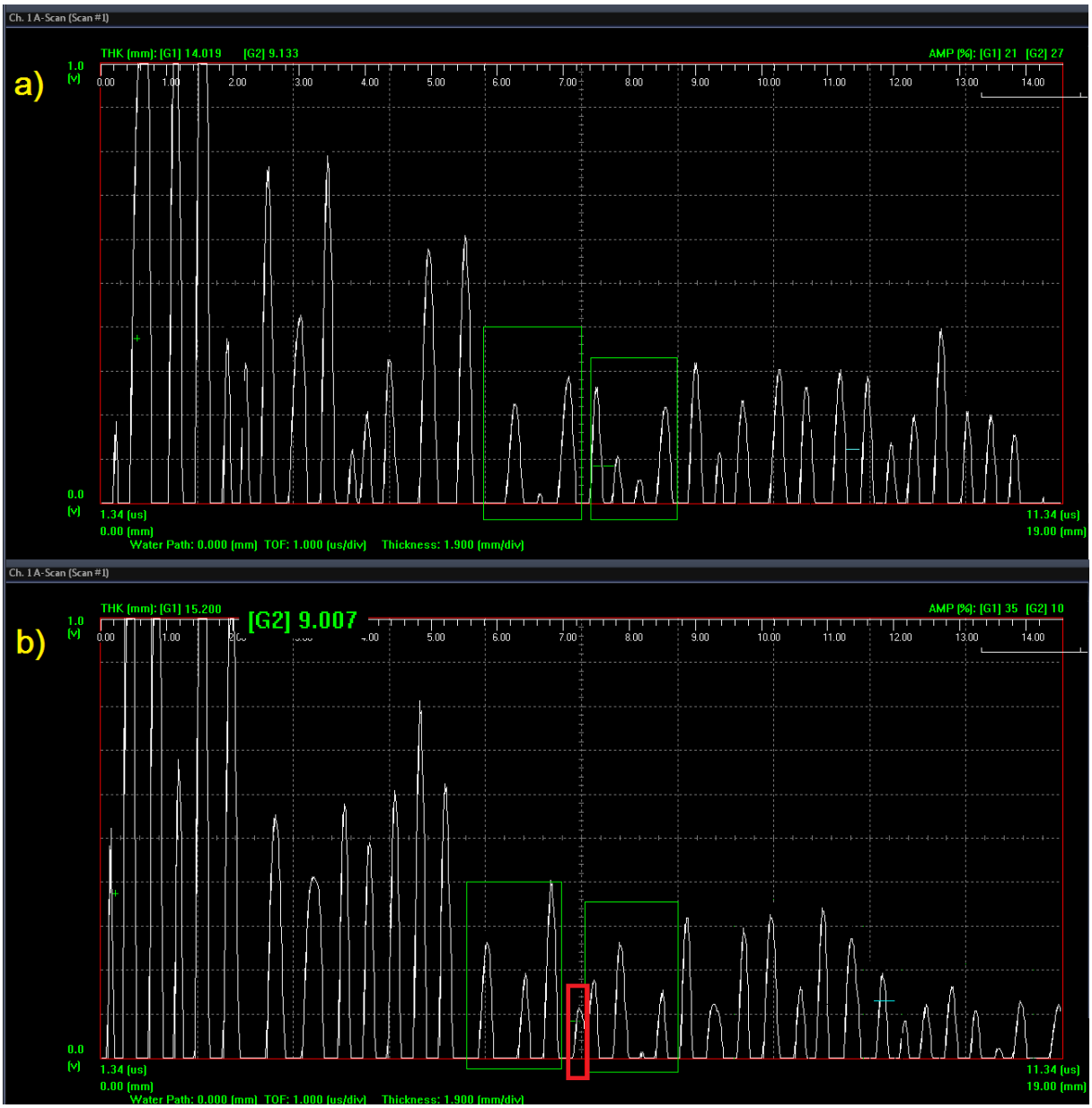

Figure 5.10 a) A-Scan on healthy area around defect No.9 b) A-Scan on defect No.9 (5 MHz).

Table 5.10 A-Scan settings for defect No.9 (5 MHz).

Transducers Frequency (MHz)					5		
No	Gain	Offset	Pulser Voltage	Damping	Energy Level	HP Filter	LP Filter
	dB	mV	V	Ohms	µJ	MHz	MHz
9	60.1	10	360	2000	470 pf	2	5

DAC SETTINGS			
Start Gain	End Gain	DAC Start	DAC End
dB	dB	µs	µs
0	7.5	0	12

Defect No.10 was detected only with the probe of 2.25 MHz.

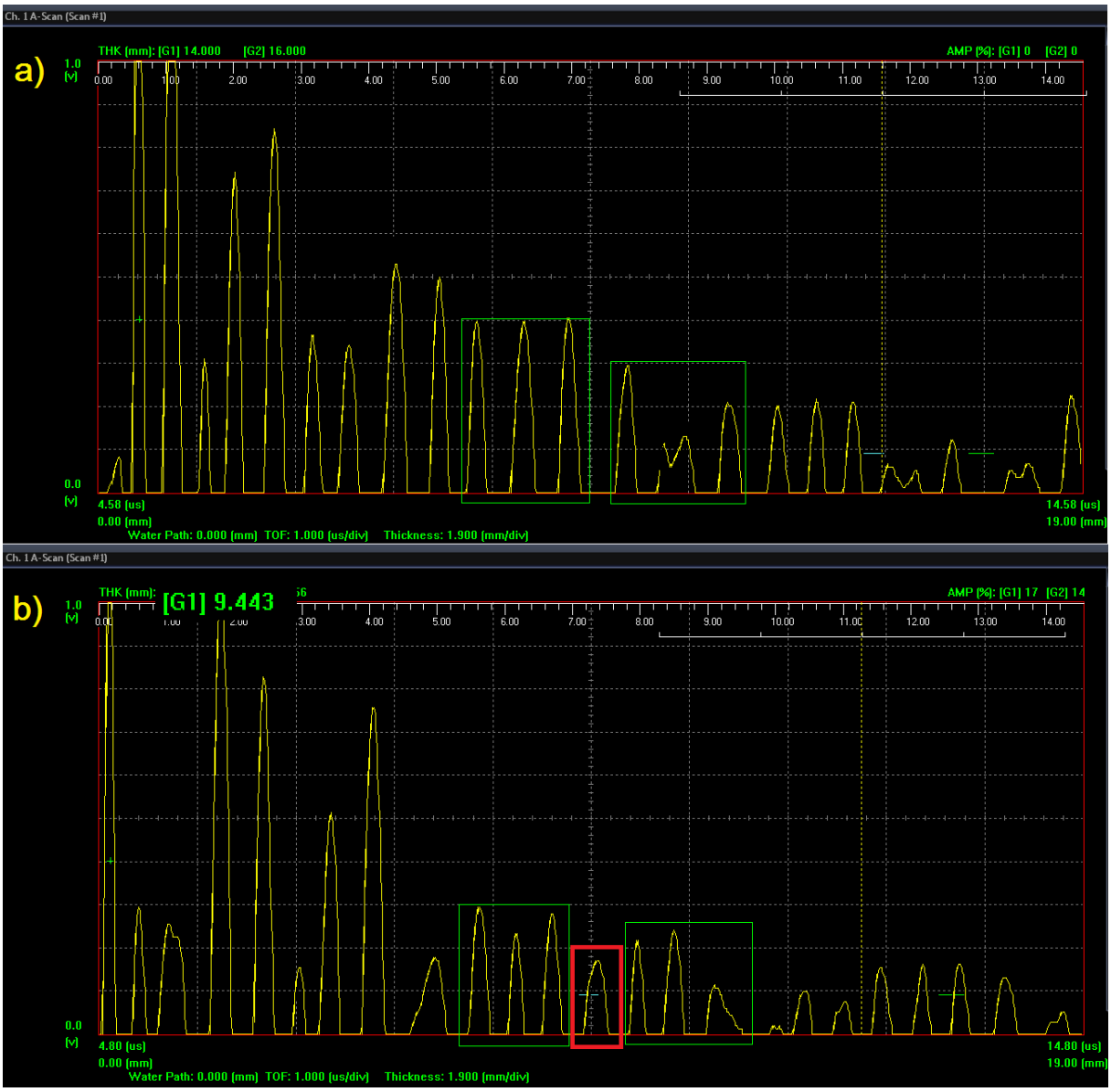

Figure 5.11 a) A-Scan on healthy area around defect No.10 b) A-Scan on defect No.10 (2.25 MHz).

Table 5.11 A-Scan settings for defect No.10 (2.25 MHz).

Transducers Frequency (MHz)					2.25		
No	Gain	Offset	Pulser Voltage	Damping	Energy Level	HP Filter	LP Filter
	dB	mV	V	Ohms	µJ	MHz	MHz
10	60.1	0	360	2000	470 pf	2	7.5

No.11 defect was the last defect of the 2nd Group detected with 5 MHz probe.

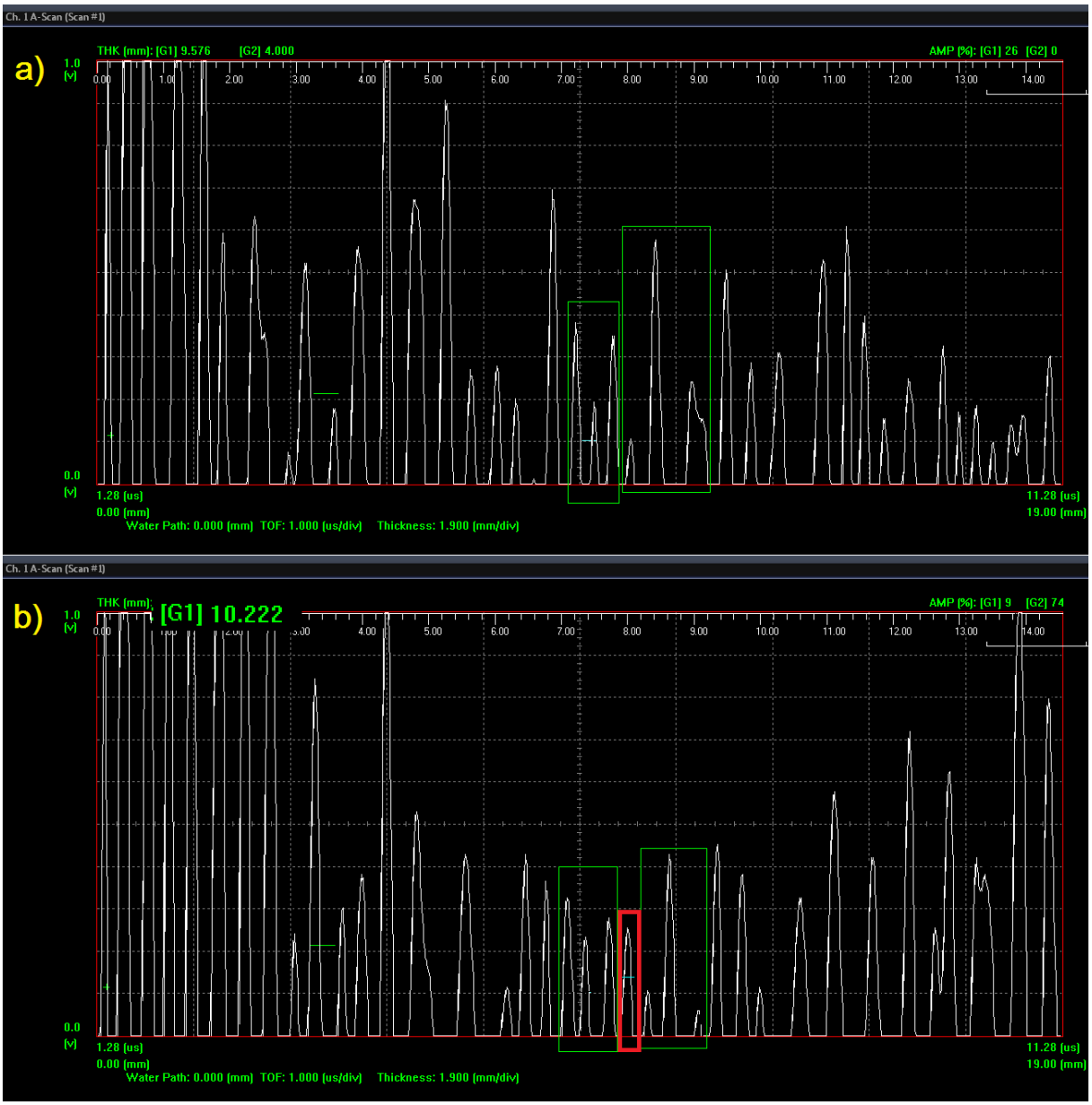

Figure 5.12 a) A-Scan on healthy area around defect No.11 b) A-Scan on defect No.11 (5 MHz).

Table 5.12 A-Scan settings for defect No.11 (5 MHz).

Transducers Frequency (MHz)					5		
No	Gain	Offset	Pulser Voltage	Damping	Energy Level	HP Filter	LP Filter
	dB	mV	V	Ohms	µJ	MHz	MHz
11	60.1	10	360	2000	470 pf	2	7.5

DAC SETTINGS			
Start Gain	End Gain	DAC Start	DAC End
dB	dB	µs	µs
0	7.5	0	12

The rest of the defects of the 2nd Group were detected only with the transducer with frequency 2.25 MHz. The signals and settings of them are presented below.

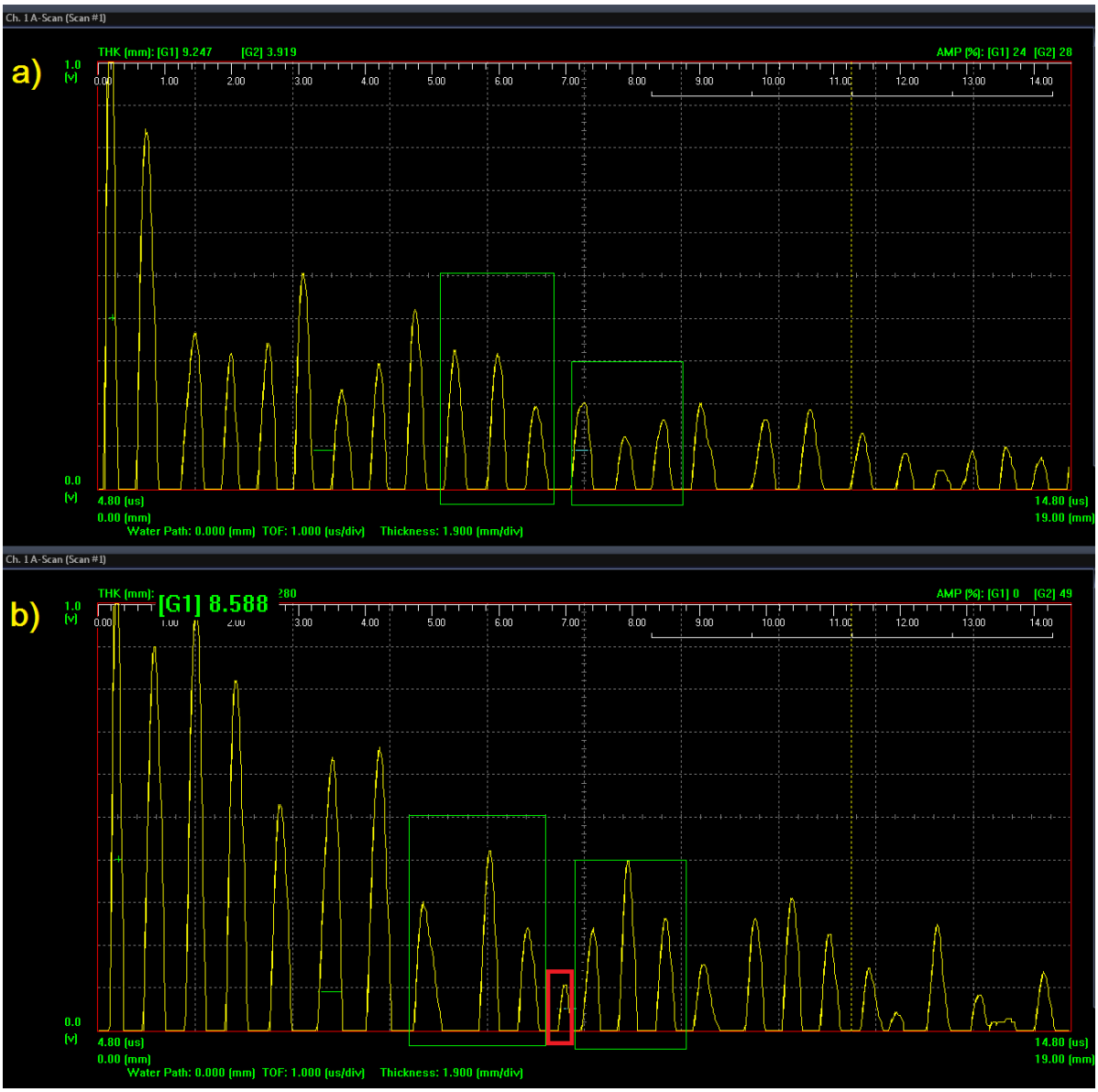

Figure 5.13 a) A-Scan on healthy area around defect No.12 b) A-Scan on defect No.12 (2.25 MHz).

Table 5.13 A-Scan settings for defect No.12 (2.25 MHz).

Transducers Frequency (MHz)					2.25		
No	Gain	Offset	Pulser Voltage	Damping	Energy Level	HP Filter	LP Filter
	dB	mV	V	Ohms	μJ	MHz	MHz
12	60.1	0	360	2000	470 pf	2	7.5

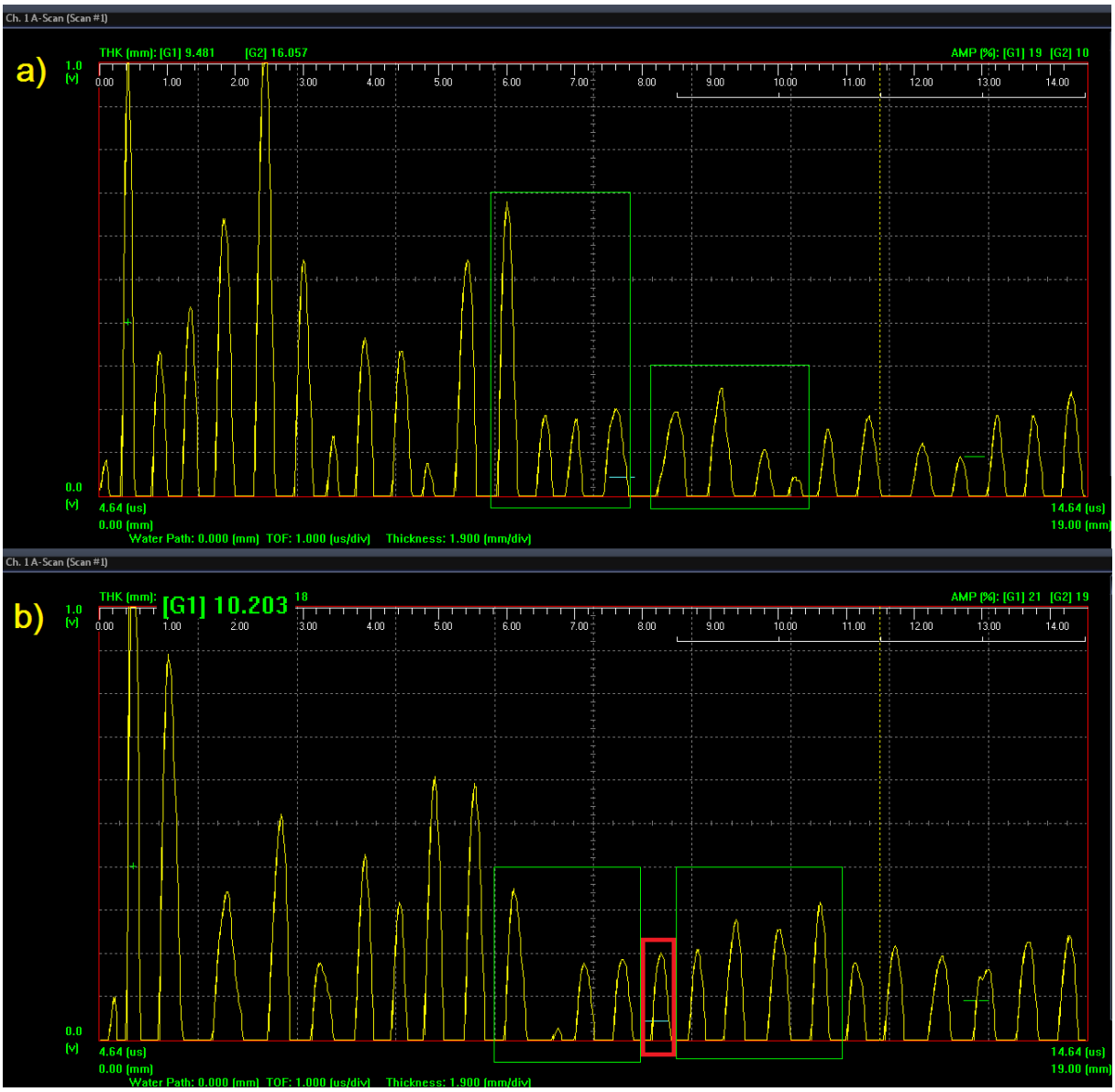

Figure 5.14 a) A-Scan on healthy area around defect No.13 b) A-Scan on defect No.13 (2.25 MHz).

Table 5.14 A-Scan settings for defect No.13 (2.25 MHz).

Transducers Frequency (MHz)					2.25		
No	Gain	Offset	Pulser Voltage	Damping	Energy Level	HP Filter	LP Filter
	dB	mV	V	Ohms	µJ	MHz	MHz
13	60.1	0	360	2000	470 pf	2	7.5

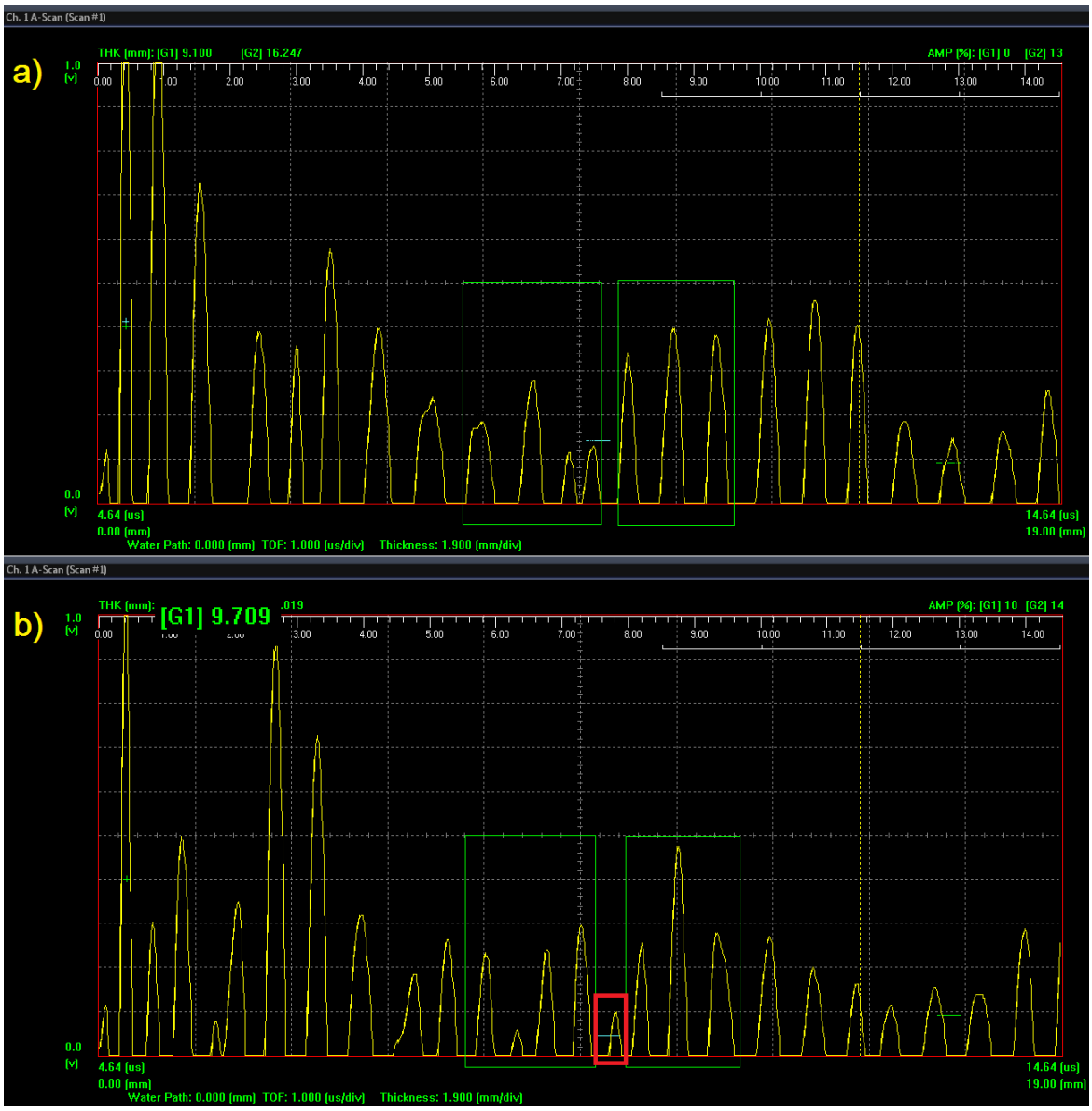

Figure 5.15 a) A-Scan on healthy area around defect No.14 b) A-Scan on defect No.14 (2.25 MHz).

Table 5.15 A-Scan settings for defect No.14 (2.25 MHz).

Transducers Frequency (MHz)					2.25		
No	Gain	Offset	Pulser Voltage	Damping	Energy Level	HP Filter	LP Filter
	dB	mV	V	Ohms	µJ	MHz	MHz
14	60.1	0	360	2000	470 pf	2	7.5

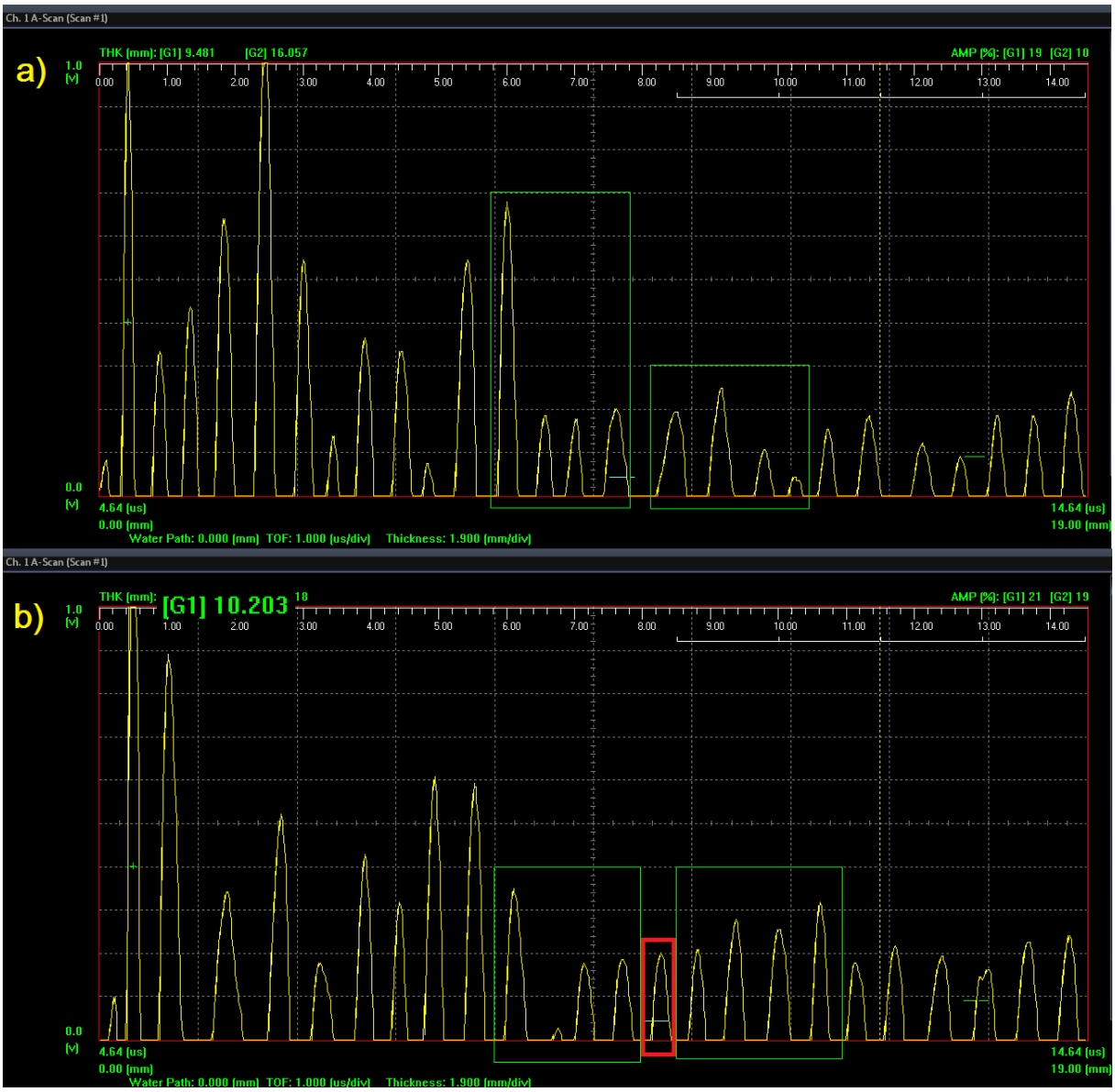

Figure 5.16 a) A-Scan on healthy area around defect No.15 b) A-Scan on defect No.15 (2.25 MHz).

Table 5.16 A-Scan settings for defect No.15 (2.25 MHz).

Transducers Frequency (MHz)					2.25		
No	Gain	Offset	Pulser Voltage	Damping	Energy Level	HP Filter	LP Filter
	dB	mV	V	Ohms	µJ	MHz	MHz
15	60.1	0	360	2000	470 pf	2	7.5

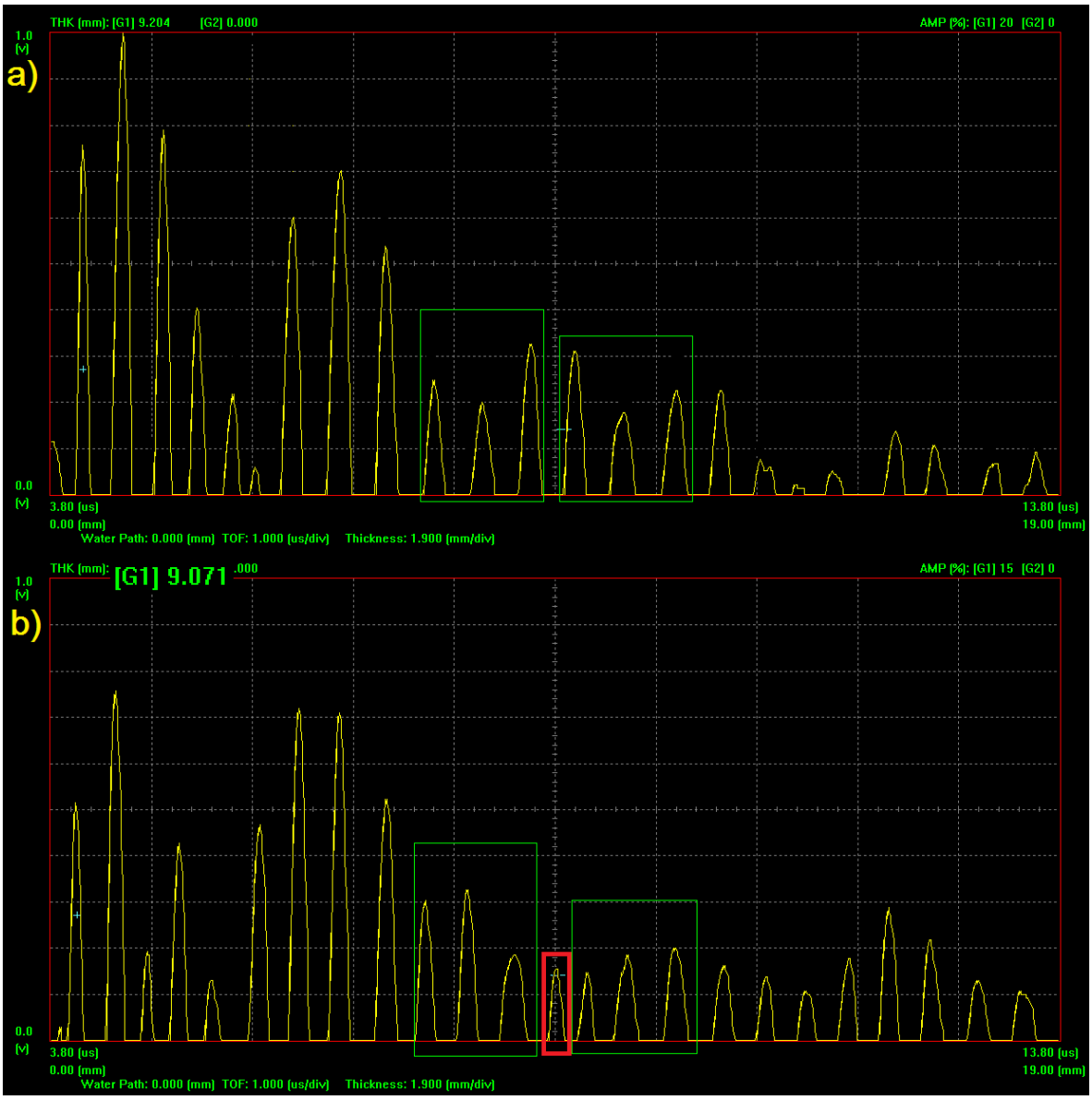

Figure 5.17 a) A-Scan on healthy area around defect No.16 b) A-Scan on defect No.16 (2.25 MHz).

Table 5.17 A-Scan settings for defect No.16 (2.25 MHz).

Transducers Frequency (MHz)					2.25		
No	Gain	Offset	Pulser Voltage	Damping	Energy Level	HP Filter	LP Filter
	dB	mV	V	Ohms	µJ	MHz	MHz
16	60.1	0	380	2000	470 pf	2	7.5

The last Group of defects (d=4 mm) starts with No.17, which was detected with both probes.

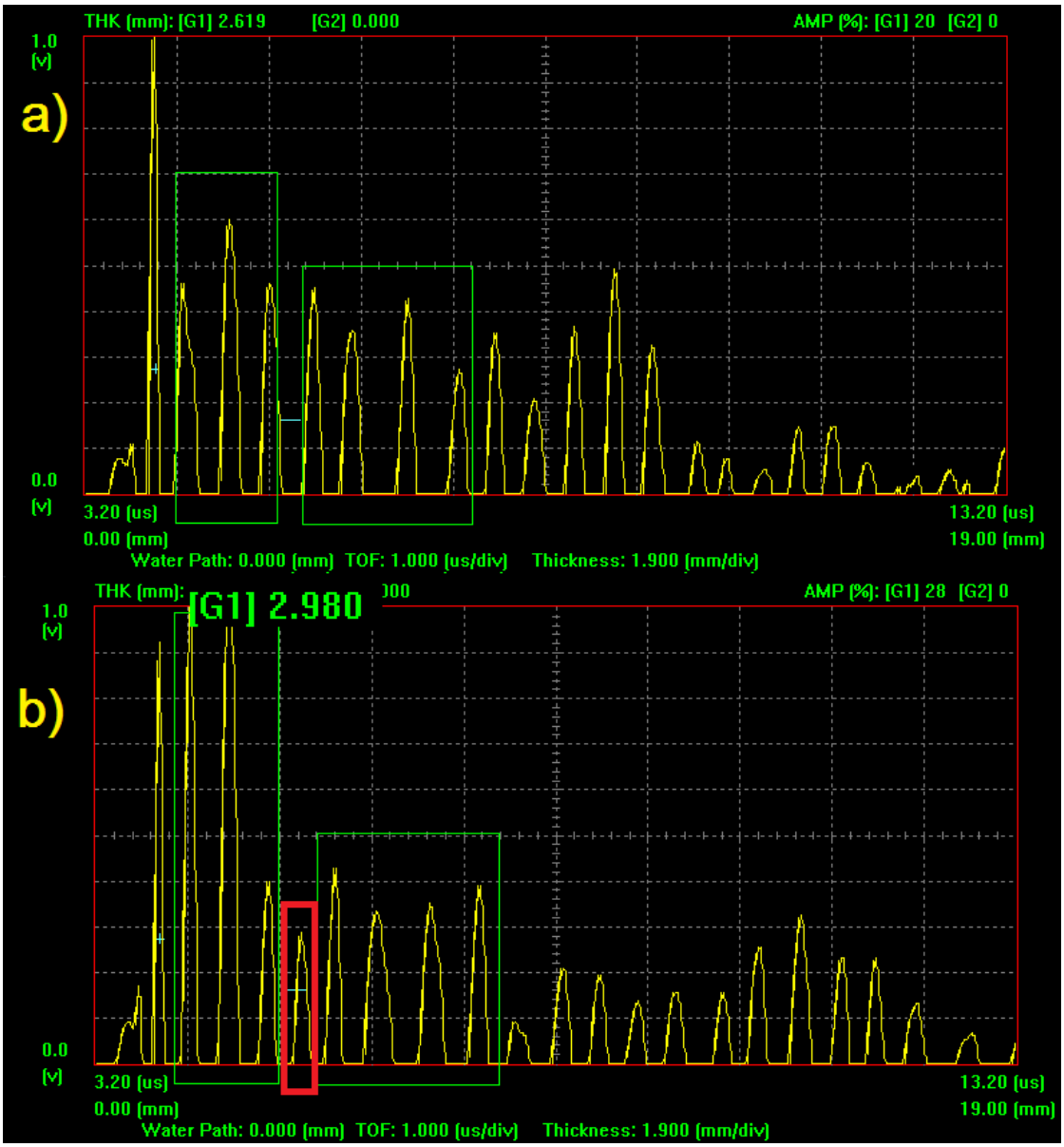

Figure 5.18 a) A-Scan on healthy area around defect No.17 b) A-Scan on defect No.17 (2.25 MHz).

Table 5.18 A-Scan settings for defect No.17 (2.25 MHz).

Transducers Frequency (MHz)					2.25		
No	Gain	Offset	Pulser Voltage	Damping	Energy Level	HP Filter	LP Filter
	dB	mV	V	Ohms	µJ	MHz	MHz
17	60.1	9	380	40.5	820 pf	2	5

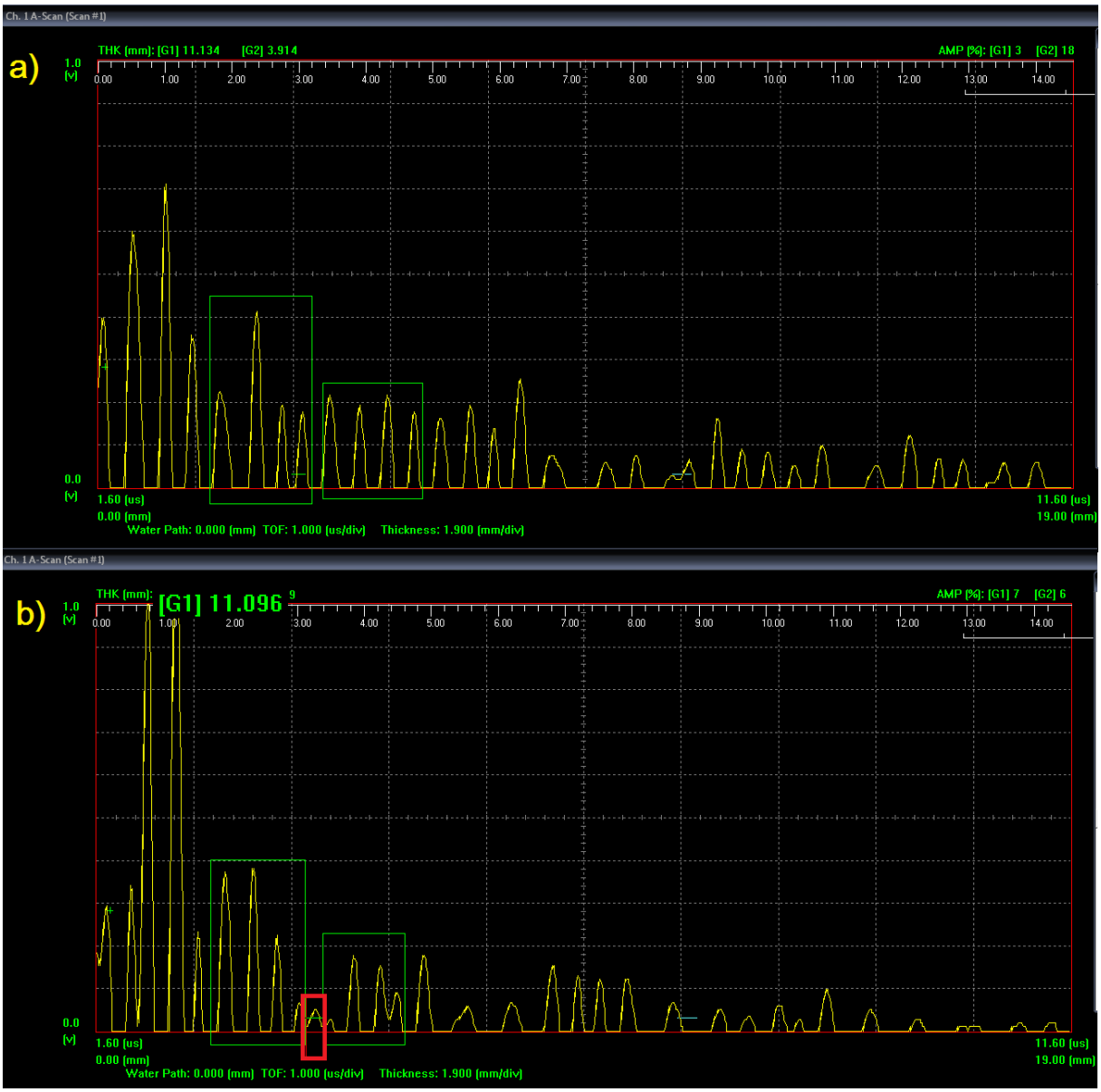

Figure 5.19 a) A-Scan on healthy area around defect No.17 b) A-Scan on defect No.17 (5 MHz).

Table 5.19 A-Scan settings for defect No.17 (5 MHz).

Transducers Frequency (MHz)					5		
No	Gain	Offset	Pulser Voltage	Damping	Energy Level	HP Filter	LP Filter
	dB	mV	V	Ohms	µJ	MHz	MHz
17	60.1	0	360	43.8	470 pf	2	5

No.18 and No.20 were detected with 2.25 MHz probe, while No.19 was detected with 5 MHz probe.

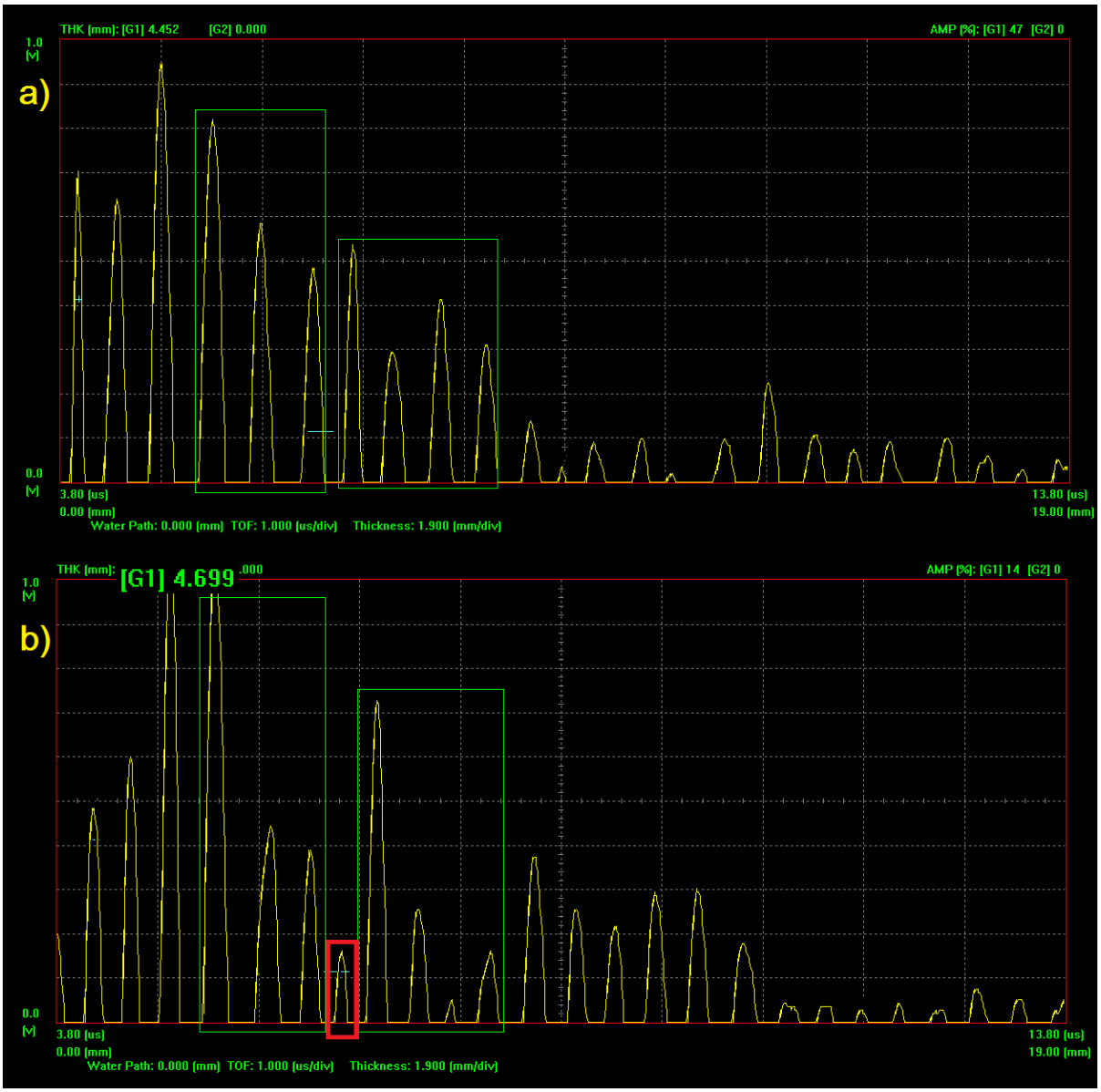

Figure 5.20 a) A-Scan on healthy area around defect No.18 b) A-Scan on defect No.18 (2.25 MHz).

Table 5.20 A-Scan settings for defect No.18 (2.25 MHz).

Transducers Frequency (MHz)					2.25		
No	Gain	Offset	Pulser Voltage	Damping	Energy Level	HP Filter	LP Filter
	dB	mV	V	Ohms	µJ	MHz	MHz
18	60.1	10	380	40.5	820 pf	2	5

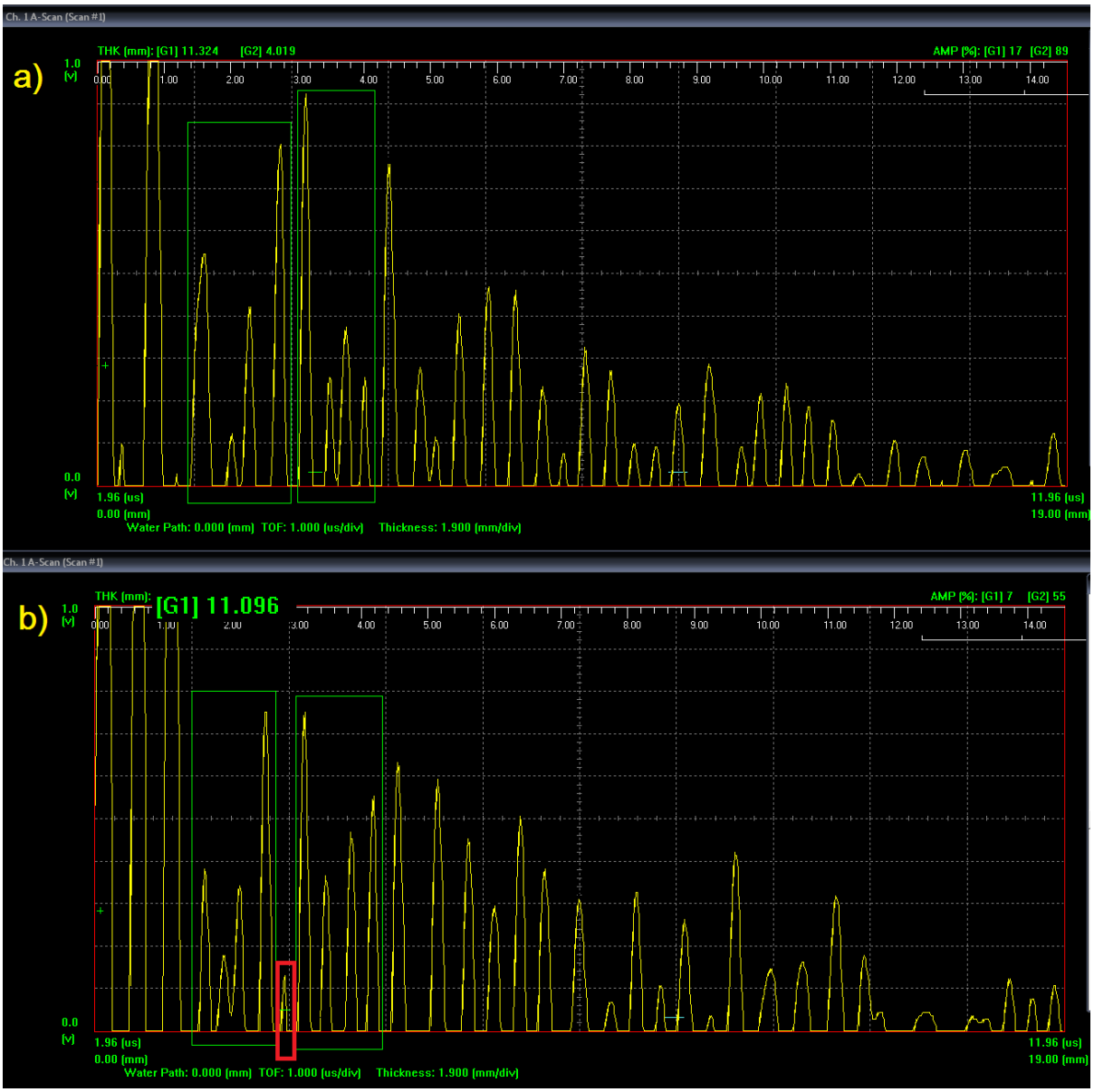

Figure 5.21 a) A-Scan on healthy area around defect No.19 b) A-Scan on defect No.19 (5 MHz).

Table 5.21 A-Scan settings for defect No.19 (5 MHz).

Transducers Frequency (MHz)					5		
No	Gain	Offset	Pulser Voltage	Damping	Energy Level	HP Filter	LP Filter
	dB	mV	V	Ohms	µJ	MHz	MHz
19	60.1	0	360	43.8	470 pf	2	5

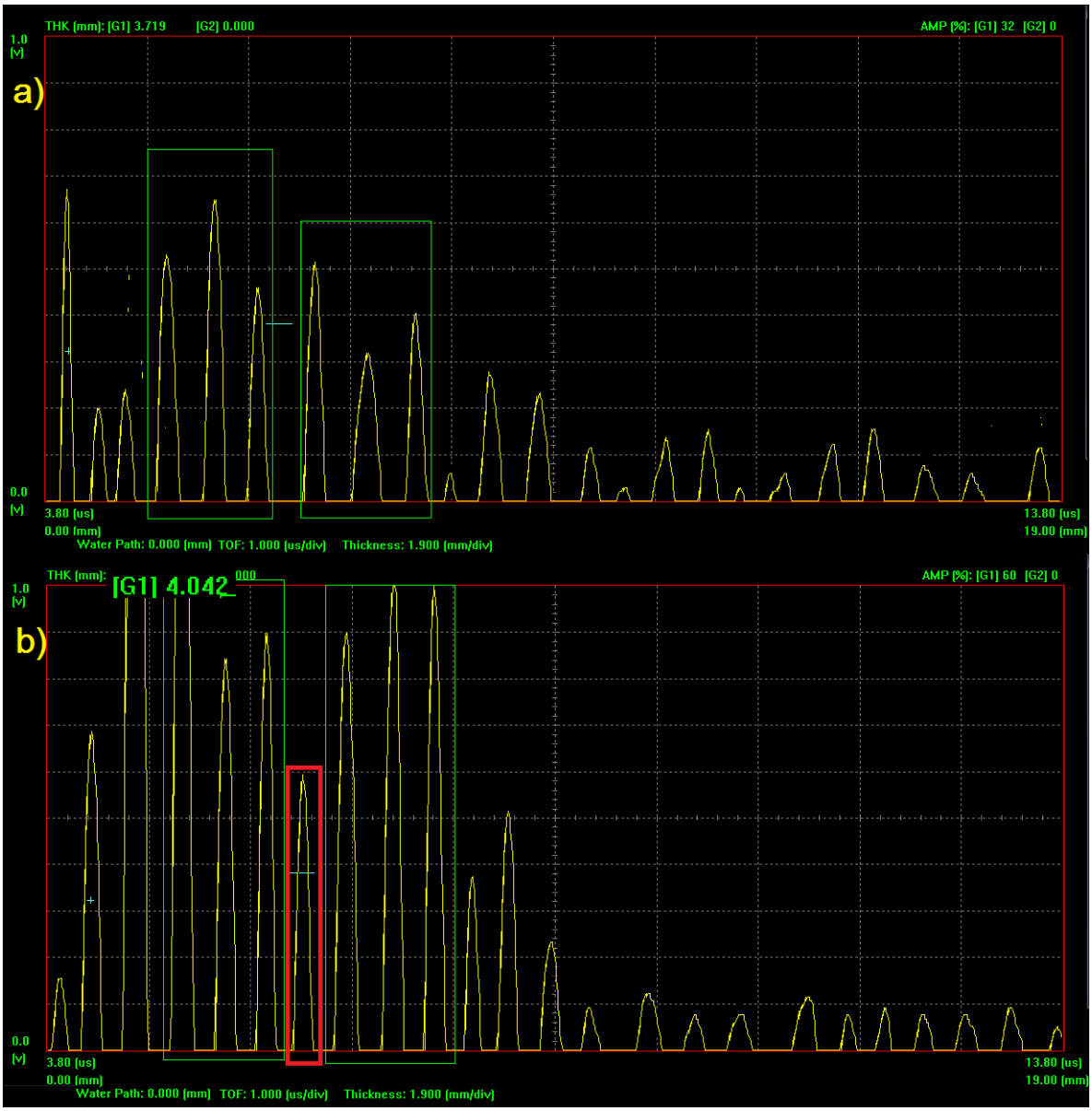

Figure 5.22 a) A-Scan on healthy area around defect No.20 b) A-Scan on defect No.20 (2.25 MHz).

Table 5.22 A-Scan settings for defect No.20 (2.25 MHz).

Transducers Frequency (MHz)					2.25		
No	Gain	Offset	Pulser Voltage	Damping	Energy Level	HP Filter	LP Filter
	dB	mV	V	Ohms	µJ	MHz	MHz
20	60.1	10	380	40.5	470 pf	2	7.5

Defect No.21 was detected with both probes. No. 22 and No. 23 were detected with 2.25 MHz probe.

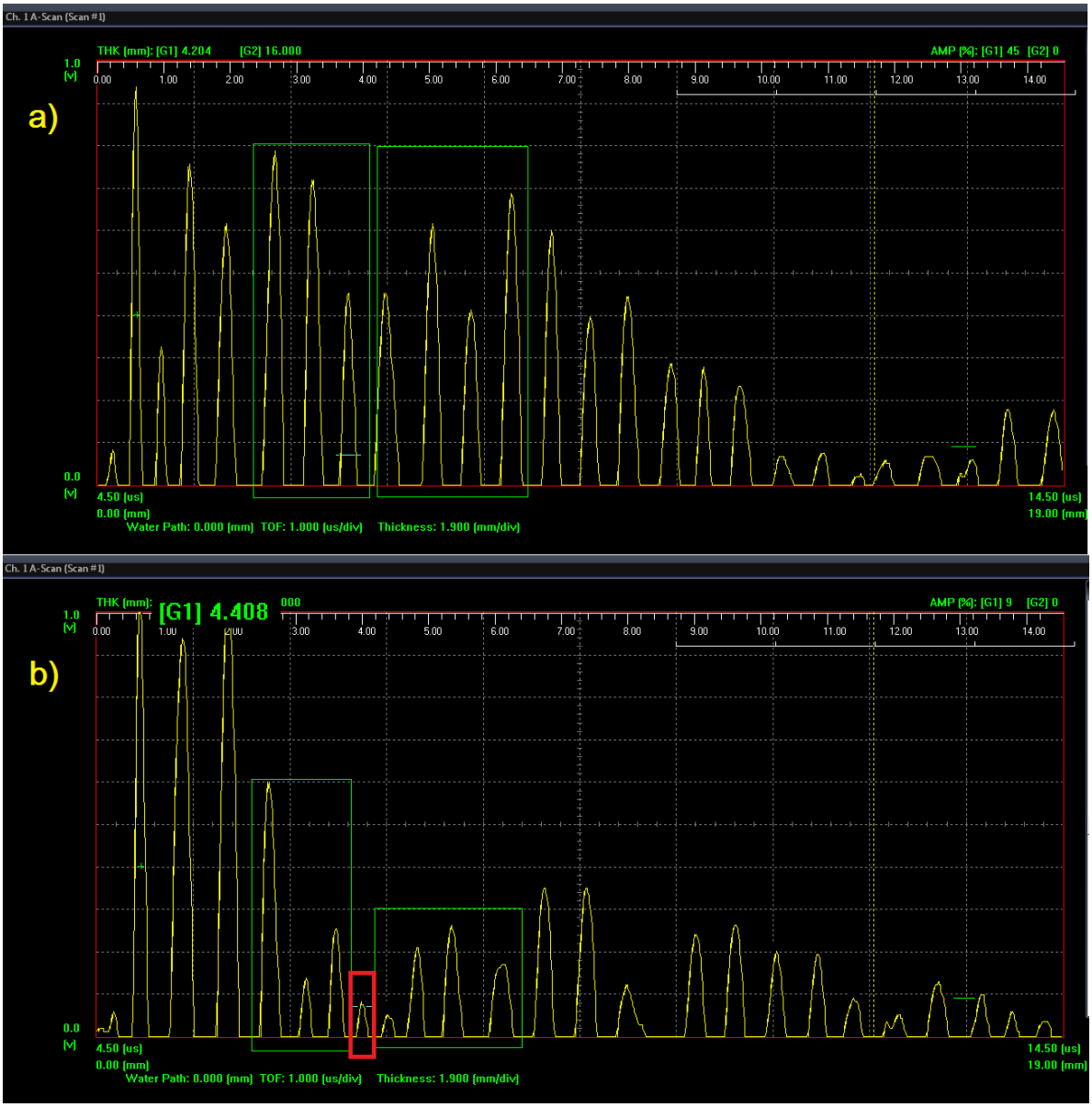

Figure 5.23 a) A-Scan on healthy area around defect No.21 b) A-Scan on defect No.21 (2.25 MHz).

Table 5.23 A-Scan settings for defect No.21 (2.25 MHz).

Transducers Frequency (MHz)					2.25		
No	Gain	Offset	Pulser Voltage	Damping	Energy Level	HP Filter	LP Filter
	dB	mV	V	Ohms	µJ	MHz	MHz
21	60.1	0	360	43.8	470 pf	2	7.5

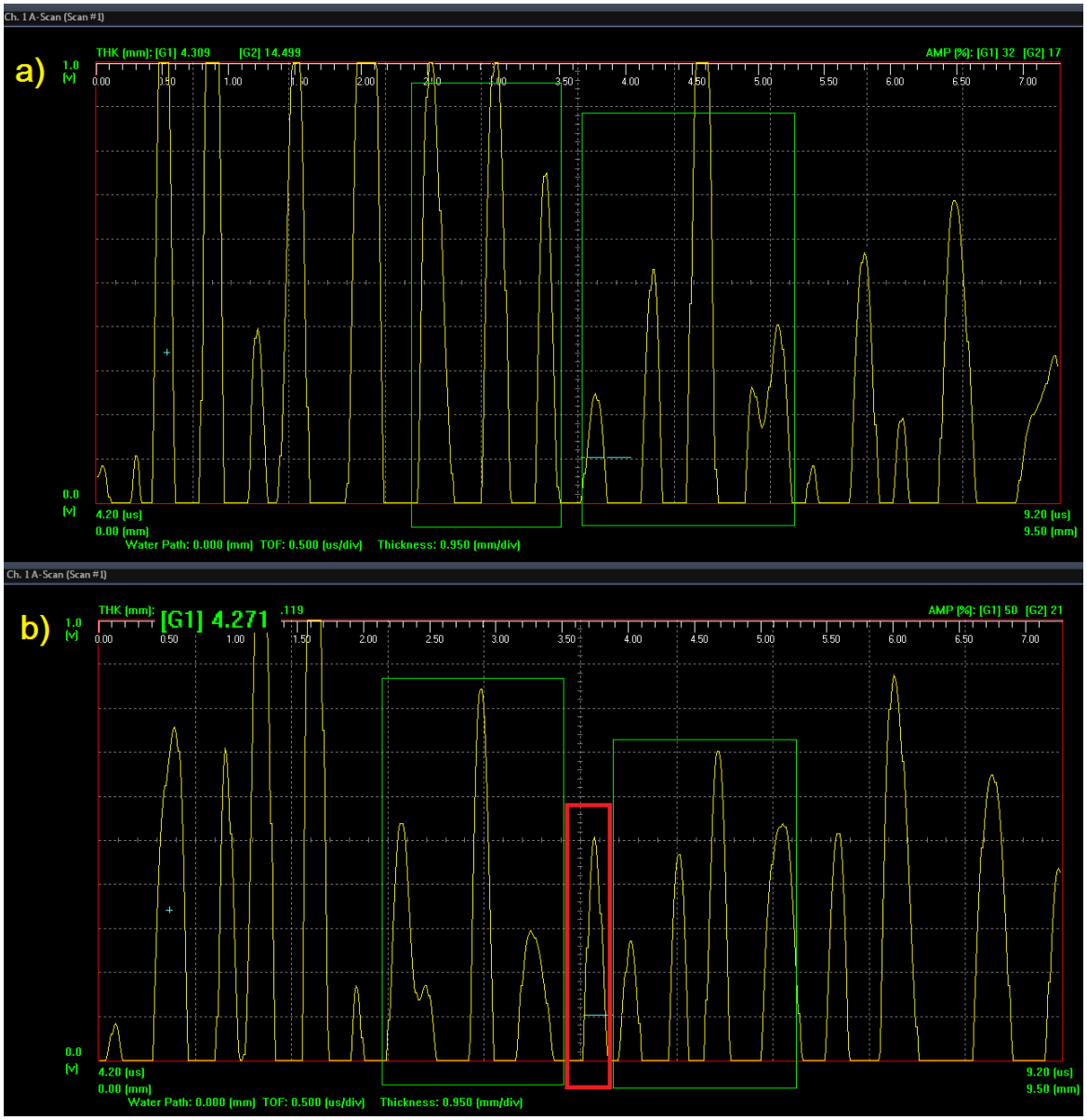

Figure 5.24 a) A-Scan on healthy area around defect No.21 b) A-Scan on defect No.21 (5 MHz).

Table 5.24 A-Scan settings for defect No.21 (5 MHz).

Transducers Frequency (MHz)					5		
No	Gain	Offset	Pulser Voltage	Damping	Energy Level	HP Filter	LP Filter
	dB	mV	V	Ohms	µJ	MHz	MHz
21	60.1	0	380	43.8	470 pf	2	7.5

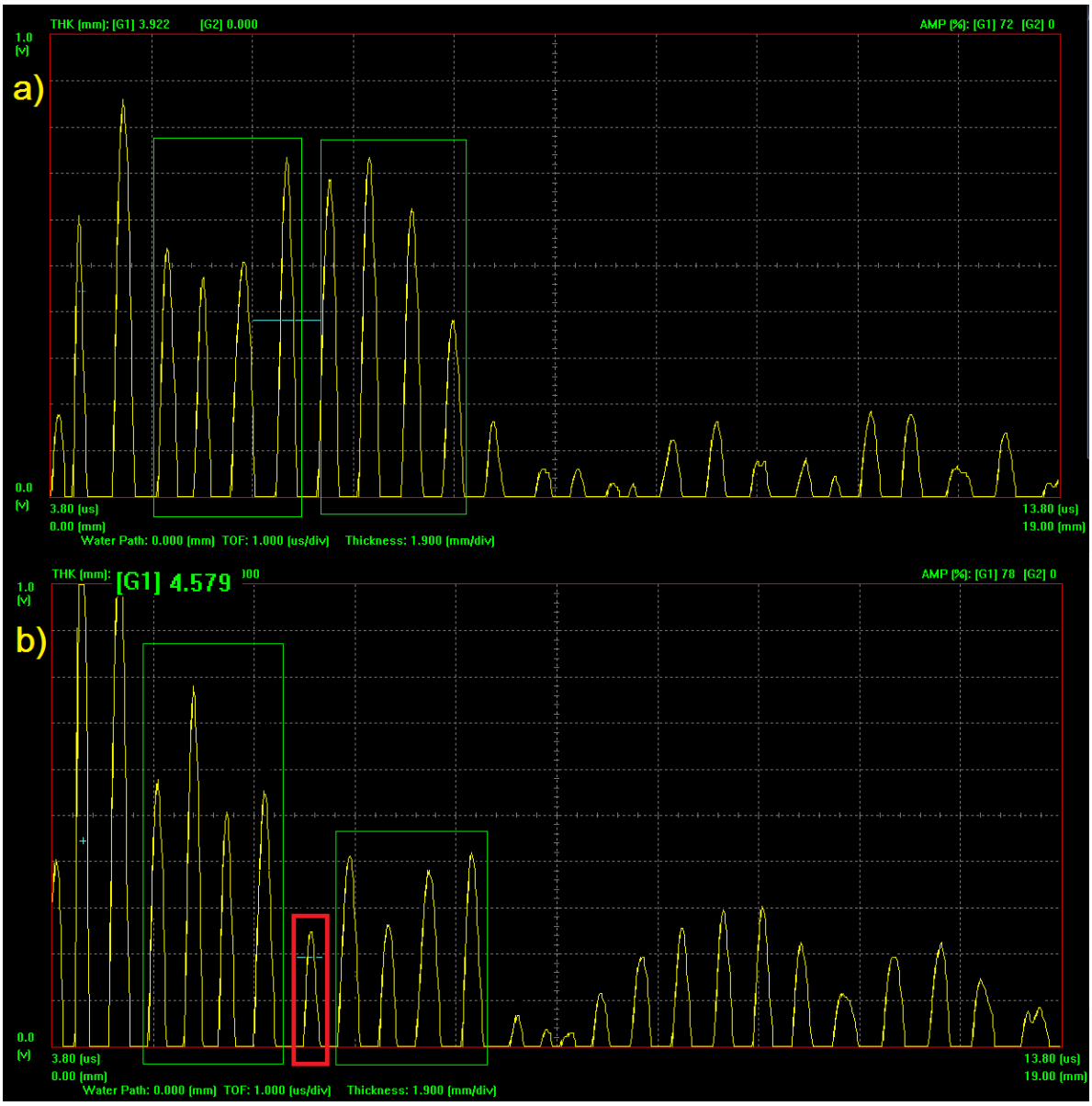

Figure 5.25 a) A-Scan on healthy area around defect No.22 b) A-Scan on defect No.22 (2.25 MHz).

Table 5.25 A-Scan settings for defect No.22 (2.25 MHz).

Transducers Frequency (MHz)					2.25		
No	Gain	Offset	Pulser Voltage	Damping	Energy Level	HP Filter	LP Filter
	dB	mV	V	Ohms	µJ	MHz	MHz
22	60.1	10	380	40.5	470 pf	2	7.5

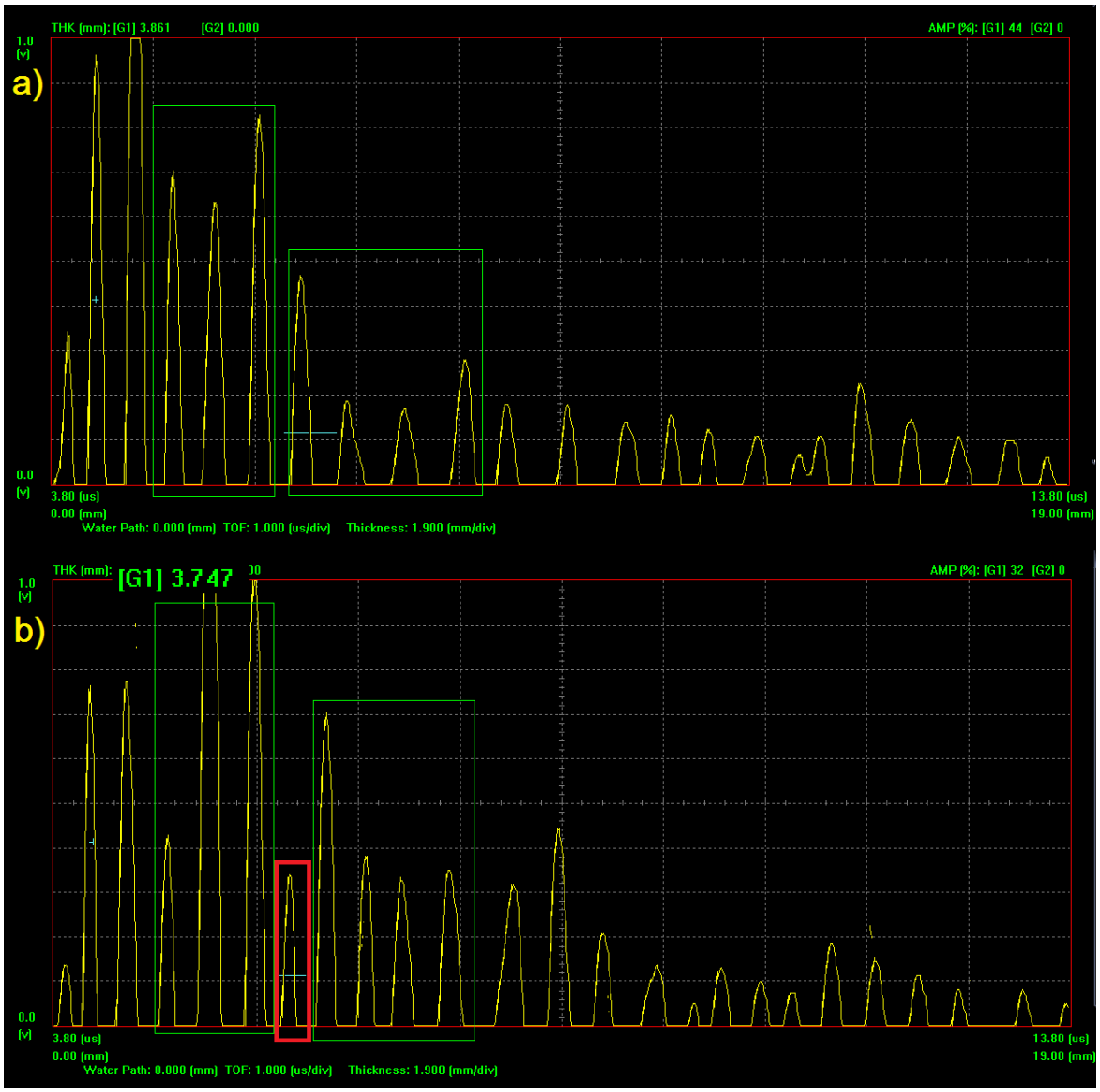

Figure 5.26 a) A-Scan on healthy area around defect No.23 b) A-Scan on defect No.23 (2.25 MHz).

Table 5.26 A-Scan settings for defect No.23 (2.25 MHz).

Transducers Frequency (MHz)					2.25		
No	Gain	Offset	Pulser Voltage	Damping	Energy Level	HP Filter	LP Filter
	dB	mV	V	Ohms	µJ	MHz	MHz
23	60.1	0	360	43.8	470 pf	2	7.5

The last defect, No. 24, was detected with the 5 MHz frequency probe.

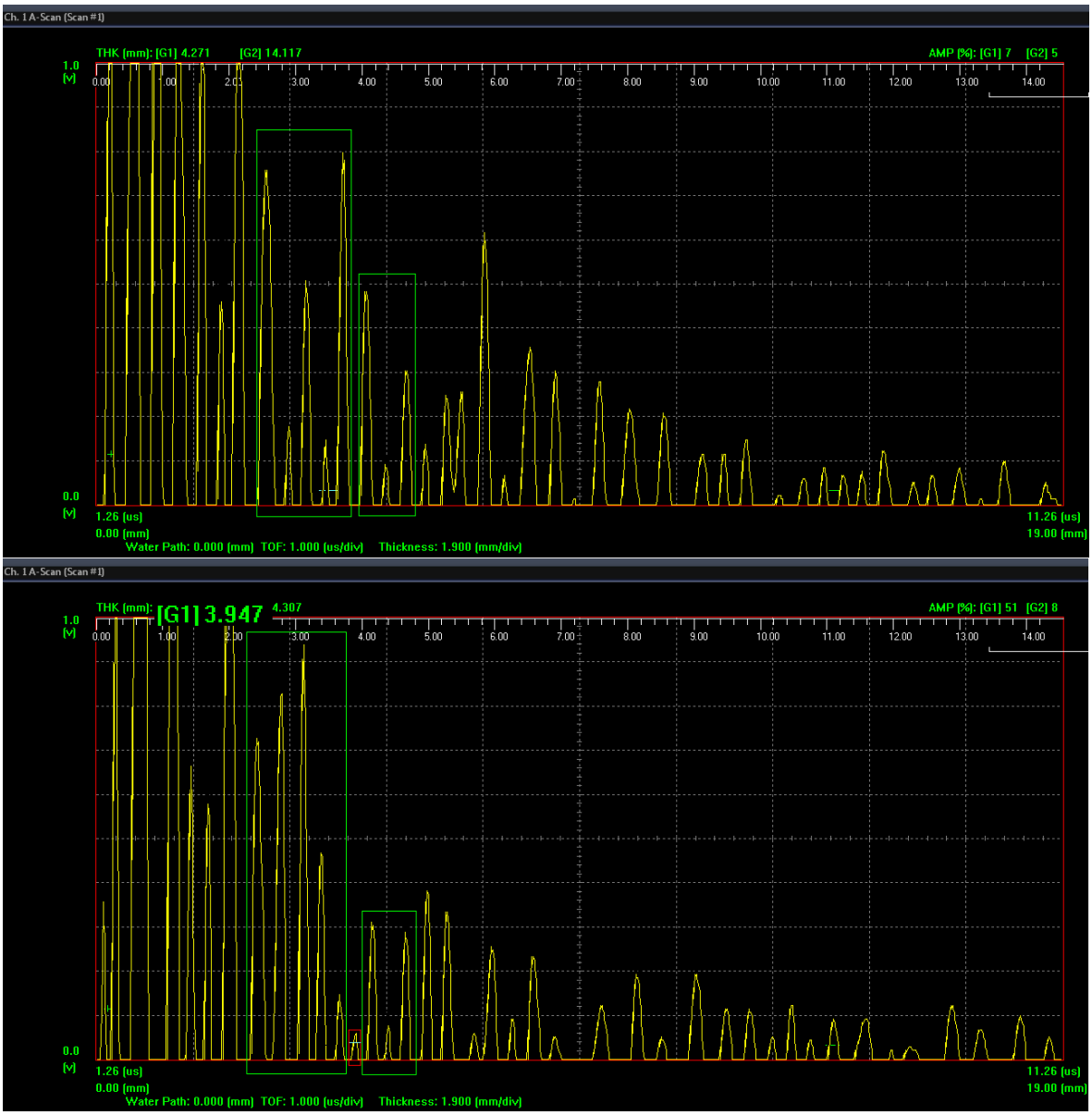

Figure 5.27 a) A-Scan on healthy area around defect No.24 b) A-Scan on defect No.24 (5 MHz).

Table 5.27 A-Scan settings for defect No.24 (5 MHz).

Transducers Frequency (MHz)					5		
No	Gain	Offset	Pulser Voltage	Damping	Energy Level	HP Filter	LP Filter
	dB	mV	V	Ohms	µJ	MHz	MHz
24	60.1	10	360	43.8	470 pf	2	7.5

5.1.2. Aggregated results of A- Scan

One third of the defects could not be detected with A-Scanning, using only 2.25 MHz probe. Meanwhile 5 MHz probe was useful for the detection of less that the half defects. That is reasonable, due to the high penetration skills that are needed for composite materials. Both probes detected overall 22 out of 24 defects. For Group 1, which contains the deepest

defects, 2.25 MHz probe gave results for almost all the defects, namely for 6 out of 8 defects. This group of defects was not satisfyingly detectable from 5 MHz probe, which gave results for 2 out of 8 defects. That was expected according to the previous reference that high penetration occurs with low frequency probes. In the medium depth of 9.25mm (Group 2), 2.25 MHz probe gave more results, namely 6 out of 8 defects. As expected, some of the defects that belong to Group 3 and lay closer to the surface of the cylinder were detected with 2.25 MHz, while other were detected with 5 MHz probe, which provides better resolution, but lower penetration.

All the above mentioned information is summed up in Table 5.28. It allows certain conclusions to be drawn, such as that deviations from the theoretical data do not exceed 1mm and that lower frequency indeed led to better results, especially in deeper distances.

Table 5.28 A-Scan results.

Theoretical Data					A-Scan Calculations		Deviation	
	Angular Position	Longitudinal Position	Defect Diameter	Depth Theoretical	2.25 MHz Depth Calculated	5 MHz Depth Calculated	2.25 MHz	5 MHz
No[1]	φ (deg)	Lx (mm)	2r (mm)	d_th (mm)	d_calc (mm)	d_calc (mm)	(mm)	
1	50	50	10	14.2	14.3	-	0.1	-
2	200	50	20	14.2	-	-	-	-
3	160	170	40	14.2	14.5	-	0.3	-
4	270	180	30	14.2	14.33	13.6	0.13	0.6
5	45	240	20	14.2	14.6	-	0.4	-
6	280	320	40	14.2	-	-	-	-
7	90	320	30	14.2	14.3	-	0.1	-
8	340	390	10	14.2	14.6	14	0.4	0.2
9	50	45	40	9.25	-	9	-	0.25
10	270	180	10	9.25	9.4	-	0.15	-
11	60	50	30	9.25	-	10.2	-	0.95
12	300	220	20	9.25	8.6	-	0.65	-
13	120	120	10	9.25	10.2	-	0.95	-
14	230	310	30	9.25	9.7	-	0.45	-
15	120	130	20	9.25	10.2	-	0.95	-
16	330	350	40	9.25	9	-	0.25	-
17	85	40	10	4	2.98	4	1.02	0
18	200	50	40	4	4.7	-	0.7	-
19	60	150	20	4	-	3.5	-	0.5
20	220	200	10	4	4	-	0	-
21	120	300	30	4	4.4	4.27	0.4	0.27
22	300	230	30	4	4.6	-	0.6	-
23	90	380	40	4	3.7	-	0.4	-
24	340	370	20	4	-	3.9	-	0.1

[1] defects No. 3, 7, 10, 12, 17, 18, 20, 21, 24 have thickness of 2mm.

5.2. C-Scan Results

5.2.1. Detailed Presentation of the C-Scan Results

The procedure described in section 4.5 led to the results below. The produced image of the scanning of each defect is also illustrated in the Figures below (Figure 5.28 to Figure 5.48). The left part of each figure illustrates the depth that corresponds to the echo of the maximum amplitude at each point. The part that is considered to represent the defect is in a red circle. The measurement received from the Gate is written on the caption, according to the scale on the left of the figure. On the right side the maximum amplitude is being illustrated for each point. Furthermore, Table 5.29 with the basic settings of the equipment is available. The same settings were applied for all the defects.

Table 5.29 C-Scan settings for 2.25 MHz probe.

Transducers Frequency (MHz)				2.25		
Gain	Offset	Pulser Voltage	Damping	Energy Level	HP Filter	LP Filter
dB	mV	V	Ohms	μJ	MHz	MHz
45	4	380	2000	820 pf	2	7.5

Table 5.30 C-Scan settings for 3.5 MHz probe.

Transducers Frequency (MHz)				3.5		
Gain	Offset	Pulser Voltage	Damping	Energy Level	HP Filter	LP Filter
dB	mV	V	Ohms	μJ	MHz	MHz
45	5	360	2000	820	2	7.5

Starting with Group 1 (d=14.25mm), the results for each defect will be presented. No.1, No.2, No.3, No.4, No.5 and No.8 defects were detected only with the 2.25 MHz probe, while No.6 defect was not detectable at this point of the experimental procedure. Defect No. 7 gave a controversial result, which was not considered reliable and is not presented.

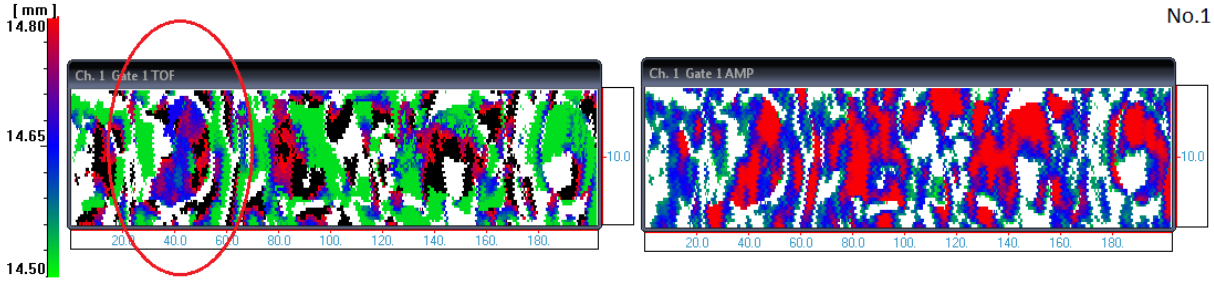

Figure 5.28 C- Scan (2.25 MHz) result No.1 (50, 50, 14.5), d_calc= 14.6 mm.

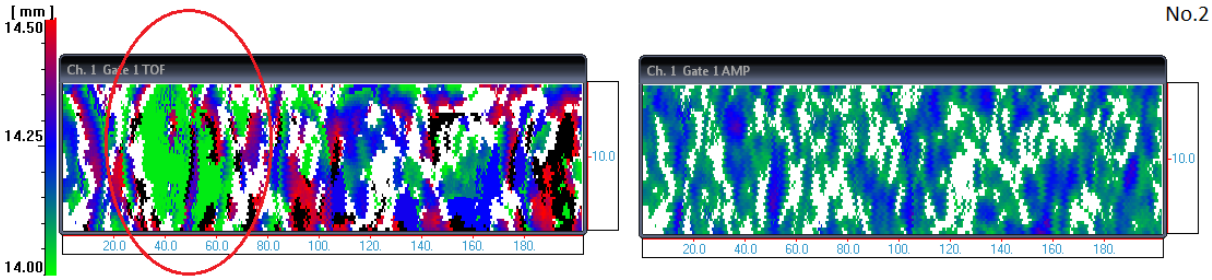

Figure 5.29 C- Scan (2.25 MHz) result No.2 (200, 50, 14.5), d_calc= 14.0 mm.

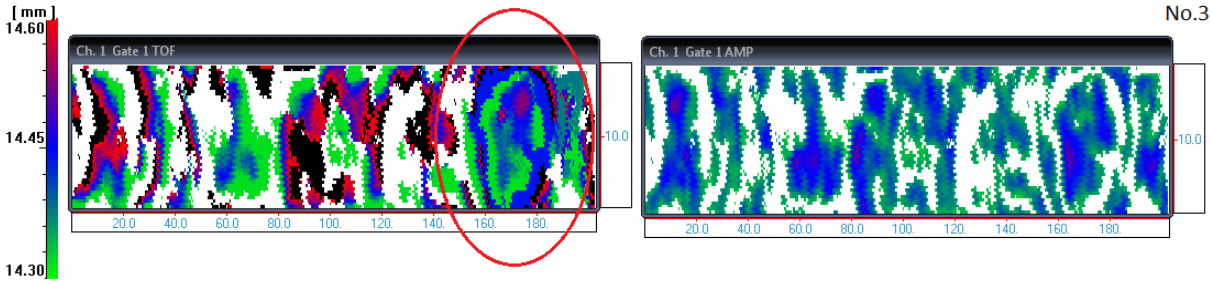

Figure 5.30 C- Scan result (2.25 MHz) No.3 (160, 170, 14.5), d_calc= 14.4 mm.

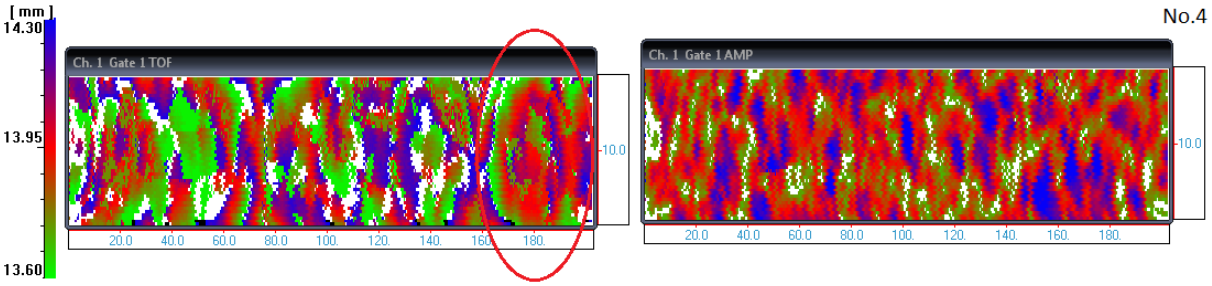

Figure 5.31 C- Scan result (2.25 MHz) No.4 (270, 180, 14.5), d_calc= 13.9 mm.

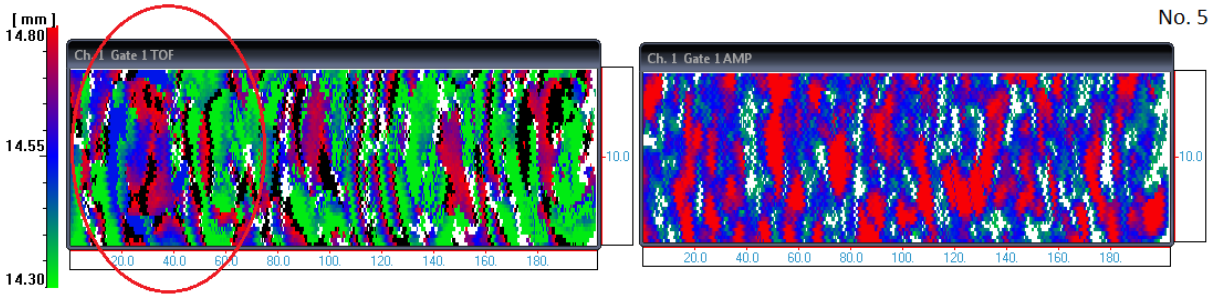

Figure 5.32 C- Scan result (2.25 MHz) No.5 (45, 240, 14.5), d_calc= 14.6 mm.

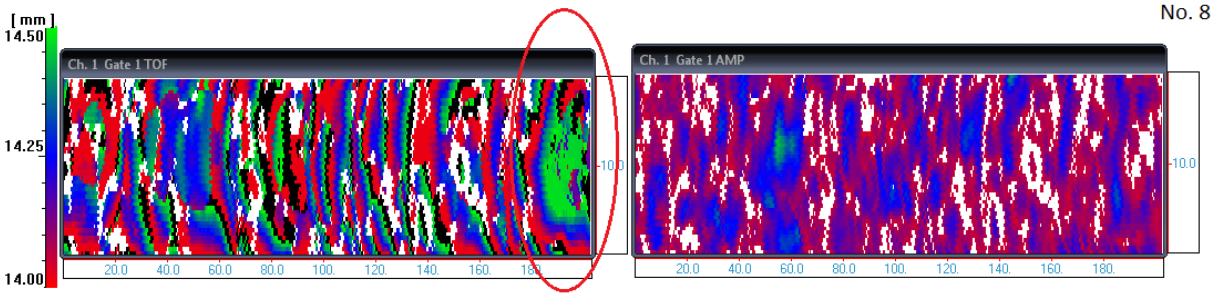

Figure 5.33 C- Scan result (2.25 MHz) No.8 (340, 390, 14.5), d_calc= 14.5 mm.

The 2nd Group of defects is at the depth of 9.25 mm. Defects No.9, No. 10, No. 11, No. 13, No.15 and No.16 were detected with 2.25 MHz probe, while No. 12 and No. 14 could not be detected.

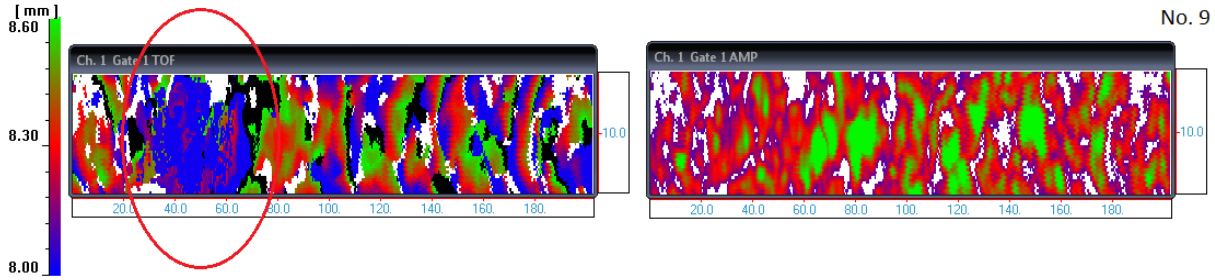

Figure 5.34 C- Scan result (2.25 MHz) No.9 (50, 45, 9.25), d_calc= 8 mm.

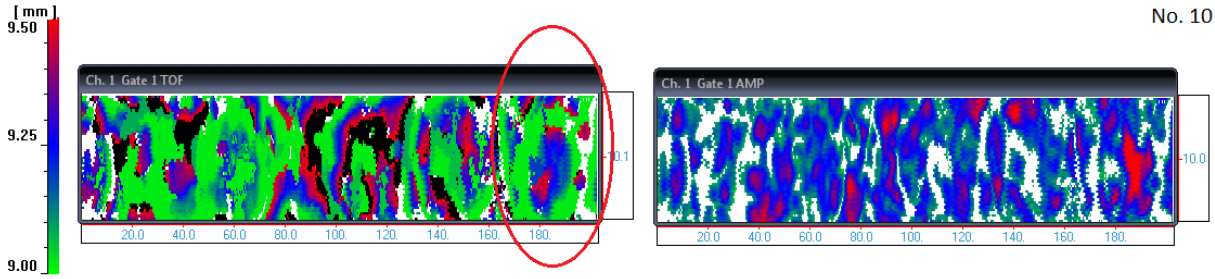

Figure 5.35 C- Scan result (2.25 MHz) No.10 (270, 180, 9.25), d_calc= 9.2 mm.

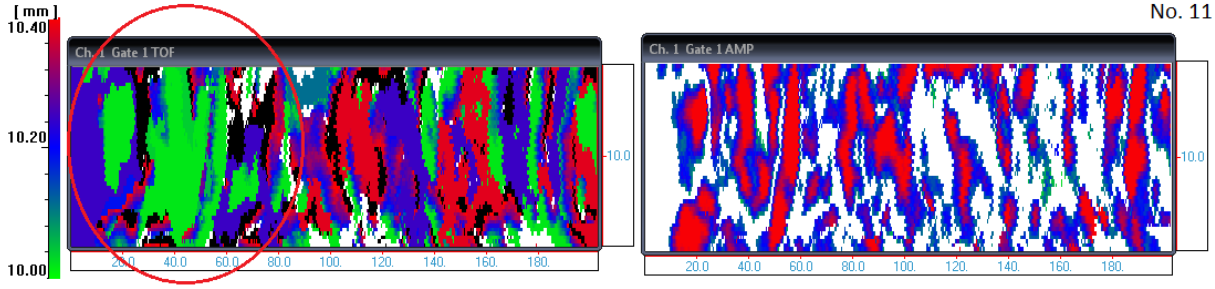

Figure 5.36 C- Scan result (2.25 MHz) No.11 (60, 50, 9.25), d_calc= 10 mm.

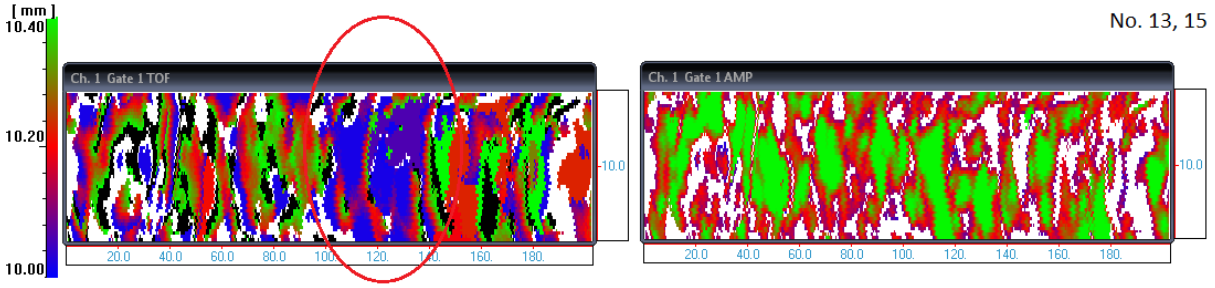

Figure 5.37 C- Scan result (2.25 MHz) No.13 (120, 120, 9.25) + No. 15 (120, 130, 9.25), d_calc=10 mm.

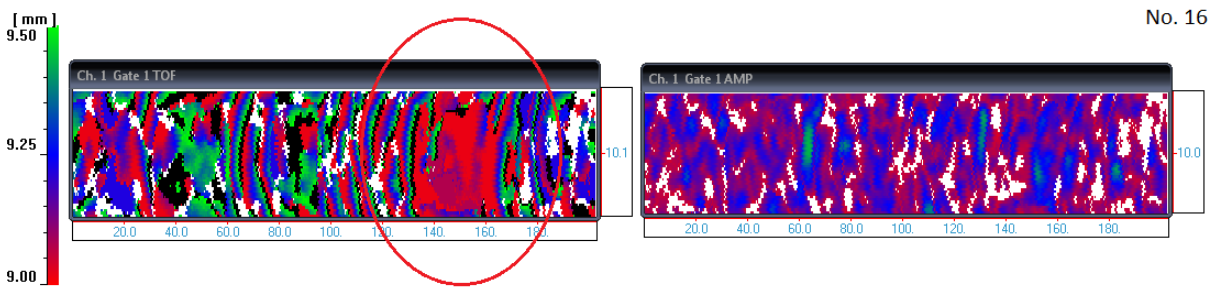

Figure 5.38 C- Scan result (2.25 MHz) No. 16 (330, 350, 9.25), d_calc=9 mm.

The last Group contains defects at the depth of 4 mm. All defects from No. 17 to No. 24 were detected with 2.25 MHz probe. Only defects No. 20 and No. 22 were also detected with probe of 3.5 MHz frequency. The figures below present the results.

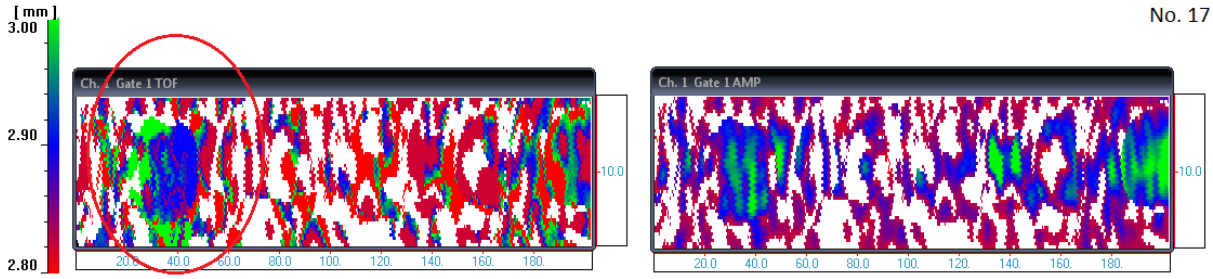

Figure 5.39 C- Scan result (2.25 MHz) No. 17 (85, 40, 4), d_calc=2.9 mm.

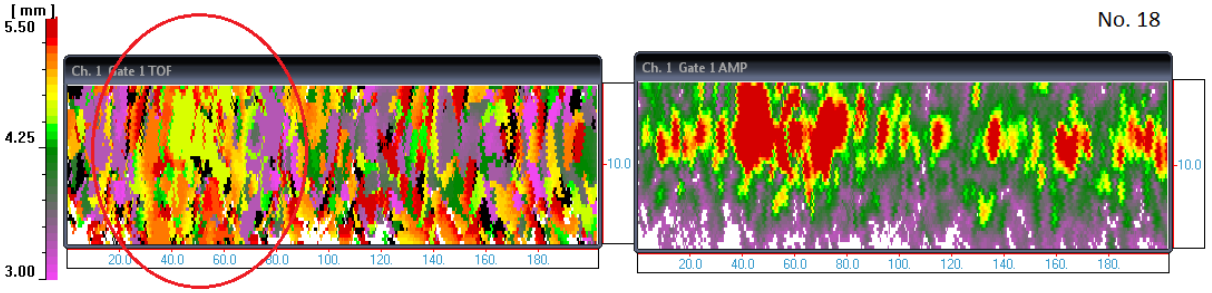

Figure 5.40 C- Scan result (2.25 MHz) No. 18 (200, 50, 4), d_calc=4.75 mm.

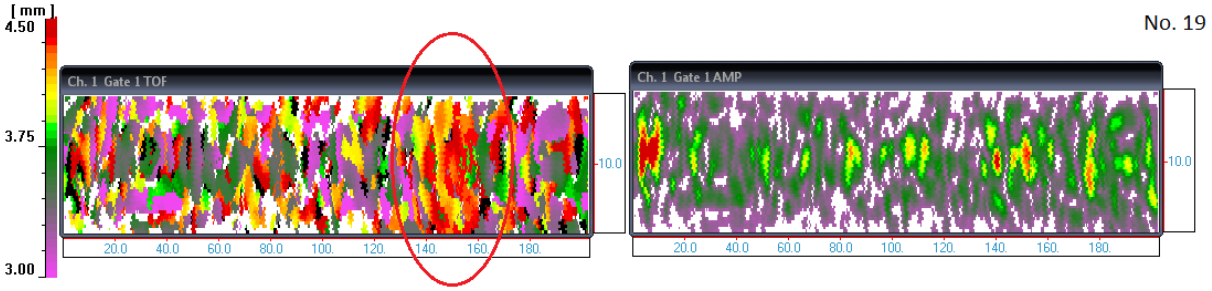

Figure 5.41 C- Scan result (2.25 MHz) No. 19 (60, 150, 4), d_calc=4.2 mm.

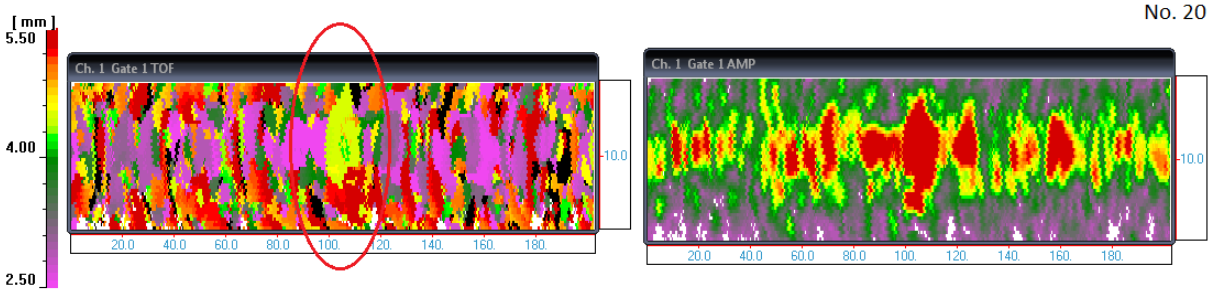

Figure 5.42 C- Scan result (2.25 MHz) No.20 (220, 200, 4), d_calc=4.75 mm.

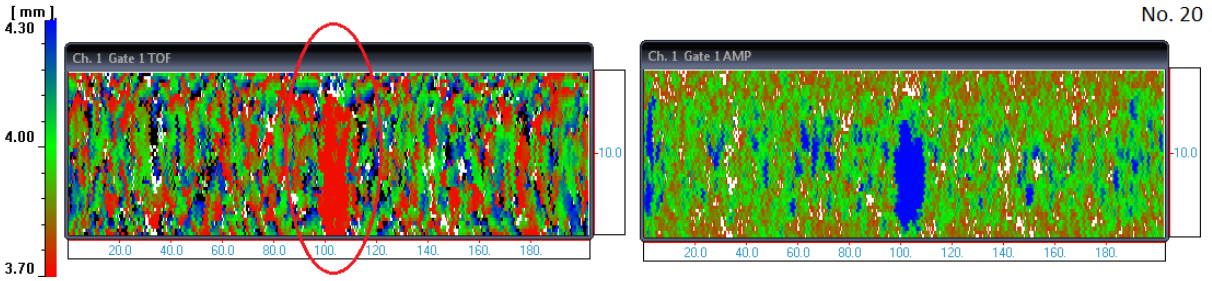

Figure 5.43 C- Scan result (3.5 MHz) No.20 (220, 200, 4), d_calc=3.7 mm.

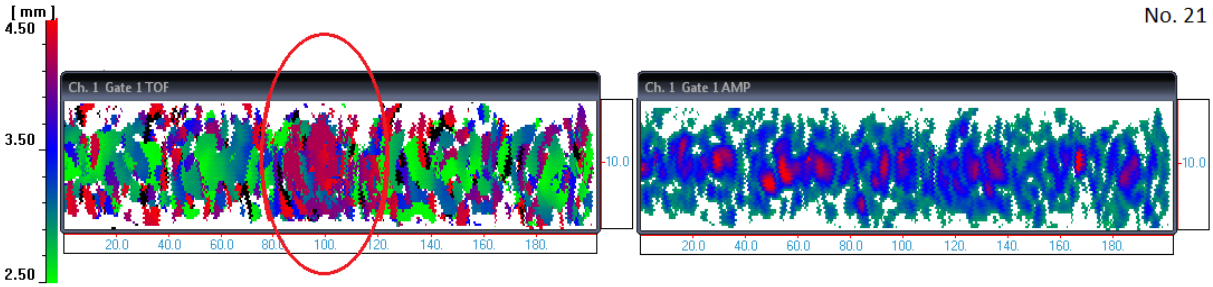

Figure 5.44 C- Scan result (2.25 MHz) No.21 (120, 300, 4), d_calc=4 mm.

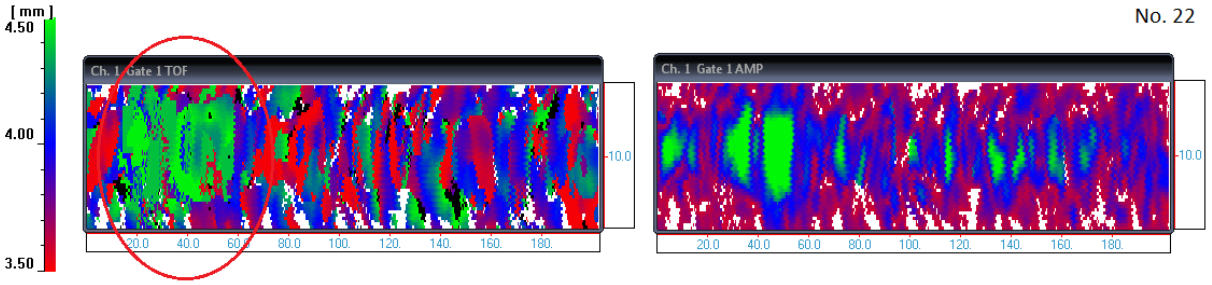

Figure 5.45 C- Scan result (2.25 MHz) No.22 (300, 230, 4), d_calc=4.5 mm.

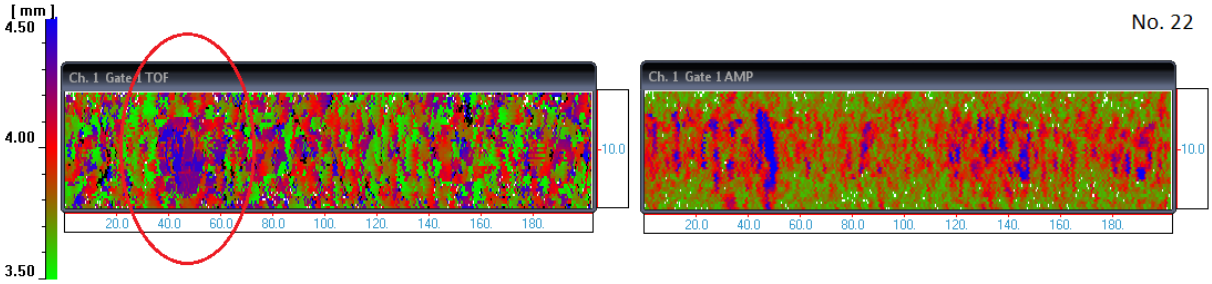

Figure 5.46 C- Scan result (3.5 MHz) No.22 (300, 230, 4), d_calc=4.5 mm.

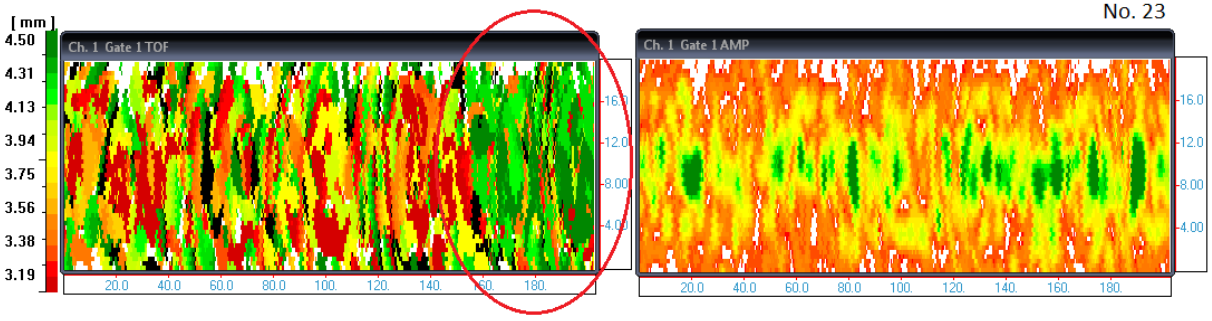

Figure 5.47 C- Scan result (2.25 MHz) No.23 (90, 380, 4), d_calc=4.3 mm.

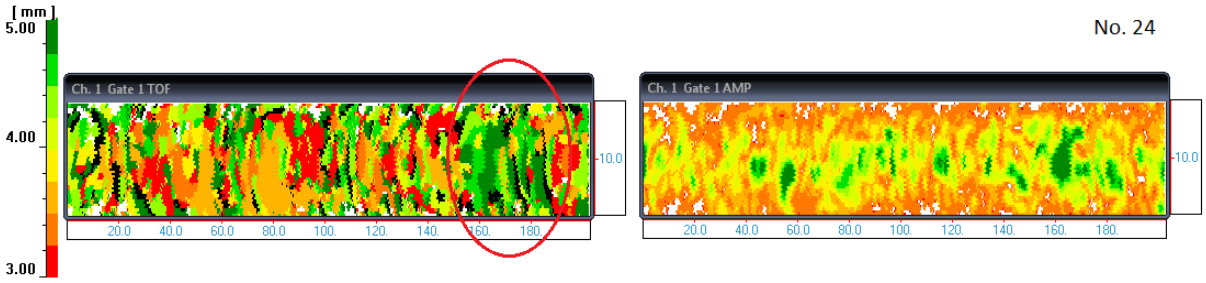

Figure 5.48 C- Scan result (2.25 MHz) No.24 (340, 370, 4), d_calc=4.5 mm.

5.2.2. Aggregated Results of C-Scan

It was impossible to detect most of the defects by using 3.5 MHz probe, contrariwise 2.25 MHz probe provided satisfying results for almost all the defects, except of three of them. All the above mentioned information is summed up in Table 5.31. It allows certain conclusions to be drawn, such as that deviations from the theoretical data do not exceed 1.5 mm and that lower frequency indeed led to more results, especially in deeper distances, as expected according to the higher penetration of the lower frequency transducers.

Table 5.31 C-Scan results.

Theoretical Data					C-Scan Calculations		Deviation	
	Angular Position	Longitudinal Position	Defect Diameter	Depth Theoretical	2.25 MHz Depth Calculated	3.5 MHz Depth Calculated	2.25 MHz	3.5 MHz
No[2]	φ (deg)	Lx (mm)	2r (mm)	d_th (mm)	d_calc (mm)	d_calc (mm)	(mm)	
1	50	50	10	14.2	14.75	-	0.55	-
2	200	50	20	14.2	14.5	-	0.3	-
3	160	170	40	14.2	14.5	-	0.3	-
4	270	180	30	14.2	13.75	-	0.45	-
5	45	240	20	14.2	14.3	-	0.1	-
6	280	320	40	14.2	-	-	-	-
7	90	320	30	14.2	-	-	-	-
8	340	390	10	14.2	14.05	-	0.15	-
9	50	45	40	9.25	8	-	1.25	-
10	270	180	10	9.25	9.2	-	0.05	-
11	60	50	30	9.25	10	-	0.75	-
12	300	220	20	9.25	-	-	0.5	-
13	120	120	10	9.25	10	-	0.75	-
14	230	310	30	9.25	-	-	-	-
15	120	130	20	9.25	10	-	0.75	-
16	330	350	40	9.25	9	-	0.25	-
17	85	40	10	4	2.9	-	1.1	-
18	200	50	40	4	4.75	-	0.75	-
19	60	150	20	4	4.2	-	0.2	-
20	220	200	10	4	4.75	3.7	0.75	0.3
21	120	300	30	4	4	-	0	-
22	300	230	30	4	4.5	4.5	0.5	0.5
23	90	380	40	4	4.3	-	0.3	-
24	340	370	20	4	4.5	-	0.5	-

[2] defects No. 3, 7, 10, 12, 17, 18, 20, 21, 24 have thickness of 2mm.

5.3. Results' Assessment and Conclusions

5.3.1. Aggregated Results

Table 5.32 contains both A and C-Scan results. From Table 5.32 it is obvious that 2.25 MHz probe was more effective for the ultrasonic examination of a CFRP specimen both for A-Scan and C-Scan. Higher penetration is absolutely necessary for composites. The laboratory possessed no transducer of lower frequency, therefore it was not possible to examine the specimen with an even lower frequency.

Table 5.32 A-Scan and C-Scan results.

Theoretical Data					1st A-Scan Calculations		C-Scan Calculations	
No.	Angular Position	Longitudinal Position	Defect Diameter	Depth Theoretical	2.25 MHz	5 MHz	2.25 MHz	3.5 MHz
					Depth Calculated	Depth Calculated	Depth Calculated	Depth Calculated
#	φ (deg)	Lx (mm)	2r (mm)	d_th (mm)	d_a (mm)	d_a (mm)	d_c (mm)	d_c (mm)
1	50	50	10	14.2	14.3	15.2	14.6	-
2	200	50	20	14.2	-	-	14	-
3	160	170	40	14.2	14.5	-	14.4	-
4	270	180	30	14.2	14.33	13.6	13.9	-
5	45	240	20	14.2	14.6	-	14.6	-
6	280	320	40	14.2	-	-	-	-
7	90	320	30	14.2	14.3	-	-	-
8	340	390	10	14.2	14.6	14	14.5	-
9	50	45	40	9.25	8.46	9	8	-
10	270	180	10	9.25	9.4	-	9.2	-
11	60	50	30	9.25	-	10.2	10	-
12	300	220	20	9.25	8.6	-	8.75	-
13	120	120	10	9.25	10.2	-	10	-
14	230	310	30	9.25	9.7	-	-	-
15	120	130	20	9.25	10.2	-	10	-
16	330	350	40	9.25	9	-	9	-
17	85	40	10	4	2.98	4	2.9	-
18	200	50	40	4	4.7	-	4.75	-
19	60	150	20	4	-	3.5	4.2	-
20	220	200	10	4	4	-	4.75	3.7
21	120	300	30	4	4.4	4.27	4	-
22	300	230	30	4	4.6	-	4.5	4.5
23	90	380	40	4	3.7	-	4.3	-
24	340	370	20	4	-	3.9	4.5	-

In Table 5.33 the most representative results are chosen, corresponding to A and C scan results of minor deviations. A comparison is made between A and C-Scan results, as well as between the Scan results and the theoretical data.

Table 5.33 Choice of final measurements and comparison.

REPRESENTATIVE CALCULATIONS					DEVIATIONS		
Theoretical Data			A-SCAN	C-SCAN	**A .vs. TH**	**C .vs. TH**	**A .vs. C**
No.	Angle	Theoretical Depth	Depth Calculated	Depth Calculated	**Deviation**	**Deviation**	**Deviation**
#	φ	d_th	d_a	d_c	**|d_a-d_th|**	**|d_c-d_th|**	**|d_a-d_c|**
	(deg)	(mm)	(mm)	(mm)	**(mm)**	**(mm)**	**(mm)**
1	50	14.20	14.30	14.60	0.10	0.40	0.30
2	200	14.20	-	14.00	-	0.20	-
3	160	14.20	14.50	14.40	0.30	0.20	0.10
4	270	14.20	13.60	13.90	0.60	0.30	0.30
5	45	14.20	14.60	14.60	0.40	0.40	0.00
6	280	14.20	-	-	-	-	-
7	90	14.20	14.30	-	0.10	-	-
8	340	14.20	14.60	14.50	0.40	0.30	0.10
9	50	9.25	8.46	8.00	0.79	1.25	0.46
10	270	9.25	9.40	9.20	0.15	0.05	0.20
11	60	9.25	10.20	10.00	0.95	0.75	0.20
12	300	9.25	8.60	8.75	0.65	0.50	0.15
13	120	9.25	10.20	10.00	0.95	0.75	0.20
14	230	9.25	9.70	-	0.45	-	-
15	120	9.25	10.20	10.00	0.95	0.75	0.20
16	330	9.25	9.00	9.00	0.25	0.25	0.00
17	85	4.00	2.98	2.90	1.02	1.10	0.08
18	200	4.00	4.70	4.75	0.70	0.75	0.05
19	60	4.00	3.50	4.20	0.50	0.20	0.70
20	220	4.00	4.00	4.75	0.00	0.75	0.75
21	120	4.00	4.27	4.00	0.27	0.00	0.27
22	300	4.00	4.60	4.50	0.60	0.50	0.10
23	90	4.00	3.70	4.30	0.30	0.30	0.60
24	340	4.00	3.90	4.50	0.10	0.50	0.60
Median (mm)					0.43	0.40	0.20

For the above measurements deviation between A-Scan and theoretical data is not ideal, as the median of the deviations is 0.43 mm and the maximum deviation is 1.02 mm (defect No. 17). The deviation between C-Scan and the theoretical data is not good enough as well, as the median is 0.4 mm and the maximum deviation is 1.25 mm (defect No.9). Maximum deviation is a noticeable value for the specific specimen, as it constitutes almost the 6% of the specimen's thickness. As mentioned above, the choice of the measurements was made based on the comparison of A-Scan with C-Scan and not with the theoretical data. Therefore, it is logical that the deviation between scan results and theoretical data may be significant.

What matters more is the deviation between A and C-Scan measurements, which should agree. Maximum deviation there is 0.75 mm, for No. 20, and the median is 0.2 mm. The representative value of the median of the deviations is considered low enough. In Table 5.33 a colored scale is applied on each column of deviations in order to compare them. Green is

minimum and red is maximum value. For the column of A .vs. C-Scan only the 3rd group of defects shows significant deviations.

It is noticed that A-Scan always underestimated the result in comparison to C-Scan for these cases. This could be explained, because for A-Scan the near field of the transducer interferes with the echoes of the inside of the specimen and there is a possibility that the operator comes to false conclusions as regards the first echo or a measurement. C-Scan does not entail this risk, as the probe was situated far enough from the specimen.

Table 5.34 Percentage discrepancy between measured and theoretical data.

SELECTED MEASUREMENTS					PERCENTAGE DISCREPANCY	
Theoretical Data			A-SCAN	C-SCAN	A .vs. TH	C .vs. TH
No	Angle	Theoretical Depth	Depth Calculated	Depth Calculated		
#	φ	d_th	d_a	d_c		
	deg	mm	mm	mm	%	%
1	50	14.2	14.3	14.6	0.70	2.82
2	200	14.2	-	14	-	1.41
3	160	14.2	14.5	14.4	2.11	1.41
4	270	14.2	13.6	13.9	4.23	2.11
5	45	14.2	14.6	14.6	2.82	2.82
6	280	14.2	-	-	-	-
7	90	14.2	14.3	12.75	0.70	10.21
8	340	14.2	14.6	14.5	2.82	2.11
9	50	9.25	8.46	8	8.54	13.51
10	270	9.25	9.4	9.2	1.62	0.54
11	60	9.25	10.2	10	10.27	8.11
12	300	9.25	8.6	8.75	7.03	5.41
13	120	9.25	10.2	10	10.27	8.11
14	230	9.25	9.7	-	4.86	-
15	120	9.25	10.2	10	10.27	8.11
16	330	9.25	9	9	2.70	2.70
17	85	4	2.98	2.9	25.50	27.50
18	200	4	4.7	4.75	17.50	18.75
19	60	4	3.5	4.2	12.50	5.00
20	220	4	4	4.75	0.00	18.75
21	120	4	4.27	4	6.75	0.00
22	300	4	4.6	4.5	15.00	12.50
23	90	4	3.7	4.3	7.50	7.50
24	340	4	3.9	4.5	2.50	12.50

The percentage discrepancy between the theoretical and the calculated data is also illustrated in Table 5.34, but as mentioned above this difference is not the criterion of the results' assessment. A final table with the comparison between A and C-Scan is below. Table 5.35 shows the percentage discrepancy of A-Scan from C-Scan measurements, using a colored scale. C-Scan is considered to be a more reliable method therefore C-Scan measurements are used as the values from which the discrepancy is measured.

Table 5.35 Percentage discrepancy between A and C-Scan measured data.

SELECTED CALCULATIONS				PERCENTAGE DISCREPANCY
No.	Theoretical Depth	A-SCAN Depth Calculated	C-SCAN Depth Calculated	A .vs. C
#	d_th	d_a	d_c	|d_a-d_c|/d_c
	(mm)	(mm)	(mm)	(%)
1	14.2	14.3	14.6	2.05
2	14.2	-	14	-
3	14.2	14.5	14.4	0.69
4	14.2	13.6	13.9	2.16
5	14.2	14.6	14.6	0.00
6	14.2	-	-	-
7	14.2	14.3	-	-
8	14.2	14.6	14.5	0.69
9	9.25	8.46	8	5.75
10	9.25	9.4	9.2	2.17
11	9.25	10.2	10	2.00
12	9.25	8.6	8.75	1.71
13	9.25	10.2	10	2.00
14	9.25	9.7	-	-
15	9.25	10.2	10	2.00
16	9.25	9	9	0.00
17	4	2.98	2.9	2.76
18	4	4.7	4.75	1.05
19	4	3.5	4.2	16.67
20	4	4	4.75	15.79
21	4	4.27	4	6.75
22	4	4.6	4.5	2.22
23	4	3.7	4.3	13.95
24	4	3.9	4.5	13.33

5.3.2. Lessons Learned and Conclusions

During the A and C-Scan procedure various conclusions were drawn. As regards the transducers' choice for testing a filament wound CFRP specimen, the conclusion was that frequencies higher than 2.25 MHz are not suggested. This material also requires high Gain, Voltage and Damping, as all composites, while closer to the surface lower Damping and Voltage seem helpful for a better result.

As regards the specimen, wound filament composites with curved surfaces are very difficult to examine. Layers are not definite, as in composites from laminated FRP fabrics. Composite materials entail on their own the difficulty of strong attenuation and diffusion, all the more when the specimen is curved. Lack of flatness leads to loss of a great part of the signals. These specimens require much effort, in order to eliminate the risk of a false measurement. C-Scan results produce more reliable measurements and that leads to the

necessity of scanning in a laboratory and not on the construction site. Furthermore, the thickness of the specimen was not ideal. Thinner specimens are easier to handle, since a clear back-wall echo is received. According to the thickness of the specimen and the depth of the defect, the diameter and the frequency of the transducer have to be chosen. That would determine the near field length that should better be avoided. The thinner the specimen is, the smaller the diameters and the lower the frequencies of the transducer should be.

Additionally, Teflon was used for the simulation of delaminations. Vacuum behaves differently inside a composite material, in terms of ultrasonic examination. There would be a stronger echo, due to the great impedance difference between the two areas. Vacuum has the characteristic of reflecting 100% of the incidental wave, while Teflon surrounded by resin would naturally absorb a percentage of the transmitted energy. Vacuum, therefore, would lead to stronger echo and clearer results. Also since the ultrasound would not be transmitted through vacuum, after the delamination no signal would be received.

5.3.3. Suggested Research

As presented above, plenty of difficulties occurred not only with manual scanning (A-Scan), but also with automated scanning (C-Scan). Further research is suggested to areas that would simplify the procedure, minimize human mistakes and lead to more reliable results.

This could be scanning thinner tubes or tubes with a liner that would lead to more complete and reliable signals. Having a clear back-wall echo is very important for Ultrasonic Testing of materials. When it comes to composites, thick specimens do not allow a clear back-wall echo.

Furthermore, it is suggested that further research is made with examination accessories, such as a rotated base or a bar rotator. These would allow the automated rotation of the cylinder and therefore the more accurate detection of the defects. Heads and accessories that can be adjusted to the shape of the specimen could also be used, e.g. spring loaded swivelling heads, contoured wedges.

Useful would also be the examination of a CFRP cylinder with a transducer of smaller diameter or lower frequency (e.g., 0.5 MHz) that would lead to higher penetration, shorter near field and probably a clearer back-wall echo. However, the strong attenuation of ultrasonic waves inside composite materials made by filament winding method could always lead to weak or non-existent back-wall echo, especially for thick specimens. Delay line transducers could also be used, because they have a wedge, which is a short piece of plastic or epoxy material at the front. These probes place the dead zone and the near field outside the under examination specimen, offering improved resolution near the surface and allowing more accurate measurements.

APPENDIX A

As mentioned in Chapter 5, before the main experimental procedure practice had to be done for A-Scan. First a metal plate with a weld and then three composites from the diploma thesis of Mr. Themelakis were examined.

Stainless Steel A1 Plate

This specimen is a stainless steel plate with a weld. Both geometrical characteristics of the plate and information for the flaws are given in the NDE inspection report shown in Figure A. 1. The three types of flaws that occur are incomplete root penetration, porosity and side-wall crack.

sonaspection

'Quality Flaws Assured'

NDE INSPECTION REPORT

ULTRASONIC

Customer	Nitrammon		Date	02/10/2006.
Specimen ID	PL 10307		Specimen Type	Plate
Dimensions	300 x 20	mm	Acceptance Spec.	SI/08/88

Weld/Specimen Cross Section(s)

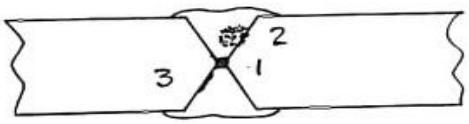

To Scale

Flaw No	Flaw Type	Flaw Length mm	Distance from 0 mm	Max UT Indication dB	Max UT Indication Angle
1	Incomplete Root Penetration	18	48	+4	60
2	Porosity	22	166	+0	60
3	Side Wall Crack	22	236	+2	60

Comments:

Inspector	Gary Stott	Signed

SONASPECTION INTERNATIONAL LTD.

Figure A. 1 NDE inspection report of S/S A1 plate.

Two angle probes were used for the examination of the weld. Both probes had a frequency of 4MHz. The first had a 60^{O} angle, while the second had a 70^{O} angle. A V2 calibration block was used in order to determine the velocity of sound in the material.

In order to detect a flaw in or around a weld some calculations have to be made. The most important calculation is the appropriate position of the probe (skip distance) and should be determined according to Figure A. 2 [30]. θ_R in our case is either 60^{O} or 70^{O}. The probe is transferred accordingly to the desired end-up-point. The desired end-up-point varies according to the area that should be examined (root, toe, heat affected zone, etc).

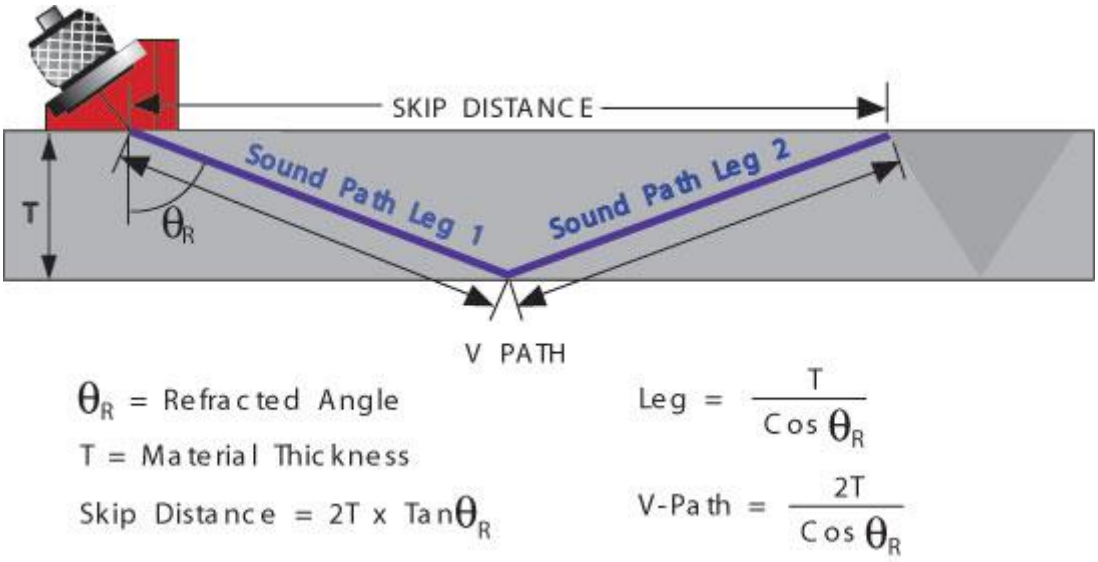

Figure A. 2 Sound path and important calculations for weld inspection.

Flaws' lengths were measured and flaws' positions were detected. The calculations agreed at a satisfactory level with the data from the NDE inspection report.

COMPOSITE SPECIMENS

As mentioned above these specimens were constructed and examined from Mr. Themelakis. Therefore all data regarding flaw depths and specimens' geometry were taken from his diploma thesis [31]. The specimens A, B1, B2 seen in Figure A. 3 were used. For the sake of brevity, the general procedure will be explained, but only one numerical example will be presented.

Firstly, velocity was calculated on each material of each specimen itself. No calibration block was used. Each part was examined from both sides, but that did not always led to results. Steel matrix in specimens B1 and B2 led to easier examination of the specimens, as the echo that represented the interface GFRP-steel had high amplitude.

More specifically, flaw No.1 of specimen A (Figure A. 4) will be used as a numerical example. Specimen A is a sandwich type composite, where skin is GFRP of thickness 2.5 mm each. Matrix is Balsa with thickness 30 mm. As seen in Figure A. 5 flaw No.1 was detected at the depth of 28 mm, which is an accurate measurement.

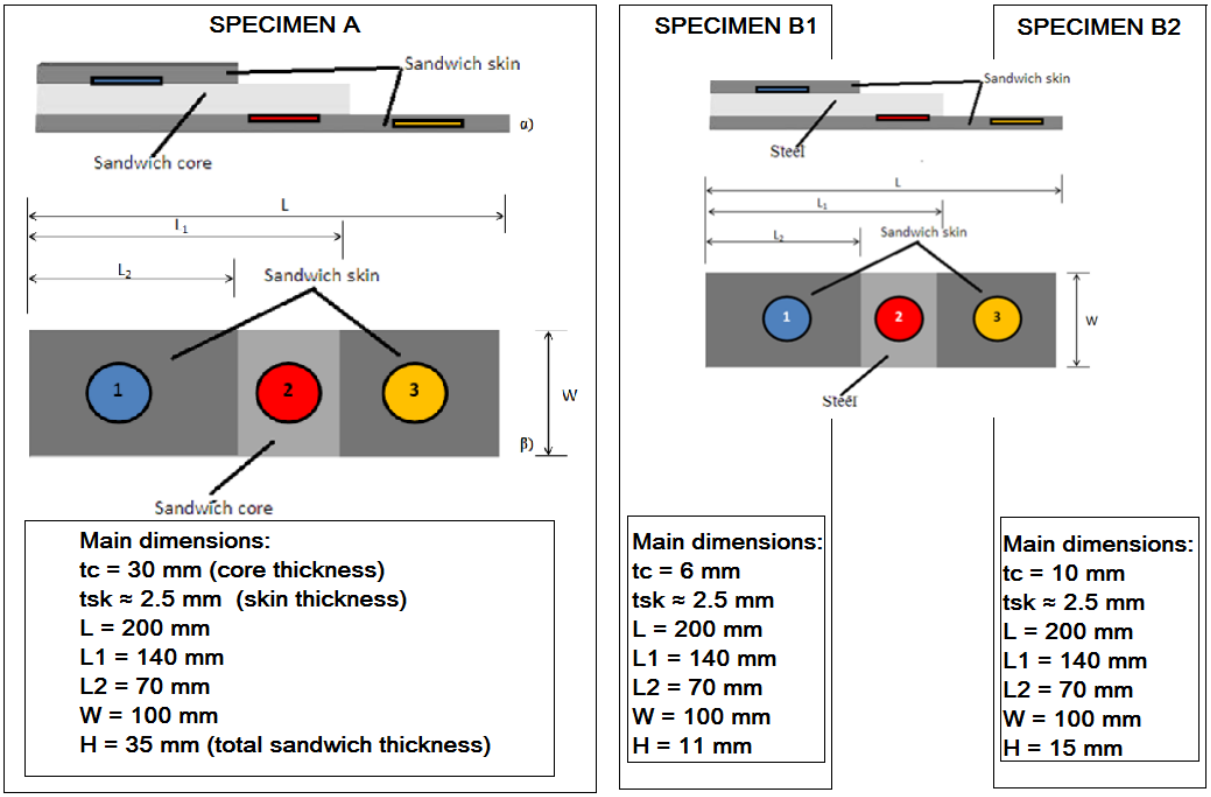

Figure A. 3 Specimens examined for practice.

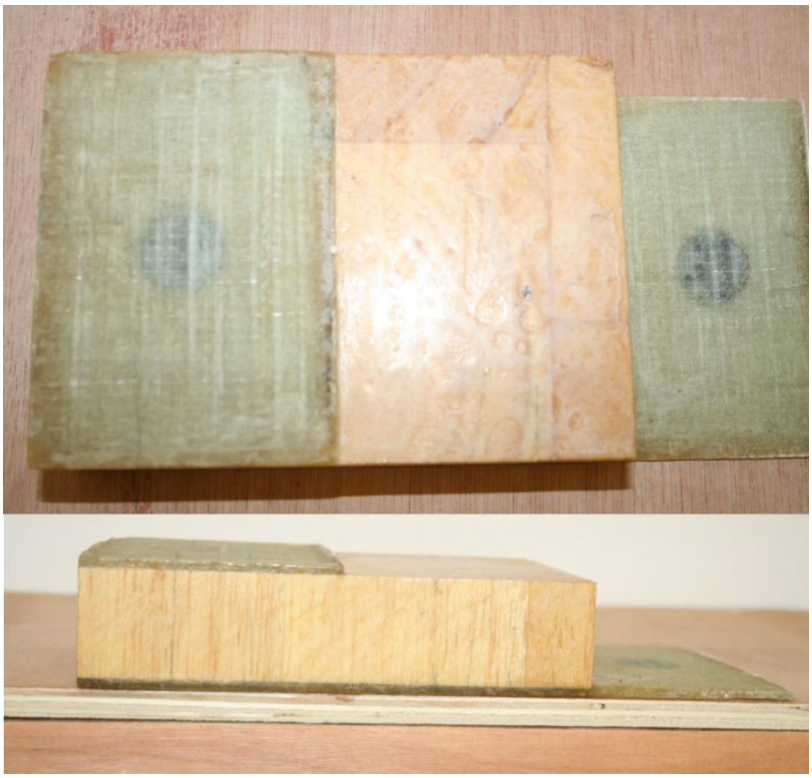

Figure A. 4 Specimen A.

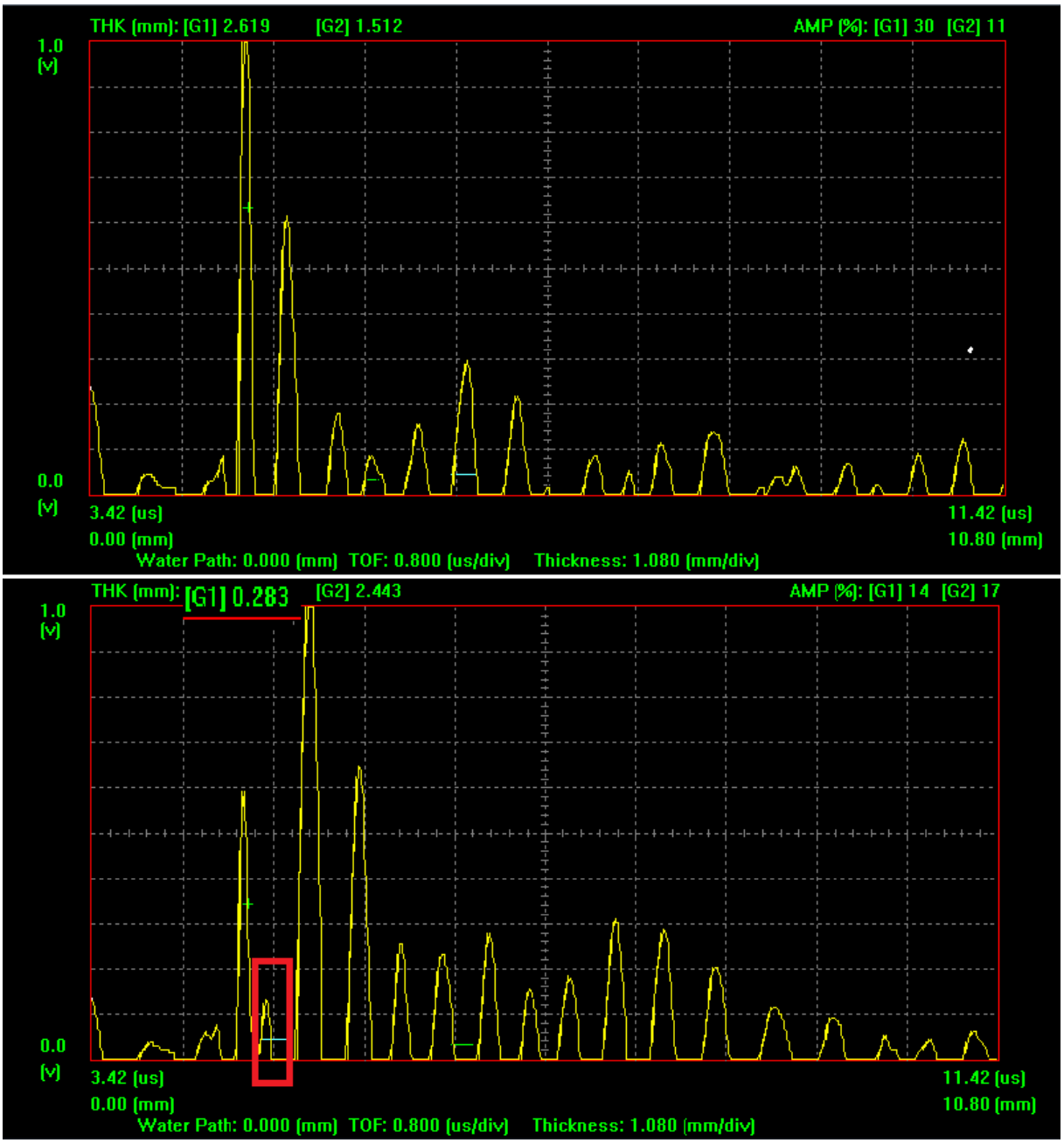

Figure A. 5 Flaw No.1 detection (specimen A).

The steps Mr. Themelakis mentions led to accurate measurements and set the basis for familiarity with UT inspection of composites.

BIBLIOGRAPHY

[1] Handbook of Composites. “Handbook of Composites | S.T. Peters | Springer.” *Springer.Com*, 2019, www.springer.com/gp/book/9781461563891.

[2] Notes ‘ΕΙΣΑΓΩΓΗ ΣΤΑ ΣΥΝΘΕΤΑ ΥΛΙΚΑ ΚΑΙ ΧΡΗΣΕΙΣ ΤΟΥΣ ΣΤΗ ΝΑΥΠΗΓΙΚΗ’, Tsouvalis N., Composite Materials, National Technical University of Athens

[3] Raftogiannis, I. *Σύνθετα Υλικά*. Vol. 1, Εκδόσεις Συμεών, 2013.

[4] Reddy, Rahul. “COMPOSITE MATERIALS -HISTORY, TYPES, FABRICATION TECHNIQUES, ADVANTAGES, AND APPLICATIONS.” *International Journal of Advances in Science Engineering and Technology*, vol. 4, no. 3, 2016, pp. 2321–9009, www.iraj.in/journal/journal_file/journal_pdf/6-291-147712140487-92.pdf.

[5] Peters, S T. *Composite Filament Winding*. Materials Park, Asm International, 2011.

[6] “A Filament-Wound Structure Technology Overview.” Materials Chemistry and Physics, vol. 42, no. 2, Nov. 1995, pp. 96–100, www.sciencedirect.com/science/article/pii/025405849501554X , 10.1016/0254-0584(95)01554-x.

[7] Rosato, Dominick V, and Cornelius S Grove. *Filament Winding: Its Development, Manufacture, Applications, and Design*. New York, Interscience Publishers, 1964.

[8] “Pipex Px® - Producing Excellence » Products.” *Pipexpx.Com*, 2012, www.pipexpx.com/marine-naval/products/.

[9] Optix Solutions Ltd 2012. “Pipex Px® - Producing Excellence » COMPOSITE PRESSURE VESSELS (ASME X, BS 4994 & BS EN13923).” *Pipexpx.Com*, 2012, www.pipexpx.com/products/composite-pressure-vessels-asme-x-bs-4994-bs-en13923/58/.

[10] Greene, Eric. Marine Composites. Annapolis, Md., Eric Greene Associates, 1999.

[11] J Graham-Jones. Marine Applications of Advanced Fibre-Reinforced Composites. Oxford, Elsevier Woodhead Publishing, 2016.

[12] Hayman B, Berggreen C, Tsouvalis NG, “A Review of the Causes of Production Defects in Marine Composite Structures and Their Influence on Performance.” Core.Ac.Uk, 2019, core.ac.uk/display/38461080, oai:dspace.lib.ntua.gr:123456789/35303.

[13] 055 -NORWEGIAN OIL AND GAS RECOMMENDED GUIDELINES FOR NDT OF GRP PIPE SYSTEMS AND TANKS NORWEGIAN OIL AND GAS ASSOCIATION (Norwegian Oil and Gas).

[14] P, Pai S, et al. “Structural Design Criteria for Filament-Wound Composite Shells.” Core.Ac.Uk, 2019, core.ac.uk/display/42788116, oai:casi.ntrs.nasa.gov:19940019929.

[15] “Definition of WAVE.” Merriam-Webster.Com, 2018, www.merriamwebster.com/dictionary/wave .

[16] Russell, Daniel A. “Dan Russell’s Acoustics and Vibration Animations.” Psu.Edu, 2011, www.acs.psu.edu/drussell/demos.html .

[17] “Wave Propagation.” Nde-Ed.Org, 2019, www.nde-ed.org/EducationResources/CommunityCollege/Ultrasonics/Physics/wavepropagation.htm .

[18] Beer, Ferdinand, et al. Mechanics of Materials. 7th ed., New York, Ny, Mcgraw-Hill Education, 2015.

[19] Krautkrämer, Josef, and Herbert Krautkrämer. Ultrasonic Testing of Materials. New Delhi, Springer Science & Business Media, 2003.

[20] kenan12. “Attenuation.” Liberal Dictionary, Liberal Dictionary, 14 Nov. 2018, www.liberaldictionary.com/attenuation/.

[21] Δρ. Μπαδογιάννης Γ. Ευστράτιος, Παχυμετρήσεις και Έλεγχος Συγκολλήσεων με Υπερήχους, Άσκηση 3, Αναλυτικές Εργαστηριακές Σημειώσεις «Ναυπηγική Τεχνολογία και Εργαστήριο», National Technical University of Athens, 2009.

[22] American Society For Nondestructive Testing. *Nondestructive Testing Handbook*. edited by Paul McIntire, Columbus, Oh, American Society For Nondestructive Testing.
[23] Fresnel, Augustin. Plane Waves and Wave Propagation, 2001, pp.24-26.
[24] "Community College Ultrasonic Testing." Nde-Ed.Org, 2019, www.nde-ed.org/EducationResources/CommunityCollege/Ultrasonics/cc_ut_index.htm .
[25] Vatansever, D., et al. "Alternative Resources for Renewable Energy: Piezoelectric and Photovoltaic Smart Structures." Global Warming - Impacts and Future Perspectives, 9 June 2012, www.intechopen.com/books/global-warming-impacts-and-future-perspective/alternative-resources-for-renewable-energy-piezoelectric-and-photovoltaic-smart-structures, 10.5772/50570.
[26] "Piezoelectric Effect." Pc-Control.Co.Uk, 2008, www.pc-control.co.uk/piezoelectric_effect.htm .
[27] Birks, Albert S, et al. Nondestructive Testing Handbook. Volume 7, Ultrasonic Testing. Columbus, Ohio, American Society For Nondestructive Testing, 1991.
[28] "An Introduction to Ultrasonic Transducers for Nondestructive Testing | Olympus IMS." Olympus-Ims.Com, 2015, www.olympus-ims.com/en/resources/white-papers/intro-ultrasonic-transducers-ndt-testing/ .
[29] National Composites Network Best Practice Guide Non-Destructive Testing of Composite Materials.
[30] Ndt.Net, 2019, www.ndt.net/ndtaz/content.php?id=435 .
[31] Θεμελάκης, Άγγελος; Themelakis, Angelos. "Εφαρμογή Της Μεθόδου Μη Καταστροφικού Ελέγχου Με Υπέρηχους Για Την Ανίχνευση Ατελειών Σε Σύνθετα Υλικά." Ntua.Gr, 2016, dspace.lib.ntua.gr/handle/123456789/43281, http://dspace.lib.ntua.gr/handle/123456789/43281 .
[32] "International Organization for Standardization." ISO, 2 Oct. 2019, www.iso.org .
[33] Acucert Ultrasonic Manual, 20.12.2010
[34] "3.4 Pulser and Receiver Operation | Olympus IMS." *Olympus-Ims.Com*, 2015, www.olympus-ims.com/en/ndt-tutorials/flaw-detection/pulser-and-receiver/ .
[35] "UT Material Properties Tables." Nde-Ed.Org, 2019, www.nde-ed.org/GeneralResources/MaterialProperties/UT/ut_matlprop_plastics.htm .
[36] Wuchinich, D. "Acoustic Properties of Selected High Strength Thermosetting Plastic Composites at Ultrasonic Frequencies." Physics Procedia, vol. 63, 2015, pp. 208–216, 10.1016/j.phpro.2015.03.034.
[37] Tanmay Majhi. "Basic Ut Principles." Slideshare.Net, 10 Nov. 2015, www.slideshare.net/TanmayMajhi/basic-ut-principles .
[38] 055 -NORWEGIAN OIL AND GAS RECOMMENDED GUIDELINES FOR NDT OF GRP PIPE SYSTEMS AND TANKS NORWEGIAN OIL AND GAS ASSOCIATION (Norwegian Oil and Gas).
[39] National Composites. "Non-Destructive Testing of Composite Materials - PDF." Docplayer.Net, 2014, docplayer.net/5401279-Non-destructive-testing-of-composite-materials.html.
[40] Bergant, Zoran, et al. "Ultrasonic C-Scan Testing of Epoxy/Glass Fiber Composite." 14th International Conference of the Slovenian Society for Non-Destructive Testing, Sep 4-6, 2017, Bernardin, Slovenia (NDT-Slovenia 2017). Session: Ultrasonic / Acoustic Emission Testing.
[41] Generalov, A, et al. TESTING OF CARBON FIBER-REINFORCED PLASTICS UNDER ULTRASONIC HIGH- FREQUENCY ECHO-METHOD.
[42] Wróbel, Gabriel & Wierzbicki, Łukasz & Pawlak, Sebastian. (2007). A method for ultrasonic quality evaluation of glass/polyester composites. Archives of Materials Science and Engineering. 28.
[43] ASTM. Practice for Measuring Ultrasonic Velocity in Materials. 10.1520/e0494-15.

[44] Sicard, Rene. International Workshop SMART MATERIALS, STRUCTURES & NDT in AEROSPACE INSPECTION OF COMPLEX COMPOSITE AEROSPACE STRUCTURES USING AUTOMATED 3D ULTRASONIC-SCANNING.
[45] “NDT Ultrasonic Testing Equipment Calibration | SDI INC Lab Products.” Structural Diagnostics, Inc, 2019, www.sdindt.com/.
[46] B&T Composites. Cylinder Data Sheet, 2011.
[47] Μελέτη Κατασκευής Κυλίνδρου με Τεχνητές Κατασκευαστικές Ανωμαλίες και Ποιοτικού Ελέγχου με Ακουστικά Συστήματα και Υπερήχους, Παράρτημα Δ
[48] “ASTM E1495 / E1495M - 17 Standard Guide for Acousto-Ultrasonic Assessment of Composites, Laminates, and Bonded Joints.” Astm.Org, 2014, http://www.astm.org/Standards/E1495.
[49] «Δοχείο αποθήκευσης ρευστών υπό πίεση κατασκευασμένο από σύνθετα υλικά (Ίνες άνθρακα και εποξειδικές ρητίνες)», Μη Καταστροφικός έλεγχος Δοχείων, Έργο επιχειρισιακών προγραμμάτων «Ανταγωνιστικότητα & Επιχειρηματικότητα»
[50] Θεμελάκης, Άγγελος Γ. Εφαρμογή Της Μεθόδου μη Καταστροφικού Ελέγχου με Υπερήχους για την Ανίχνευση Ατελειών σε Σύνθετα Υλικά. edited by Νικόλαος Γ. Τσούβαλης, Apr. 2016.
[51] 055 -NORWEGIAN OIL AND GAS RECOMMENDED GUIDELINES FOR NDT OF GRP PIPE SYSTEMS AND TANKS NORWEGIAN OIL AND GAS ASSOCIATION (Norwegian Oil and Gas).